Searching for a mouse model of non-alcoholic steatohepatitis (NASH): the contribution of liver iron, aging and transcription factor *Nrf2*

Sílvia Maria Sousa Chambel
Mestrado em Biologia Celular e Molecular
Departamento de Biologia
2015

Orientador
Doutor Tiago Duarte, Investigador no Grupo Basic and Clinical Research on Iron Biology, Instituto de Biologia Molecular e Celular, Universidade do Porto

Todas as correções determinadas pelo júri, e só essas, foram efetuadas.

O Presidente do Júri,

Porto, _____/_____/_____

Agradecimentos

Gostaria de agradecer ao Doutor Tiago Duarte e à Doutora Graça Porto pela oportunidade de desenvolver esta dissertação no Grupo *Basic and Clinical Research on Iron Biology* do Instituto de Biologia Molecular e Celular. Em particular um agradecimento ao meu orientador, Tiago Duarte, por toda a disponibilidade, orientação, bom humor e simpatia demonstrados ao longo deste ano.

Um agradecimento ao staff do Corelab do Centro Hospitalar do Porto – Hospital Geral de Santo António pelo processamento das amostras de soro dos ratinhos.

Gostaria de agradecer à Ana Luísa, por todos os ensinamentos valiosos e ajuda no desenvolvimento de todo o trabalho, mas principalmente pela amizade, boa-disposição e simpatia sempre presentes. Aos restantes BCRIBs, e aos elementos dos grupos III e MP, especialmente à Mónica, João e Gina pelos constantes momentos de divertimento que sempre proporcionaram, um muito obrigada.

À Andreia, companheira de todas as horas (literalmente), obrigada pela interminável paciência, ajuda e amizade constantes, não só este ano, mas nos últimos 5. Ao Steeve e ao Rui, agradeço por todo o apoio, gargalhadas e amizade sempre presentes. Aos restantes MBCMs, principalmente às miguitas Ana e Patrícia, obrigada por tornarem estes dois anos de mestrado em momentos memoráveis.

Aos meus pais, pelo apoio ao longo destes 24 anos e por terem contribuído para que pudesse concluir todos estes anos de estudo, muito obrigada.

This work was funded by FEDER funds through the Operational Competitiveness Programme – COMPETE and by National Funds through FCT – Fundação para a Ciência e a Tecnologia under the project FCOMP-01-0124-FEDER-028447 (PTDC/BIM-MET/0739/2012).

UNIÃO EUROPEIA
Fundo Social Europeu

Abstract

Nonalcoholic steatohepatitis (NASH) is a liver pathology associated with steatosis, inflammation, and impaired liver function. NASH arises from nonalcoholic fatty liver disease (NAFLD) possibly as a consequence of oxidative stress caused by over-nutrition. The human HFE protein plays a crucial role in systemic iron homeostasis and individuals homozygous for certain *Hfe* gene mutations develop Hereditary Hemochromatosis (HH). As steatosis is commonly observed in HH patients, and current evidence suggests a link between iron and NAFLD, we investigated the potential contribution of *Hfe* mutations to the development of hepatic steatosis, inflammation and fibrosis in young *Hfe*$^{-/-}$ mice (at 8 weeks of age) on a C57BL/6 background fed high-fat (HFD) or normal diet (ND) for 4, 8 or 12 weeks. As iron deposits have repeatedly been observed both in parenchymal and reticuloendothelial liver cells of NAFLD patients, we additionally challenged wt and *Hfe*$^{-/-}$ mice of the same age with 8 weeks of HFD or ND and bimonthly intraperitoneal injections of iron dextran complex, for 8 weeks. Mice were assessed for liver injury, hepatic iron deposition and inflammation and pro-fibrogenic parameters. Loss of *Hfe* alone and loss of *Hfe* coupled with iron administration in HFD-fed mice were not sufficient to trigger the development of NASH. Another potential aggravating factor in NAFLD is the insufficient production of antioxidant defense mechanisms in response to hepatic steatosis. We tested the contribution of NRF2, a central regulator of antioxidative response elements-mediated gene expression, in the progression of NAFLD/NASH. Moreover, as the control of hepatic lipidogenesis by NRF2 appears to be age-dependent, we challenged young (8 weeks old) and middle-aged (52 weeks old) wt and *Nrf2*$^{-/-}$ mice with standard diet (SD) or HFD for 12 weeks to evaluate the development of hepatic steatosis, inflammation and fibrosis. We determined that aging promoted obesity, glucose intolerance, steatosis and steatohepatitis upon HFD feeding. Middle-aged wt mice and *Nrf2*$^{-/-}$ mice fed HFD displayed signs of hepatocyte ballooning and injury, as well as increased inflammatory and fibrotic markers. Importantly, we demonstrate that *Nrf2* deletion leads to rapid progression of nutritional steatohepatitis in both young and middle-aged mice on HFD. Since iron overload-related disorders have a late onset in HFE-HH patients, we also investigated the development of these features in middle aged *Hfe*$^{-/-}$ mice. Whilst young *Hfe*$^{-/-}$ mice did not develop NASH in response to HFD, middle-aged animals the same genotype developed liver tumors.

Keywords: *Hfe,* Iron, NAFLD, NASH, *Nrf2*, Western-type diet, aging.

Resumo

A esteatohepatite não-alcoólica (NASH) é uma patologia do fígado associada a esteatose, inflamação e função hepática comprometida. A NASH surge da doença não-alcoólica do fígado gordo (NAFLD) como consequência de stress oxidativo provocado por sobrenutrição. A proteína humana HFE desempenha um papel crucial na homeostasia do ferro sistémico e indivíduos homozigóticos para certas mutações genéticas no gene *Hfe* desenvolvem Hemocromatose Hereditária (HH). Uma vez que a esteatose é comum em doentes de HH e que evidências recentes sugerem uma ligação entre o ferro e a NAFLD, investigámos a potencial contribuição de mutações no gene *Hfe* para o desenvolvimento de esteatose, inflamação e fibrose em murganhos *Hfe*$^{-/-}$ com fundo genético C57BL/6 às 8 semanas de idade, quando alimentados com um dieta rica em gordura e sacarose (HFD) ou uma dieta normal (ND) durante 4, 8 e 12 semanas. Como têm sido documentados depósitos de ferro parenquimatosos e mesenquimatosos em doentes de NAFLD, administrámos ferro dextrano, em conjunto com 8 semanas de HFD, a murganhos wt e *Hfe*$^{-/-}$ com a mesma idade. Foram avaliados parâmetros como lesão e deposição de ferro hepáticos e inflamação e fibrose. A ausência do gene *Hfe*, assim como a ausência de *Hfe* em conjunto com a administração de ferro a murganhos alimentados com HFD não foram suficientes para despoletar NASH. Outro fator potencialmente agravante da NAFLD é a insuficiência de mecanismos antioxidantes de resposta à esteatose. Assim, testámos a contribuição do fator de transcrição NRF2 no desenvolvimento de NASH. Adicionalmente, como a regulação da lipidogénese hepática pelo NRF2 aparenta ser dependente da idade, alimentámos murganhos wt e *Nrf2*$^{-/-}$ novos (8 semanas de idade) e de meia-idade (52 semanas) com HFD e dieta standard (SD) durante 12 semanas para avaliar o desenvolvimentos de NASH. Apurámos que o envelhecimento em murganhos wt alimentados com HFD levou ao desenvolvimento de obesidade, intolerância à glicose, esteatose e NASH. Adicionalmente, em murganhos wt e *Nrf2*$^{-/-}$de meia-idade foram observados hepatócitos em balão, lesão hepática, inflamação e fibrose. Demonstrámos também que a falta de *Nrf2* propicia a NASH em murganhos novos e de meia-idade. Uma vez que a sobrecarga de ferro hepático leva a uma manifestação tardia da sintomatologia em doentes HH, investigámos ainda o desenvolvimento de NASH em murganhos *Hfe*$^{-/-}$ de meia-idade alimentados com HFD ou SD. Apesar de os murganhos novos não terem desenvolvido NASH, a HFD promoveu o desenvolvimento de tumores hepáticos em animais de meia-idade.

Palavras-chave: Dieta tipo ocidental, Ferro, *Hfe,* NAFLD, NASH, *Nrf2*, envelhecimento.

Table of contents

List of figures

List of tables

List of abbreviations

AFLD	Alcoholic Fatty Liver Disease
ALT	Alanine aminotransferase
ARE	Antioxidant response element
AUC	Area under the curve
BMP	Bone morphogenetic protein
cDNA	Complementary deoxyribonucleic acid
CP	Ceruloplasmin
CREB-H	Cyclic AMP response element–binding protein H
DAG	Di-a-cylglycerol
DCYTB	Duodenal cytochrome b
ddH_2O	Deionized and distilled water
Di-P PA	Di-palmitoyl phosphatic acid
DMT1	Divalent metal transporter 1
DNA	Deoxyribonucleic acid
ECM	Extracellular matrix
ER	Endoplasmic reticulum
FA	Fatty acid
Fe	Iron
Fe^{2+}	Ferrous iron
Fe^{3+}	Ferric iron
FeDx	Iron dextran
FFA	Free fatty acid
FPN1	Ferroportin 1
GSH	Glutathione
H&E	Hematoxylin and eosin
H_2O_2	Hydrogen peroxide
HAMP	Hepcidin
HCC	Hepatocellular carcinoma
HEPH	Hephaestin
HFD	High-fat diet
HFE	Human hemochromatosis protein
HH	Hereditary Hemochromatosis
HJV	Hemojuvelin
HO	Heme oxygenase
Hprt	Hypoxanthine phosphoribosyltransferase gene
HSC	Hepatic stellate cell
IGTT	Intraperitoneal glucose tolerance test
IL-6	Interleukin 6
ISC	Iron sulfur cluster
JH	Juvenile hemochromatosis
KC	Kupffer cell
KEAP1	Kelch-like ECH associating protein 1

LCFA	Long chain fatty acids
LIP	Labile iron pool
MAF	Musculo-aponeurotic fibrosarcoma protein
MDA	Malondialdehyde
MHC	Major histocompatibility complex
mRNA	Messenger ribonucleic acid
NaCl	Sodium chloride
NAFLD	Non-alcoholic fatty liver disease
NAS	NAFLD Activity Score
NASH	Non-alcoholic steatohepatitis
ND	Normal diet
NP-40	Nonidet P-40
Nqo1	NAD(P)H dehydrogenase [quinone] 1 gene
NRF2	Transcription factor nuclear factor-erythroid 2-related factor 2
NTBI	Non-transferrin bound iron
O_2^-	Superoxide
OH•	Hydroxyl radical
PBS	Sodium phosphate buffer
PCR	Polimerase chain reaction
qPCR	Real-time polimerase chain reaction
RNA	Ribonucleic acid
ROS	Reactive oxygen species
RT	Room temperature
RT-PCR	Reverse transcription polymerase chain reaction
SD	Standard diet
STEAP	Six transmembrane epithelial antigen of the prostate
TAG	Tri-acylglycerol
TBARS	Tiobarbituric acid-reactive substances
Tf	Transferrin
TfR	Transferrin receptor
TG	Triglyceride
TIBC	Total iron binding capacity
Tnf-α	Tumor necrosis factor alpha
VLDL	Very low density lipoprotein
Wt	Wild-type
ZIP14	Zinc transporter Zrt-Irt-like protein 14
α-Sma	Alpha-smooth muscle actin

Introduction

1. Anatomy and physiology of the liver

The liver, a versatile organ and the largest gland in the human body, plays an important role in a variety of critical functions, including the detoxification of the systemic and portal blood, and the production and secretion of blood and bile components. The liver is also involved in protein, steroid, and fat metabolism, as well as vitamin, iron, and sugar storage. The classical structural unit of the liver is the hepatic lobule, which encompasses the portal triads consisting of the hepatic artery, bile duct, and portal vein. The liver receives its supply of hydrophilic nutrients through the portal vein and delivers metabolized products to the other organs through the central vein. The hepatic artery, located in the vicinity of the portal vein, supplies the liver with blood enriched in oxygen (Katz et al., 1977). Parenchymal cells or hepatocytes that radiate from the central vein to the perimeter of the lobule define the basic functional unit of the liver, known as the acinus. The liver acinus is demarcated into three discrete zones, based upon oxygen supply: zone 1 is the periportal region that encircles the portal tracts where the oxygenated blood from hepatic arteries enters; zone 2 is the midlobular region; and zone 3 is the pericentral region around the central veins where oxygenation is poor **(Figure 1)** (Jungermann and Kietzmann, 1996; LeCluyse et al., 2012; Rappaport, 1977).

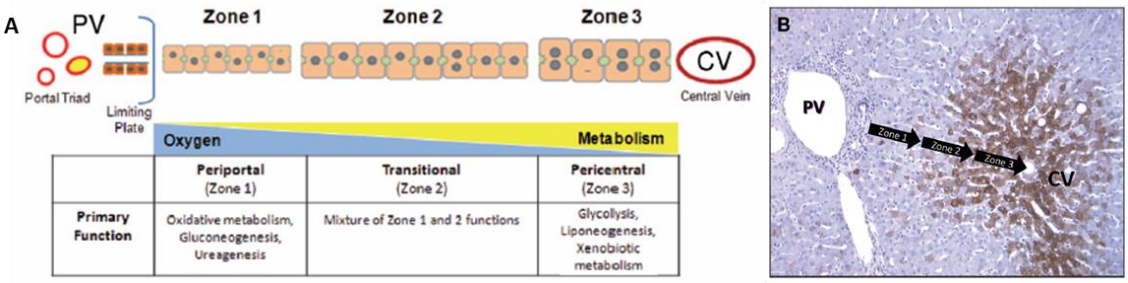

Figure 1. Structural and functional zonation of the liver. **(A)** Discrete zones of the liver between the portal vein (PV) and central vein (CV) illustrating the differences in cell size, phenotype and gradients in oxygen tension and metabolism. **(B)** Histological zones of the human liver. Adapted from (LeCluyse et al., 2012).

2. Hepatic lipid metabolism

The liver plays a key role in the processing of lipids, which includes the synthesis and degradation of fatty acids (FA), and the regulation of blood glucose and cholesterol levels. Hepatocytes convert the excess dietary glucose into FA, in an insulin-dependent process involving acetyl-CoA precursors entitled lipogenesis. FA can be stored as triglycerides (TG) in lipid droplets or used in the generation of phospholipids (Huang J,

2011; Serviddio et al., 2013). Under normal conditions, TG, along with cholesterol and phospholipids, are assembled into very low density lipoprotein (VLDL) particles that can be secreted into the bloodstream for storage in other tissues in the form of lipid droplets, thus preventing TG accumulation in hepatocytes (Huang J, 2011; Stein and Shapiro, 1960). On the other hand, when the available glucose cannot meet energy demands, hepatocytes break down TG and cholesterol stored in lipid droplets through a lysosomal degradative pathway designated lipophagy. The breakdown of TG supplies free fatty acids (FFA) required to sustain rates of mitochondrial *β*-oxidation for the generation of ATP (Liu and Czaja, 2013). FA degradation also occurs in peroxisomes (*β*-oxidation) and in the endoplasmic reticulum (ER) (*ω*-oxidation).

When FA input exceeds the capacity of *β*-oxidation, fat begins to accumulate in hepatocytes (hepatosteatosis), which is a hallmark of both alcoholic (AFLD) and non-alcoholic fatty liver disease (NAFLD) (Zambo et al., 2013). Hepatic steatosis increases FFA *β*-oxidation, resulting in increased rates of electron leakage from the mitochondrial respiratory chain (Seifert et al., 2010), higher free radical formation, and increased hydrogen peroxide production in the peroxisomes.

3. NAFLD: prevalence and etiology

The increase in obesity and diabetes has become an alarming public health trend in the industrialized world (Boudreau et al., 2009; Ford et al., 2002). Obesity is associated with altered physiological functions in the organism and the development of an array of other health risk factors that increase the propensity of cardiovascular disease or type 2 diabetes. These risk factors include abdominal obesity, atherogenic dyslipidemia, hypertension and insulin resistance and have been termed the metabolic syndrome (Alberti et al., 2006). NAFLD is the hepatic manifestation of the metabolic syndrome and is fast becoming one of the most common causes of chronic liver disease worldwide (Byrne and Targher, 2015). In western countries, NAFLD is estimated to affect 20-30% of the general population and up to 90% of the severely obese population (Fabbrini and Magkos, 2015). It starts with the relatively benign accumulation of TG in hepatocytes (steatosis) and hepatic lipid accumulation is a risk factor for disease development. In 30-40% of NAFLD patients, steatosis can progress to the more severe non-alcoholic steatohepatitis (NASH), which is associated with inflammation, fibrosis, impaired liver function (cirrhosis) and hepatocellular carcinoma (HCC) (Dietrich and Hellerbrand, 2014). Development of hepatic fibrosis occurs in 40-50% of people with NASH (Ekstedt et al., 2006).

The pathological mechanisms leading to the transition from lipid deposition to necro-inflammation and cytotoxicity remain unclear, but a “two-hit” theory is widely accepted (Day and James, 1998). The first hit relates to ‘simple’ hepatocellular lipid accumulation without evidence of hepatocellular injury (Enomoto et al., 2015). This lipid accumulation results from increased inflow of FFA derived from insulin resistant adipose tissue, increased hepatic *de novo* lipogenesis and impaired TG export from hepatocytes. The second hit is associated with a hepatic response to counter the steatotic state, promoting lipid peroxidation by *β*- and *ω*-oxidation and evidencing hepatocellular injury (e.g., ballooning degeneration). Lipid oxidation increases the production of reactive oxygen species (ROS) in the liver, resulting in mitochondrial dysfunction, up-regulation of proinflammatory adipocytokines, Kupffer cell (KC) triggering and activation of quiescent hepatic stellate cells (HSCs). Once activated, HSCs begin to proliferate, increasing the production of collagen and stimulating the progression of liver fibrosis (Elpek, 2014) **(Figure 2)**. Fibrosis is a hepatic response to repeated and chronic liver injury, such as the one caused by NASH. Myofibroblasts are cells responsible for deposition of extracellular matrix (ECM) and are usually absent from the healthy liver, accumulating in response to hepatic cell injury, and serving as the main cell effector of fibrogenesis (Koyama and Brenner, 2015). Alpha-smooth muscle actin (α-SMA) is a commonly employed marker of hepatic stellate cell differentiation into myofibroblast (Nagamoto et al., 2000).

Although the role of HSC activation is still uncertain in the progression of NAFLD, many studies have reported the activation of HSCs in NASH (Kaji et al., 2011). Another factor associated with NASH-related fibrogenesis is insulin resistance, as insulin promotes HSC activation and insulin sensitizers are able to attenuate hepatic fibrosis in NAFLD (Elpek, 2014). In addition to directly inducing cellular destruction by membrane lipoperoxidation, ROS can act as secondary messengers in the regulation of pro-inflammatory and pro-fibrogenic genes such as α-SMA and cytokines such as tumor necrosis factor alpha (TNF-α) and interleukin-6 (IL-6) (Angulo, 2002).

Even though obesity is strongly correlated with NAFLD, recent studies suggest that body fat mass alone is not sufficient to trigger the pathogenesis of NAFLD, but adipose tissue dysfunction might be. It is still not known whether NAFLD is the cause or the consequence of insulin resistance, but there is mounting evidence that hepatic lipid accumulation is capable of causing hepatic/peripheral insulin resistance and hepatic inflammation, by the production of lipid products derived from long chain fatty acids (LCFA) such as di-a-cylglycerols (DAG) and tri-acylglycerols (TAG) and intermediate products such as ceramides and di-palmitoyl phosphatic acid (Di-P PA). The increased

production of these lipid products causes ‘resistance’ in the hepatic insulin signaling pathway, promoting hepatic inflammation and liver disease (Byrne and Targher, 2015; Fabbrini and Magkos, 2015) **(Figure 2)**.

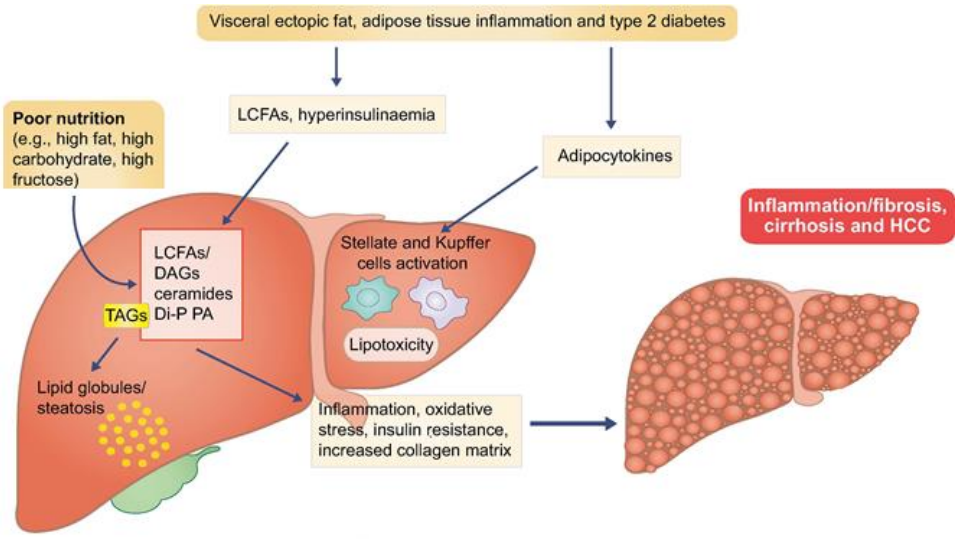

Figure 2. Development of progressive liver disease in NAFLD. Hepatic lipid accumulation begins to appear (steatosis) due to increased levels of FFA derived from insulin resistant adipose tissue, increased hepatic de novo lipogenesis or impaired lipid export from hepatocytes. However, as lipid peroxidation ensues, the liver tries to overcome its steatotic status, leading to oxidative stress, inflammation and Kupffer and hepatic stellate cells activation. HSCs then begin to proliferate, increasing collagen production and stimulating the progression of fibrosis, cirrhosis and HCC (Byrne and Targher, 2015).

4. Iron chemistry

Iron (Fe) is an essential element for nearly every form of life, serving both as an electron donor and receiver. Iron can be incorporated into multiple proteins, either in the form of organic cofactors, such as heme, or inorganic cofactors, such as iron sulfur clusters (ISC) (Evstatiev and Gasche, 2012). Iron-containing proteins carry or store oxygen (e.g. hemoglobin, myoglobin), catalyze metabolic and signaling-related redox reactions and transport or store iron (e.g. transferrin, lactoferrin, ferritin) (Ganz, 2013). These proteins also take part in transcription factors and repressors, enzymes of intermediate metabolism and DNA synthesis and repair (Evstatiev and Gasche, 2012).

Most reactions involving iron-containing proteins show iron switching between the ferrous (Fe^{2+}) and ferric (Fe^{3+}) state (Evstatiev and Gasche, 2012), highlighting the biological importance of iron as a transition metal. Free iron can generate ROS, particularly through “Fenton-type” reactions. The Fenton reaction **(1)** represents the most important reaction of hydrogen peroxide (H_2O_2) or lipid peroxides with free or poorly liganded ferrous iron, generating a highly reactive and damaging hydroxyl radical (OH•).

Superoxide (O_2^-) can also react with ferric iron **(2)**, and this combination results in the Haber-Weiss reaction **(3)** (Kehrer, 2000; Kell, 2009; Umbreit, 2008).

$$Fe^{2+} + H_2O_2 \rightarrow Fe^{3+} + OH^- + \bullet OH \quad \textbf{(1)}$$

$$Fe^{3+} + O_2^- \rightarrow Fe^{2+} + O_2 \quad \textbf{(2)}$$

$$O_2^- + H_2O_2 \rightarrow O_2 + OH\bullet + OH^- \quad \textbf{(3)}$$

Free iron is therefore extremely toxic to cells and other biological structures, promoting oxidation of proteins, peroxidation of lipids and modification of nucleic acids (Evstatiev and Gasche, 2012; Papanikolaou and Pantopoulos, 2005), events that can eventually lead to cellular damage. To overcome this potential toxicity, organisms have developed mechanisms of iron homeostasis involving tight control of iron uptake, storage and export and its intracellular distribution (Hentze et al., 2004), thus regulating tissue iron levels.

5. Iron metabolism

5.1 Body iron distribution

The average human male adult contains about 3-5 g of iron, of which about two thirds is kept within hemoglobin of developing erythroid precursors and mature red blood cells. The remaining body iron can mainly be found in reticuloendothelial macrophages (~ 600 mg), stored in hepatocytes (~ 1000 mg) within ferritin and its degradation product, hemosiderin (Gkouvatsos et al., 2012) and in muscles, primarily in myoglobin (Papanikolaou and Pantopoulos, 2005) **(Figure 3)**. Men and non-menstruating women absorb daily 1-2 mg of iron from the diet, in order to compensate for iron losses derived from sloughing of enterocytes and minor bleeding (Ganz, 2012). These amounts are, however, insufficient to cover iron needs, as the majority of iron within blood plasma is directed to the bone marrow for erythropoiesis which, by itself, requires a daily supply of at least 20-25 mg of iron. Iron requirements are then fulfilled by the recycling of iron by reticuloendothelial macrophages. Splenic and hepatic macrophages recover the hemoglobin from senescent erythrocytes and supply iron to erythrocyte precursors for hemoglobin synthesis (Evstatiev and Gasche, 2012; Ganz, 2012; Papanikolaou and Pantopoulos, 2005).

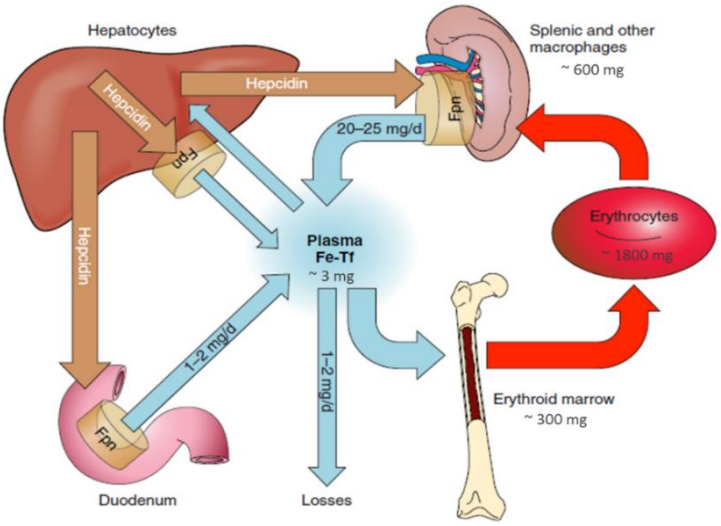

Figure 3. Iron distribution within the body. Transferrin-bound iron is represented in blue and iron in erythrocytes in red. Adapted from (Ganz, 2013).

5.2 Iron uptake

Dietary iron is absorbed in the brush border of duodenal enterocytes in two distinct forms: non-heme or inorganic iron, mainly found in cereals and vegetables, or heme-bound iron, mainly sourced from hemoproteins, hemoglobin and myoglobin in meat (Evstatiev and Gasche, 2012; Lane et al., 2015a; Silva and Faustino, 2015).

Inorganic dietary iron mostly exists in its insoluble oxidized ferric form within the intestinal lumen. For it to cross the enterocytes apical membrane, ferric iron undergoes reduction by the low pH of the stomach coupled with ascorbic acid (Sharp, 2010). Duodenal cytochrome b (DCYTB), a brush border ferriductase, and Six transmembrane epithelial antigen of the prostate *2* (STEAP2) (McKie et al., 2001) facilitate iron reduction (Silva and Faustino, 2015), which allows ferrous iron to be transported across the apical enterocyte membrane by proton-coupled Divalent metal transporter 1 (DMT1) (Ganz, 2013; Mackenzie and Garrick, 2005; Papanikolaou and Pantopoulos, 2005). Ferrous iron thus enters the “labile iron pool” (LIP), presumably binding to low molecular weight chelators and remaining available for metabolic purposes (Evstatiev and Gasche, 2012) **(Figure 4)**.

5.3 Cellular iron storage

When iron demands are low, iron can be stored within ferritin, a ubiquitous and highly conserved iron storage protein. Ferritin polymers (H and L ferritin) form a structure that accommodates up to 4500 iron ions to be stored within it. Moreover, ferritin also allows the mobilization of iron when demands increase by pathways that are yet unknown (Andrews and Schmidt, 2007; Harrison and Arosio, 1996; Theil, 2003). Ferritin is down-

regulated when there is iron deficiency, rendering iron available to meet demands. Conversely, ferritin is up-regulated in the presence of iron overload disorders, in order to protect cells from toxicity (Hentze et al., 2004). Hepatocytes and reticuloendothelial cells, such as macrophages and monocytes, are the main iron storage cell types in the human body (Yun and Vincelette, 2015).

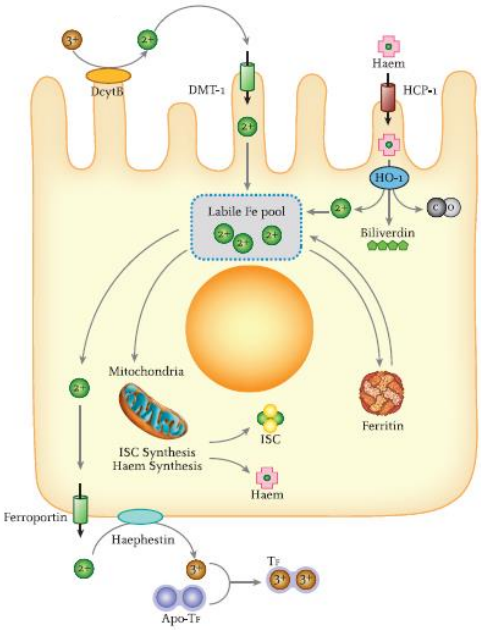

Figure 4. Uptake of heme and non-heme iron by duodenal enterocytes. Inorganic ferrous iron enters the enterocyte via DMT1 after reduction by DCYTB. Heme-bound iron enters the cytosol via putative heme transporters HCP-1. Once in the cytoplasm, iron can either be stored within ferritin, an iron storage protein, released into plasma by FPN1 or enter the LIP and becoming available for metabolic purposes (Evstatiev and Gasche, 2012).

5.4 Cellular iron export

When iron demands are high, intracellular iron is transferred across enterocytes, macrophages and hepatocytes to the circulation by a single protein, Ferroportin 1 (FPN1; also known as SLC40A1, IREG1 and MTP1), the single iron exporter identified in mammals to date (Abboud and Haile, 2000; Donovan et al., 2000; McKie et al., 2000). FPN1 is expressed in all sites involved in iron transfer to plasma, which includes the basolateral membrane of enterocytes, the membranes of macrophages, the sinusoidal surfaces of hepatocytes and the basal surface of the placental syncytiotrophoblast facing the fetal circulation (Ganz, 2013). FPN1 exports ferrous iron by mechanisms that have not yet been reported, but ferric iron is required for binding to transferrin, a protein capable or binding iron tightly but reversibly in the interstitial fluids. Iron efflux must then be coupled to oxidation. In the case of enterocytes, hephaestin (HEPH), a membrane anchored, multicopper ferroxidase oxidizes ferrous to ferric iron (Gulec et al., 2014) for

it to bind to transferrin. In what concerns hepatocytes and macrophages, ferrous iron oxidation is performed by ceruloplasmin (CP) (Andrews, 2000).

5.5 Cellular iron uptake

5.5.1 Transferrin-mediated mechanisms

Iron absorbed from the diet is distributed throughout the body bound to plasma transferrin (Tf), a monomeric protein capable of biding tightly but reversibly two atoms of ferric iron (Gkouvatsos et al., 2012). Iron chelation by Tf aims to facilitate iron transport and its cellular uptake and preserve ferric iron in a soluble form, and thus in a redox inert state, preventing the formation of toxic free radicals (Rochette et al., 2015). Under normal conditions, Tf carries nearly all serum iron and delivers it to erythroid progenitor cells and other fast dividing cell populations for uptake via the transferrin receptor-1 (TfR1) (Cheng et al., 2004).

TfR1 is expressed at low levels in most tissues and resides in the outer cell membrane of cells presenting high iron demands (e.g. intestinal epithelial cells, placental syncytiotrophoblasts and neoplasic cells), binding one Tf molecule at each of its subunits. When holo-transferrin (holo-Tf, diferric transferrin) binds to TfR1, this complex undergoes endocytosis via clathrin-coated pits. Acidification of the endosome via proton pump ATPase facilitates a conformational change in Tf, resulting in the release of ferric iron. When iron is released, apo-transferrin (apo-Tf, iron free transferrin) and TfR1 return to the cell surface. Apo-Tf is recycled back to the bloodstream and becomes available to recapture iron. Iron is then reduced by an endosomal ferrireductase (e.g., STEAP3 (Ohgami et al., 2005) or by a recently discovered mechanism involving cellular ascorbate (Lane et al., 2015b) and transported out of the endosome by DMT1 (Daniels et al., 2006; Gkouvatsos et al., 2012; Hentze et al., 2004) or Zinc transporter Zrt-Irt-like protein 14 (ZIP14) (Jenkitkasemwong et al., 2012) **(Figure 5)**.

Transferrin receptor 2 (TfR2) (Kawabata et al., 1999) is an iron-binding protein that is highly homologous to TfR1 but whose expression is largely restricted to hepatocytes (Daniels et al., 2006) and, to a lower extent, to erythroid cells, spleen, lung and muscle (Evstatiev and Gasche, 2012). TfR2 binds iron-loaded Tf with a 25-fold lower affinity compared to its homolog TfR1. Although TfR2 expression is not regulated by intracellular iron levels (Kawabata et al., 2000), mutations in this protein cause Hereditary Hemochromatosis (HH), indicating its crucial role in systemic iron homeostasis (Gkouvatsos et al., 2012).

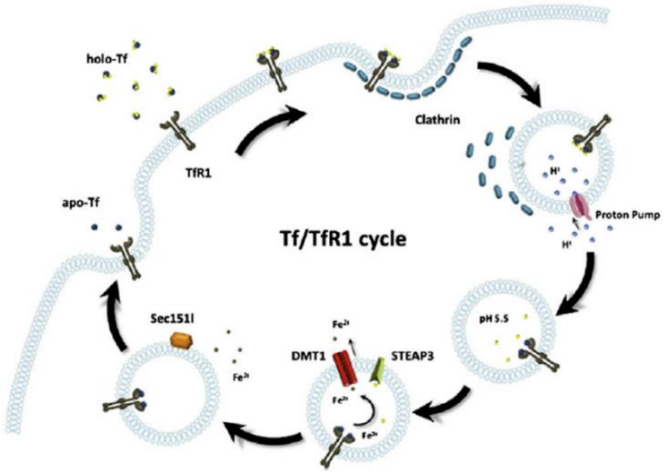

Figure 5. Cellular uptake of transferrin-bound iron. Holo-Tf binds to TfR1 and the Tf/TfR1 complex is endocytosed. A drop in pH releases ferric iron from Tf. Ferric iron is oxidized by STEAP3 to ferrous iron and it is transported to the cytosol via DMT1. TfR1 and Apo-Tf are recycled back to the cell surface and circulation, respectively (Gkouvatsos et al., 2012).

Under normal physiological conditions, approximately 30% of plasma Tf-binding sites are saturated. Tf saturation <15% indicates iron deficiency, while >45% are consistent with iron overload (Hentze et al., 2010). However, in disorders of severe iron overload, such as HH, Tf saturation exceeds 60%. Under these conditions, non-transferrin bound iron (NTBI) increases dramatically and starts to accumulate in the circulation and in tissue parenchymal cells, eventually leading to organ damage. The main site for NTBI accumulation is the liver, even though there is also some deposition in the heart and pancreas (Ganz, 2013; Gkouvatsos et al., 2012).

5.5.2 Transferrin independent mechanisms

Even though Tf is the main source of iron for all tissues, specific cell types assimilate iron through independent routes. This is the case of liver and spleen macrophages that, despite having a Tf/TfR1 dependent route, mainly obtain iron from phagocyting senescent erythrocytes, an essential process for maintaining body iron homeostasis. Phagocytosed erythrocytes are broken up in lysosomes and iron is released via Heme oxygenase 1 (HO-1), entering the LIP. Iron from the labile pool is either used for metabolic purposes, stored within ferritin or exported into the circulation via FPN1 and becoming bound to Tf after oxidation by CP (Evstatiev and Gasche, 2012). Macrophages are also able to scavenge hemoglobin via signal-inducing macrophage protein CD163, a receptor that scavenges hemoglobin by mediating endocytosis of haptoglobin-hemoglobin complexes (Kristiansen et al., 2001). HO-1 and its homologues HO-2 and HO-3 (Ryter and Tyrrell, 2000) performs the metabolic degradation of heme into bile pigments (i.e., biliverdin and bilirubin), iron and carbon monoxide (Papanikolaou and Pantopoulos, 2005; Ryter et al., 2006) **(Figure 6)**.

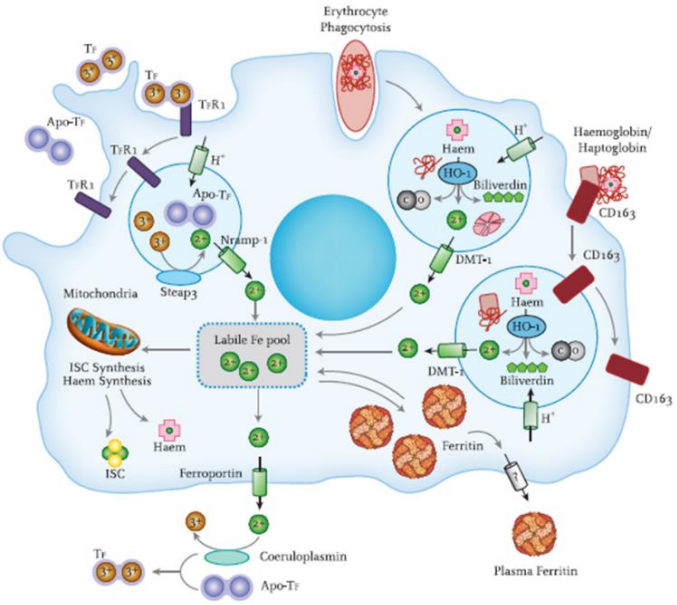

Figure 6. Macrophage iron uptake. Macrophages primarily obtain iron through the endocytosis of old red blood cells. In the cytoplasm, erythrocytes are broken up in lysosomes by HO-1 and iron enters the LIP, becomes stored in ferroportin or is exported via FPN1 and bounds to Tf. (Evstatiev and Gasche, 2012).

6. Systemic iron homeostasis

6.1 Hepcidin: the iron regulatory hormone

Hepcidin (HAMP*)* is a 25-amino-acid protein mainly produced by hepatocytes (Andrews and Schmidt, 2007). Hepcidin was first identified as an antimicrobial peptide (Park et al., 2001) but its main function was subsequently discovered to be the regulation of body iron homeostasis, as hepcidin knockout mice exhibit massive iron overload (Nicolas et al., 2001). Hepcidin exerts its biological function by post-translationally controlling the concentration of FPN1 and promoting its phosphorylation, internalization and lysosomal degradation (Nemeth et al., 2004). When hepcidin levels rise, due to, for example, inflammation or infection, iron absorbed in the gut cannot enter the circulation, remaining stored within enterocytes and being, eventually, lost by intestinal sloughing. Another consequence of increased hepcidin levels is the degradation of FPN1 in storage sites, such as hepatocytes and macrophages, resulting in low iron levels in circulation and impending iron overload (Evstatiev and Gasche, 2012). On the other hand, hepcidin levels drop when there is increased erythropoietic demand for iron, hypoxia and iron deficiency (Nicolas et al., 2002). Hepcidin levels are also low in conditions such as HH, in which increased dietary iron absorption leads to excessive iron stores (Bridle et al., 2003).

6.2 Transcriptional control of hepcidin

Iron feedback regulates hepcidin expression, so that both the toxicity associated with iron overload and the physiological consequences underlying its deficiency can be avoided (Silva and Faustino, 2015). A pathway involved in hepcidin expression by iron levels is the hemojuvelin (HJV)-bone morphogenetic protein (BMP) axis. HJV, a membrane protein, regulates hepcidin hepatic expression and acts as a BMP co-receptor, activating hepcidin transcription through the BMP-SMAD cascade. The BMP pathway, besides regulating iron in the liver, is involved in other processes such as embryonic morphogenesis, bone development, and remodeling and tissue repair (Ganz and Nemeth, 2012). When BMPs, particularly, BMP6, which, in mice, is activated by increased iron levels (Andriopoulos et al., 2009; Meynard et al., 2009), bind to BMP receptors type I and type II, the BMP-HJV signaling pathway is activated. The activated receptors phosphorylate receptor-associated SMAD proteins (R-SMADs) that, together with SMAD4, translocate to the hepatocyte nucleus, binding to BMP responsive elements (BMPREs) located in the hepcidin promoter region and inducing its transcription (Evstatiev and Gasche, 2012; Ganz, 2013; Silva and Faustino, 2015).

Hepcidin expression can also be controlled by the cell surface Human hemochromatosis protein (HFE) and TfR2. Under basal conditions, HFE is usually expressed on the cell surface of hepatocytes and binds to TfR1, a process inversely correlated with transferrin saturation (Muckenthaler, 2014). However, when serum holo-transferrin-iron levels increase, HFE is displaced from TfR1 and binds to TfR2. The holo-Tf-TfR2-HFE complex triggers the MAPK/ERK signaling pathway, thus leading to increased hepcidin transcription (Goswami and Andrews, 2006; Silva and Faustino, 2015).

It has recently been shown that HFE, TfR2 and HJV form, along with the BMP/SMAD pathway, a multimeric complex on the hepatocyte cell membrane (D'Alessio et al., 2012). HFE binds to the BMP type I receptor Alk3, stabilizing it by diminishing its polyubiquitination and degradation through the proteasome (Wu et al., 2014). Alk3, along with Alk2, are two essential BMP type I receptors responsible for aiding hepcidin expression (Steinbicker et al., 2011). However, in patients with HH associated with mutations in the *HFE* gene, the HJV-BMP signaling pathway is impaired, as HFE cell-surface expression becomes compromised (Muckenthaler, 2014). Since mutant HFE cannot translocate to the cell surface, Alk3 mRNA levels are reduced in patients with HH and, as a consequence, hepcidin transcription is compromised. As a result, HH patients develop symptoms of severe iron overload (Wu et al., 2014) **(Figure 7)**.

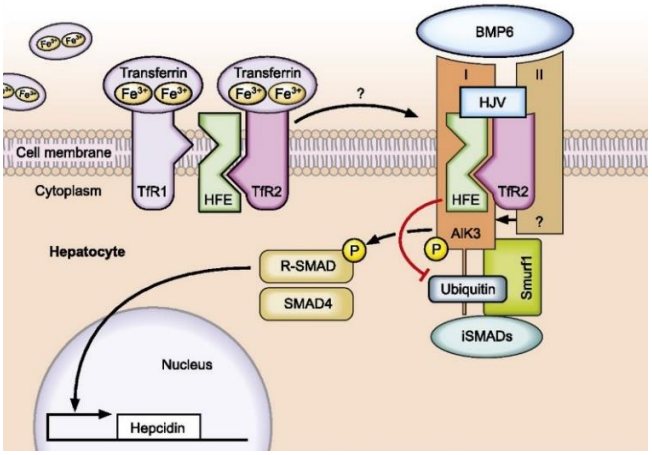

Figure 7. Cell surface interaction between HFE, TfR2, HJV, BMP receptors and BMP ligands (BMP6). HFE binds to Alk3, preventing its stabilization and proteasomal degradation, thus increasing its cell surface expression and the activation of the BMP/SMAD pathway and hepcidin transcription (Muckenthaler, 2014).

7. Hereditary Hemochromatosis

Hereditary Hemochromatosis (HH) is an autosomal recessive disorder characterized by deficient hepcidin expression. Decreased HAMP levels result in uncontrolled dietary iron absorption and, as a consequence, increased serum transferrin saturation and ferritin levels and NTBI appearance. Eventually, in males between 40 and 50 years of age and post-menopausal women, as body iron levels escalate, excessive iron begins to accumulate mainly in the liver, but also in pancreas, pituitary, heart, joints and skin. If left untreated, HH may cause clinical complications such as arthritis, hypogonadotrophic hypogonadism, diabetes mellitus, liver fibrosis, cirrhosis, hepatocellular carcinoma and heart failure (Papanikolaou and Pantopoulos, 2005).

The main mechanism affected in HH is the iron sensing-hepcidin axis. Depending on which genes might be affected, HH can be classified into four types: (i) *HFE* related HH, (ii) juvenile hemochromatosis (JH), (iii) *TfR2*-associated hemochromatosis and (iv) ferroportin disease (Silva and Faustino, 2015). The most common type of HH is attributable to a mutation in the *HFE* gene, a major histocompatibility complex (MHC) class I type molecule (Feder et al., 1996). The majority of HH patients is homozygous for a *HFE* gene C282Y polymorphism or, occasionally, compound heterozygote for a C282Y/H63D mutation. In the C282Y mutation, the cysteine-tyrosine substitution interrupts the formation of a disulfide bond essential for HFE to bind beta 2-microglubulin (β_2M), a component of MHC class I molecules (Feder et al., 1996), thus disabling HFE stabilization, transport and cell-surface expression and its interaction with TfR1 and TfR2. *HFE* related mutations depict a high prevalence (5:1000 individuals of northern European descent) (Pietrangelo, 2006); however, as the clinical penetrance of HH is, in fact, much lower (Beutler et al., 2002), other modifying factors, such as alcohol or

additional genetic variations might be involved in HH manifestations, making *HFE*-related HH the mildest form of the disease (Arezes and Nemeth, 2015). Mutations in TfR2 (HH-type III) result in a phenotype similar to HFE-related HH, as individuals present elevated transferrin and ferritin saturation levels. The other forms of HH present much more severe clinical symptoms than type I and III HH, as well as early-onset organ disease. Juvenile hemochromatosis (JH) (HH-type II) is caused by mutations either in the *HJV* (type IIA) or *HAMP* (type IIB) genes. JH is much more uncommon than the adult forms but it leads to much more severe iron accumulation. Finally, HH-type IV results from autosomal dominant mutations in the *SLC40A1* gene and the outcome can either be the gain or loss of function in FPN1 (Batts, 2007; Pietrangelo, 2010; Silva and Faustino, 2015). Currently, the standard treatment for all types of HH is iron reduction therapy (phlebotomy) and treatment should begin when ferritin levels exceed normal values. However, frequency of treatment or therapeutic endpoints vary between patients and disease severity (Pietrangelo, 2010).

8. Iron imbalance in NAFLD

Excessive hepatic iron accumulation is frequently observed in NAFLD patients and may be a potential aggravating factor in the development of NASH. The combination of steatosis and cellular iron loading, together with the increased levels of free fatty acids, can result in increased oxidative stress, which would enhance the progression from steatosis to NASH (O'Brien and Powell, 2012). This is supported by evidence that phlebotomy has beneficial effects towards NAFLD disease progression and insulin resistance-related hepatic iron accumulation. Likewise, obesity-related steatosis is a risk factor for liver injury in HFE-related HH (Powell et al., 2005). However, the role of iron in initiating liver fibrosis is not clear. Most of the evidence comes from animal studies where iron overload enhanced the fibrotic response to acute treatments with hepatic toxicants. For example, the hemochromatotic hemojuvelin knockout (Sebastiani et al., 2011) and mice fed iron-rich (carbonyl iron) diet (Arezzini et al., 2003) are more susceptible to the hepatotoxin carbon tetrachloride-induced liver fibrosis. It is also not clear why iron accumulates in some NAFLD patients, and the association between HFE mutations and NAFLD remains controversial (Hernaez et al., 2011; Valenti et al., 2010).

9. *Nrf2*: an important hepatoprotectant

The liver is the main organ responsible for the biotransformation and subsequent detoxification of xenobiotics. These events expose the organ to ROS (Serviddio et al., 2013) and electrophiles (Levonen et al., 2014) which, in turn, are increasingly implicated

in the pathogenesis of NAFLD and other chronic liver diseases. In hepatocytes, the major sites of ROS production are the mitochondria and the cytochrome P450 system. Electrophiles are produced by oxidation and nitration of unsaturated FA, resulting in the production of a series of reactive species (Levonen et al., 2014). Hepatocytes are equipped with multiple defense systems mainly composed of cytoprotective enzymes that ensure protection against the toxic effects of endogenous and exogenous oxidants and electrophiles to which they are exposed (Dinkova-Kostova et al., 2005). Importantly, many of these cytoprotective enzymes are encoded by genes containing antioxidant response elements (AREs) in their promoter regions. The ARE region is a *cis*-acting enhancer sequence that mediates transcriptional activation of genes encoding antioxidant and electrophile conjugating enzymes, ubiquitin/proteasomes, chaperone and heat-shock proteins in response to changes in the cellular redox status (Zhang et al., 2010). Transcription factor nuclear factor-erythroid 2-related factor 2 (NFE2l2/NRF2) is a basic leucine zipper redox-sensitive transcription factor that regulates transcriptional induction of ARE-containing genes (Holmstrom et al., 2013; Kensler et al., 2007; Lee et al., 2003). Under homeostatic conditions, NRF2 is sequestered in the cytosol by the actin binding protein Kelch-like ECH associating protein 1 (KEAP1) that targets NRF2 for polyubiquitination and degradation, resulting in a short protein half-life (Itoh et al., 1997) **(Figure 8A)**. During exposure to electrophiles or oxidative stress, KEAP1 becomes oxidized at critical cysteine residues and the NRF2/KEAP1 interaction is disrupted. As a result, NRF2 escapes KEAP1 control, which leads to decreased NRF2 proteasomal degradation and translocation of newly synthesized NRF2 into the nucleus. Once in the nucleus, NRF2 dimerizes with small musculo-aponeurotic fibrosarcoma proteins (MAFs) and promotes the expression of ARE-containing genes (Kansanen et al., 2012; Kensler et al., 2007; Suzuki et al., 2013) **(Figure 8B)**. The binding to and regulation of NRF2 by KEAP1 are explained by a “hinge and latch” model (Tong et al., 2006), as described in **Figure 8**.

Besides activating antioxidant and detoxification genes in response to electrophilic or oxidative stress, there is increasing evidence that NRF2 participates in hepatic fatty acid metabolism. Studies employing young adult C57BL/6 mice on a control diet have demonstrated that NRF2 represses the expression of key enzymes involved in FA synthesis with concomitant reduction in hepatic lipid levels (Tanaka et al., 2012; Yates et al., 2009). This is in contrast with studies employing older mice of the same genetic background, where NRF2 had little or no effect on hepatic fatty acid metabolism (Tanaka et al., 2008; Zhang et al., 2012). Likewise, young C57BL/6 mice fed a high-fat diet (HFD) display a mechanism of hepatic lipogenesis that is negatively regulated by NRF2 (Shin

et al., 2009; Tanaka et al., 2008). Once again, studies using older mice either failed to detect an effect (Zhang et al., 2012) or identified NRF2 as an activator of genes involved in lipid synthesis and uptake (Huang et al., 2010).

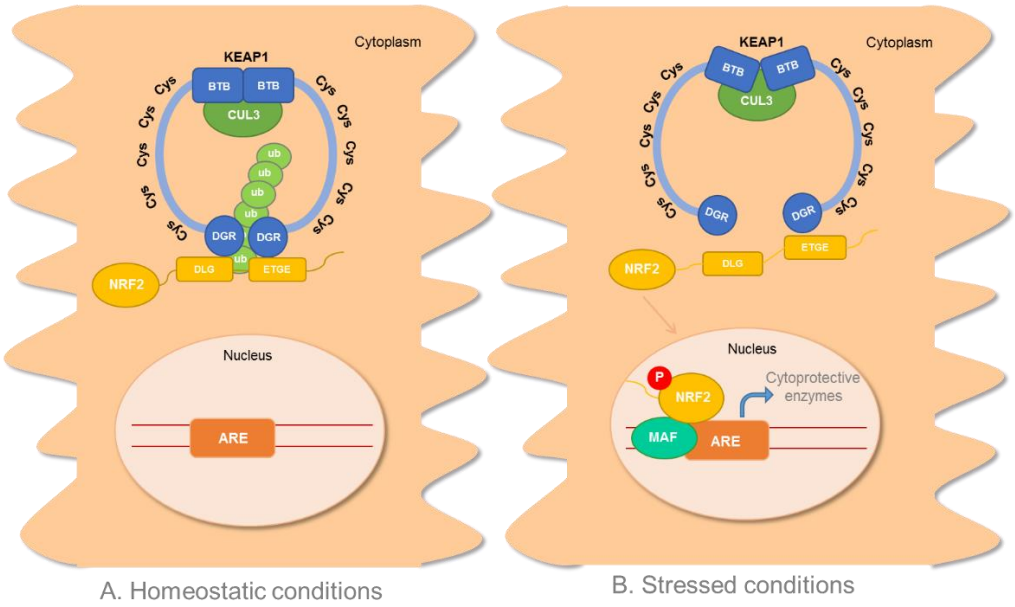

Figure 8. Activation of the KEAP1-NRF2-ARE pathway by oxidants and/or electrophiles. **(A)** Under homeostatic conditions, NRF2 is mainly localized in the cytoplasm through an interaction with KEAP1 and the actin cytoskeleton. KEAP1 is a five domain protein consisting of an N-terminal Broad complex, Tramtrack and Bric-à-brac (BTB) domain, an intervening region with cysteine (Cys) residues, a C-terminal Kelch domain with double glycine repeats (DGR) and the C-terminal domain. KEAP1 homodimerizes at the BTB domain, which is also a binding site for Cullin 3 (CUL3). The KEAP1 homodimer binds to NRF2 through the ETGE and DLG motifs of NRF2, each binding to a DGR domain in KEAP1. According to the proposed hinge and latch model (Tong et al., 2006), ETGE is a high-affinity motif ('hinge') whereas DLG is a low-affinity one ('latch'). KEAP1 functions as an adaptor protein in the CUL3-based E3 ligase complex, which results in the polyubiquitination (Ub) of the lysine residues situated between the DLG and ETGE motifs, and subsequent proteasomic degradation of NRF2. **(B)** Under stressed conditions, the modification of critical cysteine residues of KEAP1 destabilizes its binding to the DLG motif of NRF2, which blocks ubiquitination/proteasomal degradation and allows NRF2 to escape KEAP1 control and translocate into the nucleus. In the nucleus, NRF2 heterodimerizes with small MAF proteins and promotes the expression of ARE-containing genes.

In summary, NRF2 appears to protect the liver of mice against steatosis by inhibiting lipogenesis and promoting fatty acid oxidation, but the effect is controversial and the regulation of hepatic lipidogenesis by NRF2 appears to be age-dependent. This might be related with a decrease in NRF2 expression with age, leading to progressive hepatic accumulation of lipids and/or the attenuation of antioxidant defenses (Collins et al., 2009; Gupte et al., 2013). With age, there is a substantial reduction in glutathione (GSH) levels and in the expression and activity of glutamate cysteine ligase, the rate-controlling enzyme in GSH synthesis. This is accompanied by lower levels of NRF2 protein and a reduction in NRF2/ARE binding (Suh et al., 2004), as well as increased markers of

protein and lipid oxidation (Shih and Yen, 2007). Conversely, the liver of aged NRF2-null mice shows lower free radical reducing activity (Hirayama et al., 2003) and GSH synthesis. Aging has also been reported to increase the prevalence of the metabolic syndrome and of NAFLD in the human population, and to enhance the progression to NASH and fibrosis (Sheedfar et al., 2013). The reason why aging organisms gradually lose the ability to activate NRF2 is currently not understood (Hayes and Dinkova-Kostova, 2014), but a decline in NRF2 signaling is presumed to contribute to the age-related hepatic oxidative stress.

Aims

Several genetic and nutritional animal models have been reported to display a number of the metabolic abnormalities present in NASH, such as obesity, insulin resistance, dyslipidemia, and altered adipokine profile. However, an animal model of human NASH should also display steatosis, intralobullar inflammation, hepatocellular ballooning, perisinusoidal fibrosis, and susceptibility to hepatocellular carcinoma. The extrapolation of NAFLD/NASH animal models to the human disease is thus currently limited by the lack of reproducibility of important clinical and morphological features.

As a result of hepatic steatosis, hepatocytes become vulnerable to oxidative stress, which is presently accepted as one of the main drives for the progression from simple steatosis to steatosis associated with necroinflammatory activity and fibrosis in NAFLD patients. Hepatic iron overload is a candidate pathogenic cofactor in the progression of NAFLD to NASH and fibrosis. Non-hemochromatotic patients with NAFLD often present mild hepatic iron overload, which predisposes to liver injury. It is then possible to speculate that iron deposits found in some NAFLD/NASH patients may contribute to NASH development. In the first set of experiments, we aimed to determine whether excessive hepatic iron deposition, as seen in HFE-related HH, is an aggravating factor in the progression from hepatic steatosis to non-alcoholic steatohepatitis and fibrosis. For that purpose, we studied the development of hepatic steatosis, inflammation and fibrosis in *Hfe*$^{-/-}$ mice (at 8 weeks of age) fed high-fat or normal diet for 4, 8 or 12 weeks. Whilst the *Hfe*$^{-/-}$ mouse is a model of parenchymal iron deposition, iron deposits have repeatedly been observed both in parenchymal and reticuloendothelial liver cells of NAFLD patients. It is possible that iron-loaded hepatic macrophages would become activated and promote lobular inflammation and fibrosis. To address this hypothesis, separate groups of WT and *Hfe*$^{-/-}$ mice were given four 1 mg doses of iron-dextran complex (intraperitoneally) every 2 weeks, for the 8 week period of feeding control or

high-fat diet. This treatment is supposed to deliver iron to the reticuloendothelial hepatic cells.

Another potential aggravating factor in NAFLD is the insufficient production of antioxidant defense mechanisms in response to hepatic steatosis. Transcription factor NRF2 is a central regulator of antioxidative response elements-mediated gene expression. NRF2 is activated by oxidative or electrophilic stress and is highly expressed in detoxification organs, especially the liver. Thus, NRF2 may serve as a major regulator of several cellular defense pathways by which hepatic cells combat oxidative stress in the progression from NAFLD to NASH. In the second set of experiments, we aimed to test the contribution of NRF2 to the progression from NAFLD to NASH. As the control of hepatic lipidogenesis by NRF2 appears to be age-dependent, we have studied the effect of feeding control or high-fat diet to young (8 weeks of age) and middle aged (12 months of age) animals for a period of 12 weeks. In particular, we have evaluated the development of hepatic steatosis, inflammation and fibrosis, as well as other features of the metabolic syndrome in wt and *Nrf2*$^{-/-}$ mice. Since iron overload-related disorders have a late onset in HFE-HH patients, we have also investigated the development of these features in middle aged *Hfe*$^{-/-}$ mice fed a high-fat diet or standard diet by comparison with young animals. We expect this set of experiments to provide new insights into the mechanisms contributing to the development of NAFLD/NASH. By taking into account factors like age, the cellular antioxidant response, and iron deposition, we hope to contribute to the establishment of a better animal model of human NASH.

Material and Methods

1. Animals and experimental design

Wild-type (wt), *Hfe* knock-out (*Hfe*$^{-/-}$) (Zhou et al., 1998) and *Nrf2* knock-out (*Nrf2*$^{-/-}$) (Itoh et al., 1997) mice (*Mus musculus*) on a C57BL/6J background were bred at the Instituto de Biologia Molecular e Celular (IBMC) animal facility. Animals received humane care in compliance with the recommendations of the European Convention for the Protection of Vertebrate Animals used for Experimental and Other Scientific Purposes (ETS 123), the 86/609/EEC Directive and the Portuguese law (DL 129/92). Animal experimental protocols were approved by the competent national authority Direção Geral de Alimentação e Veterinária (DGAV) and by the IBMC's ethical committee. Experimental procedures did not inflict severe stress on animals and humane end-points related particularly with body weight changes were established. These consisted in providing soft food at the bottom of the cage and fluid therapy when a weight loss greater than 10 percent was detected within a few days. When a weight loss greater than 20 percent was determined, mice were immediately sacrificed.

The first set of experiments was designed to investigate the role of iron on hepatic damage development in an *Hfe*$^{-/-}$ mice model fed high-fat diet at different time points. To do that, female *Hfe*$^{-/-}$ mice (n=29) at 8 weeks of age were fed *ad libitum* with a Western-type high-fat, high sucrose diet (HFD) (ssniff EF R/M acc. TD88137 mod.) (n=14) or a Control diet (ND) (ssniff EF R/M CD88137 control) (n=15) for 4 (n=9), 8 (n=10) and 12 (n=10) weeks. Both diets included 200 mg/kg of iron. The ND was completely cholesterol-free and nutrient contents, except the fat content (energy), fat source (fatty acid composition), sugar and starch contents, were identical to the HFD. The high-fat diet had 500-600 mg/kg of cholesterol and its fat content was derived from butter fat. Diet composition is depicted in **Annex I - Table 1**.

In NAFLD patients, iron loading is often reported not only in parenchymal but also in reticuloendothelial liver cells. To evaluate whether iron-loaded hepatic macrophages become activated in response to excessive iron and promote lobular inflammation and fibrosis, wt (n=10) and *Hfe*$^{-/-}$ mice (n=14) (8 weeks-old), fed either HFD or ND, received intraperitoneal injections of iron-dextran complex (FeDx) (Sigma-Aldrich, Germany, D8517; 100 mg iron/ml). A total of 4 mg of iron dextran was administered, divided into four 1 mg doses every 2 weeks, for 8 weeks. Another group of female wt (n=10) and *Hfe*$^{-/-}$ mice (n=10) at 8 weeks of age were fed *ad libitum* with the previously described HFD ND for 8 weeks.

A separate set of experiments was conducted to study the role of age-related hepatic oxidative stress on the development of steatosis and steatohepatitis in two animal models (*Hfe* and *Nrf2* knock-out mice). Female wt (n=13), *Hfe*$^{-/-}$ (n=9) and *Nrf2*$^{-/-}$ (n=9) mice at 8 weeks of age and wt (n=12), *Hfe*$^{-/-}$ (n=10) and *Nrf2*$^{-/-}$ (n=13) mice at approximately 54 weeks of age were fed either a standard (SD) (2.6% fat and 3.9 kcal/g; 4RF21, Mucedola, Italy) or a custom pelletted Western-type diet (HFD) (21.2 % fat, 33.2 % sucrose and 5.2 kcal/g; ssniff EF R/M acc. TD88137 mod.) **(Annex I - Table 1)** for a period of 12 weeks.

At the end of the experiments, mice were fasted for 6 h and blood was collected by retro-orbital bleeding under anesthesia with isofluorane (B. Braun Medical, Portugal). Animals were then euthanized using a lethal dosage of isofluorane and cervical dislocation for organ collection. Liver and visceral fat (perigonadal, perirenal and retroperitoneal) were dissected, weighted and fragments were either snap frozen in liquid nitrogen or 10% (v/v) formalin-fixed.

2. Body weight and food and energy intake

Mice were housed according to their genetic background and body weight and food intake were determined weekly for the duration of experiments. Pre-weighted food was placed in the food hoppers and measured on a weekly basis for each cage. Food intake was estimated by subtracting the weight of the remaining food from the initially supplied dose, and expressed as grams consumed per animal and per day. Energy intake was calculated on the basis of 4.398 kcal/g for the ssniff ND, 3.952kcal/g for the Mucedola SD and 5.258 kcal/g for the ssniff HFD.

3. Serum biochemistry

After sitting at room temperature (RT) for at least 30 min, blood was centrifuged at 10,000 × g for 10 min and serum was collected and stored at -20° C. Serum alanine aminotransferase (ALT) activity, serum glucose, cholesterol, triglyceride, iron concentration, and the total iron binding capacity (TIBC) were measured in a *Cobas C8000 analyzer* (Roche Diagnostics, Germany) at the Centro Hospitalar do Porto Corelab. Transferrin saturation was calculated by dividing the serum iron concentration by the TIBC.

4. Glucose tolerance test

Glucose tolerance tests were performed on mice that received high-fat diet for 12 weeks. Animals were fasted for 6 h and baseline blood glucose levels were determined with an

Accu-chek Aviva glucometer and test strips (Roche Diagnostics, Germany). For each animal, a small drop of blood was obtained by tail clipping and placed on a test strip of the glucose meter to determine the blood glucose levels at starvation. A single dose of glucose [20% (w/v) prepared in NaCl 0.9% (v/v) solution] was then administered intraperitoneally to each mouse at 2 mg glucose per gram of body weight. Blood glucose levels were also determined at 30, 60, 90 and 120 min after glucose administration by removing the clot from the first tail incision and applying pressure to obtain a blood drop.

5. Liver non-heme iron quantification

Non-heme iron content was measured using the bathophenanthroline method (Torrance and Bothwell, 1980). Tissue samples averaging 100 mg were placed in iron-free Teflon vessels and dried in a microwave oven (MDS 2000, CEM) for 2 h. Dry tissue weights were determined and samples were digested in 1 ml of an acidic mixture [36.5 % (v/v) hydrochloric acid and 0.1 g/ml trichloroacetic acid] at 65° C, for 20 h. After digestion, the supernatant was collected and a chromogen reagent [5 volumes of deionized water, 5 volumes of saturated sodium acetate, and 1 volume of 0.1% (w/v) bathophenanthroline sulfonate/1% (v/v) thioglycolic acid] was added to the samples to react with iron and obtain a colored product that was measured spectrophotometrically at 535 nm (*µQuant*, Bio Tek, Germany). Results were expressed as micrograms of iron per gram of dry tissue weight and as the total amount of iron in the liver.

6. Liver triglyceride quantification

A liver section (100 mg of tissue) was washed in cold sodium phosphate buffer (PBS) and homogenized in 1 ml of 5% (v/v) Nonidet P-40 substitute (NP-40), using a mechanical homogenizer. Samples were slowly heated to 80°C - 100°C in a dry bath for 2-5 min or until NP-40 became cloudy. Samples were cooled down to RT and the heating step was repeated to solubilize all triglycerides. Samples were then centrifuged for 2 min at top speed, to remove any insoluble material, and diluted 10-fold with deionized and distilled water (ddH_2O). The triglyceride content was determined with a *Wako Triglyceride E-test kit* (Wako Pure Chemical Industries, Japan), according to the manufacturer's instructions, and values were normalized to liver weight.

7. Thiobarbituric acid-reactive substances (TBARS) assay

Liver samples were homogenized in a homogenizing solution [0.85 g KH_2PO_4 25 mM, 2.67 g $Na_2HPO_4.2H_2O$ 30 mM, 0.25 mL Triton X-100 0,1% (v/v) to a final volume of 250 mL, pH 7,0], in the proportion of 2 ml of this solution per gram of liver fresh weight. Total

protein was quantified with the *DC™ Protein Assay* kit (Bio-Rad, USA) as per the manufacturer's recommendations. 100 µl of the homogenate were diluted in 200 µl of 10% (v/v) trichloroacetic acid (TCA). The solution was mixed for a few seconds and centrifuged at 6000 rpm and 4°C for 1 min. 200 µl of the obtained homogenate were then incubated with 200 µl of 1% (w/v) of thiobarbituric acid in a water bath at 95°C for 40 min. Samples were cooled down to RT and the reaction product was measured spectrophotometrically at 535 nm (*µQuant*, Bio Tek, Germany). The concentration of TBARS, expressed as malondialdehyde (MDA) equivalents, was calculated against an MDA standard curve.

8. Liver histology

Tissues specimens were 10% (v/v) formalin-fixed and embedded in paraffin. Three-micrometer sections of liver were deparaffinized with xylene and hydrated by a passage through a grade of alcohols [100% (v/v), 96% (v/v), 70% (v/v) and 50% (v/v)] and distilled water. All stainings were performed using standard procedures and stained sections were mounted in Entellan (Merck Millipore, Germany). Representative pictures were obtained with an Olympus CX31 light microscope equipped with a DP-25 camera (Imaging Software Cell^B, Olympus, USA).

8.1 Perls Prussian blue staining

To visualize iron deposits in liver parenchyma and reticuloendothelial liver cells, tissue sections were stained with Perls Prussian blue. Briefly, sections were stained with Perls solution [equal parts mixture of 2% (w/v) potassium ferrocyanide (Merck Millipore, Germany) and 2% (v/v) hydrochloric acid] for 30 min, followed by several changes in ddH_2O for 5 min. Sections were then counterstained with Neutral red stain [1g of Neutral red for microscopy (Sigma-Aldrich, Germany), 100 ml of ddH_2O and 1 ml of glacial acetic acid] for 1 min, rinsed in ddH_2O and rapidly dehydrated in 70% (v/v), 96% (v/v) and 100% (v/v) ethanol and xylene.

Liver sections were graded to determine the presence of iron in parenchymal or mesenchymal cells. Iron in hepatocytes was graded as no visible iron (0), iron in very few hepatocytes (1), iron in 5 – 10% of hepatocytes (2), iron in ≥ 40% of hepatocytes (3), and abundant iron in most hepatocytes (4). Iron in Kupffer cells was classified as no iron (0), iron in < one-third of cells (1), iron in one third to ≤ two thirds of cells (2) and abundant iron in more than two-thirds of cells (3).

8.2 Hematoxylin and eosin staining

To determine the severity of histological changes, such as the presence of steatosis, inflammation, and hepatocyte ballooning, hematoxylin and eosin (H&E) staining was performed. The protocol consisted in staining the histological sections with Gill's hematoxylin solution (Merck Millipore, Germany) for 3 min, followed by rapid rinsing in 0.1% (v/v) hydrochloric acid. Sections were then stained with eosin [100 mg of eosin (Merck Millipore, Germany), 100 ml of ddH_2O and 160 µl of glacial acetic acid] for 3 min, rinsed under tap water and rapidly dehydrated in 50% (v/v), 70 % (v/v), 96% (v/v) and 100% (v/v) ethanol and xylene.

A system for scoring the features of nonalcoholic fatty liver disease called the NAFLD Activity Score (NAS) was developed as a tool to measure changes in NAFLD during therapeutic trials, evaluating traits such as steatosis, inflammation and hepatocellular ballooning (Brunt et al., 2011). Steatosis grading was made at low magnification (at most 10x and usually at 4x) and graded as absent (<5%), mild (5%–33%), moderate (>33%–66%) or severe (>66%), according to the amount of surface area of parenchyma visually determined to be involved by steatosis. The zonal distribution of steatosis was determined as zone 3 predominant (perivenular), zone 1 predominant, panacinar or azonal. Inflammation grading was determined as follows: no foci (0), <2 foci per 200X field (1), 2-4 foci per 200X field (2) and >4 foci per 200X field (3). Finally, hepatocyte ballooning was classified as: none (0), few ballooned cells (1) and many ballooned cells (2).

8.3 Sirius red staining

Fibrosis was assessed following a Sirius red staining. Liver sections were stained with Mayer's hematoxylin (Sigma-Aldrich, Germany) for 8 min and washed under running tap water for 5 min. Afterwards, sections were stained for 60 min with Picro-sirius red solution [0.5 g of Direct Red 80 (Sigma-Aldrich, Germany) in 500 ml of a saturated solution of picric acid], washed 2 times with acidified water and dehydrated in three changes of 100% (v/v) ethanol and xylene.

The percentage of hepatic fibrotic area was assessed on three random images captured at 100× magnification under polarized light using ImageJ software. The same image threshold setting was applied to all images from the same study. Liver sections were also graded according to the amount of parenchyma with visible fibrosis as none (0), mild to moderate, zone 3, or portal/periportal only (1), portal/periportal and perisinusoidal (2), bridging fibrosis (3) and cirrhosis (4) (Kleiner et al. 2005).

9. Isolation of total RNA from liver samples and DNase treatment

Total RNA was extracted from frozen liver samples using 1 ml of TRI Reagent (Sigma-Aldrich, Germany). Samples were homogenized using a mechanical homogenizer and centrifuged at 12000 × g for 10 min, at 4° C. The cleared supernatant was transferred to a new RNase-free tube and incubated for 5 min at RT. 200 µl of chloroform were added to each sample and tubes were vigorously shaken for 15 s, incubated at RT for 2-3 min and centrifuged at 12000 × g for 15 min, at 4° C. The RNA-rich aqueous phase was carefully removed and placed into a new tube and RNA was precipitated using 500 µl of isopropanol, followed by homogenization by inversion and incubation at RT for 10 min. Samples were then centrifuged at 12000 × g for 10 min, at 4° C, the supernatant was removed and the pellet was washed with 1 ml of 75% (v/v) ethanol. Afterwards, samples were briefly vortexed and centrifuged at 7500 × g for 5 min at 4° C, ethanol was removed and RNA pellets were left to air dry for 5-10 min. RNA was then resuspended in 400 µl of RNase-free water and incubated at 55°-60° C, for 10-15 min, to ensure complete solubilization. RNA was quantified by *NanoDrop* (Thermo Scientific, USA) and its purity was assessed by absorbance 260/280 and 260/230 ratios.

RNA was treated with DNase for removal of contaminating DNA using a *TURBO DNA-free kit* (Life Technologies, USA). Each reaction received 2.5 µl of 10x buffer, 1 µl of TURBO DNase, 4 µg of total RNA and RNase free water until the final volume of 25 µl. After samples were incubated at 37° C for 30 min, 2.5 µl of DNase inactivation reagent were added and reagents were well mixed to disperse the inactivation reagent. Following 2 min of incubation at RT, RNA was centrifuged at 10000 × g for 90 s and treated RNA was transferred to a new tube and stored at -80° C.

10. cDNA synthesis

First-strand cDNA was obtained with *NZY First-Strand cDNA Synthesis kit* (Nzytech, Portugal) using DNase treated RNA. In each reaction 1 µl of Oligo(dT) primer mix (50µM), 9 µl of RNA and 1 µl of 10x annealing buffer were used to perform the annealing reaction. Samples were incubated at 65° C for 5 min in a *SimpliAmp Thermal Cycler* (Applied Biosystems, Life Technologies, USA) and then placed on ice. To perform the reverse-transcription step, 10 µl of NZYRT 2x Master Mix and 2 µl of NZYRT Enzyme Mix were added to each tube. Samples were incubated at 50° C for 30 min followed by 85° C for 5 min for reaction inactivation. Finally, 1 µl of NZY RNase H (*E. coli*) was added to each sample, followed by a 37° C incubation for 20 min. All samples were diluted 1:2 with nuclease-free water and cDNA was stored at -20° C.

11. Real-time polymerase chain reaction (qPCR)

Relative gene expression levels were quantified using an *iQ5 Real-Time PCR Detection System* (Bio-Rad, USA). PCR mix was prepared by adding 10 µl *iQ SYBR Green Supermix* (Bio-Rad, USA), 0.08 µl of each primer (STAB vida, Portugal), 1 µl of cDNA sample and 8.84 µl of RNase-free water for a final volume of 20 µl. Primer sequences and respective annealing temperatures are listed in **Table 1**. The reaction plate was sealed, centrifuged briefly and placed in the Real-Time PCR Detection System. The amplification protocol consisted of denaturation at 95° C for 4 min and 40 cycles of 94° C for 30 s, followed by 59° C for 45 s, and 72° C for 30 s. Transcript quantity was estimated against the respective standard curve generated with serial dilutions of cDNA (1:1, 1:10 and 1:100) and normalized against the quantity of the endogenous control gene hypoxanthine phosphoribosyltransferase (*Hprt*). A single peak of the dissociation curve was always confirmed for each PCR reaction.

Table 1. *Mus musculus* primer sequences for genes used in real-time PCR.

Gene	Forward primer	Reverse primer	References
Hprt	AGATGGGAGGCCATCACATTGT	ATGTCCCCCGTTGACTGATCAT	[1]
α-Sma	ACCCAGCACCATGAAGATCAAG	AGGTAGACAGCGAAGCCAGGA	[1]
Tnf-α	CTGTAGCCCACGTCGTAGCA	CGGCAGAGAGGAGGTTGACT	[1]
Nqo1	GTGCAGAAGCGAGCTGGAAATACTC	CGAATCTTGATGGAGGACTGGATGC	[1]
Hamp	CATGTTCCAGAGGCGAAGGAGG	GCAGCACATCCCACACTTTGATC	[2]

[1] designed with Primer3 software (Rozen and Skaletsky, 2000); **[2]** (Ilyin et al., 2003)

12. Statistical analysis

Results are expressed as the mean ± standard deviation (SD). For statistical analyses, ANOVA one-way test was used for the different experimental groups and significance was determined using Tukey's *post hoc* test with *GraphPad Prism 6*. The trapezoidal rule was used to determine the area under the curve (AUC). Results were considered statistically significant when $p < 0,05$.

Results

Part I

To evaluate whether feeding a western-type diet leads to the development of hepatic damage in an animal model of parenchymal iron overload, *Hfe*$^{-/-}$ female mice at the age of 8 weeks were fed a high-fat, high-sucrose diet (HFD) or a normal diet (ND) for 4, 8 or 12 weeks.

1. Food/energy intake and effect of diet on body weight

The food/energy intake and body weight were monitored once every week. The percentage of body weight gain, liver weight and visceral fat weight were calculated at the end of the experiment. The daily food and energy intake of HFD-fed mice were higher than in mice fed ND **(Table 2).**

Table 2. Daily food and energy intake.

Experimental group	Food intake (g/animal/day)	Energy intake (kcal/animal/day)
ND	3.91	17.2
HFD	4.21	22.1

HFD feeding resulted in higher total body weight, compared to ND feeding **(Figure 9A)**. At the end of each time point (4, 8 and 12 weeks), mice tended to gain more weight when fed HFD, compared to their ND-fed counterparts. The most significant weight gain was observed at the end of 12 weeks of HFD feeding (p<0.01), compared to mice fed ND **(Figure 9B)**.

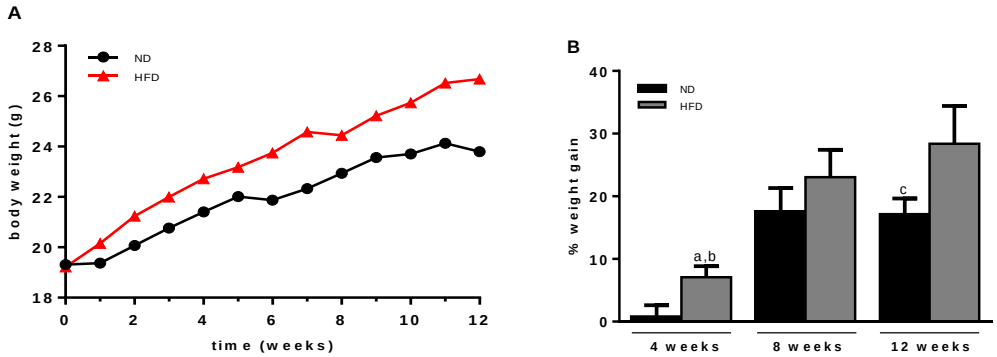

Figure 9. Eight-week old female *Hfe*$^{-/-}$ mice on a C57BL/6 background (n=5 mice per group) were placed on a normal diet (ND) or a high-fat diet (HFD) for 4, 8 or 12 weeks. **(A)** Body weight was monitored once every week. **(B)** The percentage of weight gain was calculated at the end of the experiment. a. p<0.0001 (one-way ANOVA vs. *Hfe*$^{-/-}$ mice on 8 weeks on HFD). b. p<0.0001 (one-way ANOVA vs. *Hfe*$^{-/-}$ mice on 12 weeks on HFD). c. p<0.01 (one-way ANOVA vs. *Hfe*$^{-/-}$ mice on 12 weeks on HFD).

Visceral fat tissue weight was registered since the accumulation of visceral fat is implicated in the etiology of the metabolic syndrome and NAFLD (Tilg and Moschen, 2010). Visceral fat weight tended to increase from 8 weeks of HFD feeding, compared to ND feeding, although the difference was not statistically different **(Figure 10A)**. In *Hfe*$^{-/-}$ mice fed HFD, the liver weight increased with time and the difference became statistically significant at 12 weeks ($p<0.05$) **(Figure 10B)**. There was a trend for higher liver weight and liver to body weight ratio in *Hfe*$^{-/-}$ mice fed HFD, compared to ND-fed counterparts, but statistical significance was not reached **(Figure 10C)**.

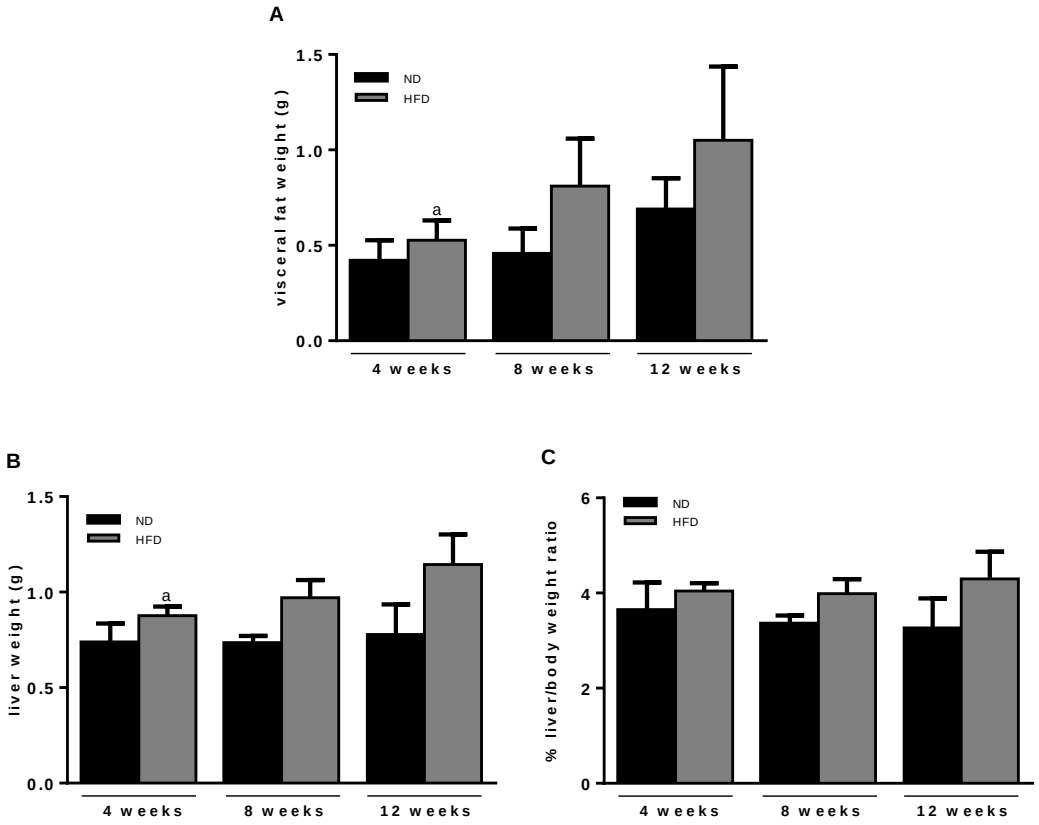

Figure 10. Visceral fat weight **(A)**, liver weight **(B)** and liver/body weight ratio **(C)** of *Hfe*$^{-/-}$ mice after 4, 8 and 12 weeks of ND or HFD feeding. a. $p<0.05$ (one-way ANOVA vs. *Hfe*$^{-/-}$ mice on 12 weeks of HFD).

2. Effect of diet on iron metabolism

The *Hfe*$^{-/-}$ mouse is a well-established model of systemic iron overload, as lack of *Hfe* gene leads to compromised hepcidin expression (Zhou et al., 1998). In this experiment, the hepatic iron stores increased significantly with time in mice fed ND ($p<0.01$) and those that received HFD ($p<0.05$) **(Figure 11A)**. The increased liver weight of mice fed HFD for 12 weeks resulted nevertheless in a significant decrease in the hepatic non-heme iron concentration ($p<0.05$) **(Figure 11B)**.

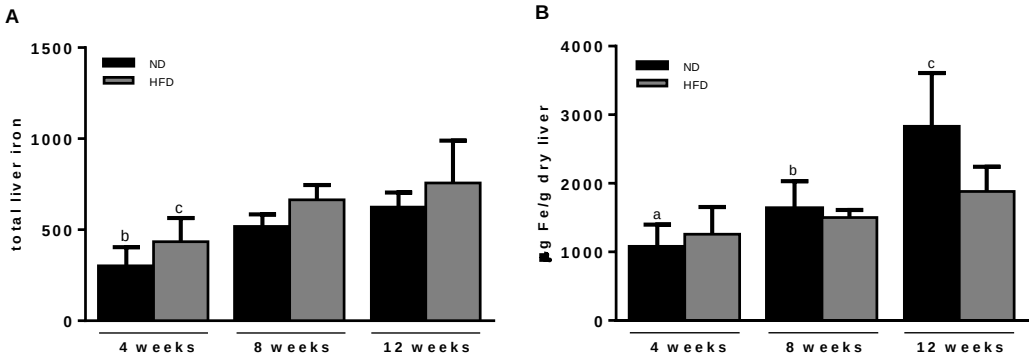

Figure 11. Hepatic non-heme iron of *Hfe*$^{-/-}$ mice after 4, 8 and 12 weeks of ND or HFD feeding. **(A)** Hepatic iron stores were expressed as total liver iron or **(B)** as micrograms of iron per gram of dry tissue weight. a. p<0.0001 (one-way ANOVA vs. *Hfe*$^{-/-}$ mice on 12 weeks of ND). b. p<0.01 (one-way ANOVA vs. *Hfe*$^{-/-}$ mice of 12 weeks on ND). c. p<0.05 (one-way ANOVA vs. *Hfe*$^{-/-}$ mice of 12 weeks on HFD).

The analysis of liver sections stained with Perls Prussian blue revealed that *Hfe*$^{-/-}$ mice accumulated iron in the parenchyma predominantly in periportal areas, which was independent from the diet **(Figure 13A)**. Parenchymal and mesenchymal iron load were assessed by blind grading of histological liver sections. In what concerns parenchymal iron load, no significant differences were found between *Hfe*$^{-/-}$ mice fed ND or HFD, irrespective of time on the diets **(Figure 12A)**. Regarding the mesenchymal iron load, iron-rich macrophages were scarcely observed in *Hfe*$^{-/-}$ mice fed ND and HFD. After 12 weeks of HFD feeding, the number of iron-rich macrophages was significantly lower than at earlier time points (p<0.05) **(Figure 12B)**.

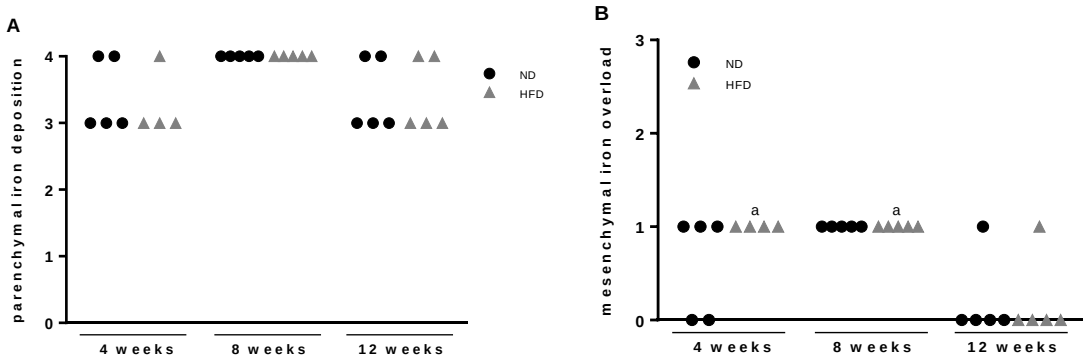

Figure 12. Histological grading of hepatic iron load saturation of *Hfe*$^{-/-}$ mice after 4, 8 and 12 weeks of ND or HFD feeding. **(A)** Parenchymal iron deposition. Iron in hepatocytes was graded as 0. No visible iron, 1. Iron in very few hepatocytes, 2. Iron in 5 – 10% of hepatocytes, 3. Iron in ≥ 40% of hepatocytes, and 4. Abundant iron in most hepatocytes (4). **(B)** Mesenchymal iron deposition. Iron in Kupffer cells was classified as 0. No iron, 1. Iron in < one-third of cells, 2. Iron in one third to two thirds of cells and, 3.Abundant iron in more than two-thirds of cells. a. p<0.05 (one-way ANOVA vs. *Hfe*$^{-/-}$ mice on 12 weeks of HFD).

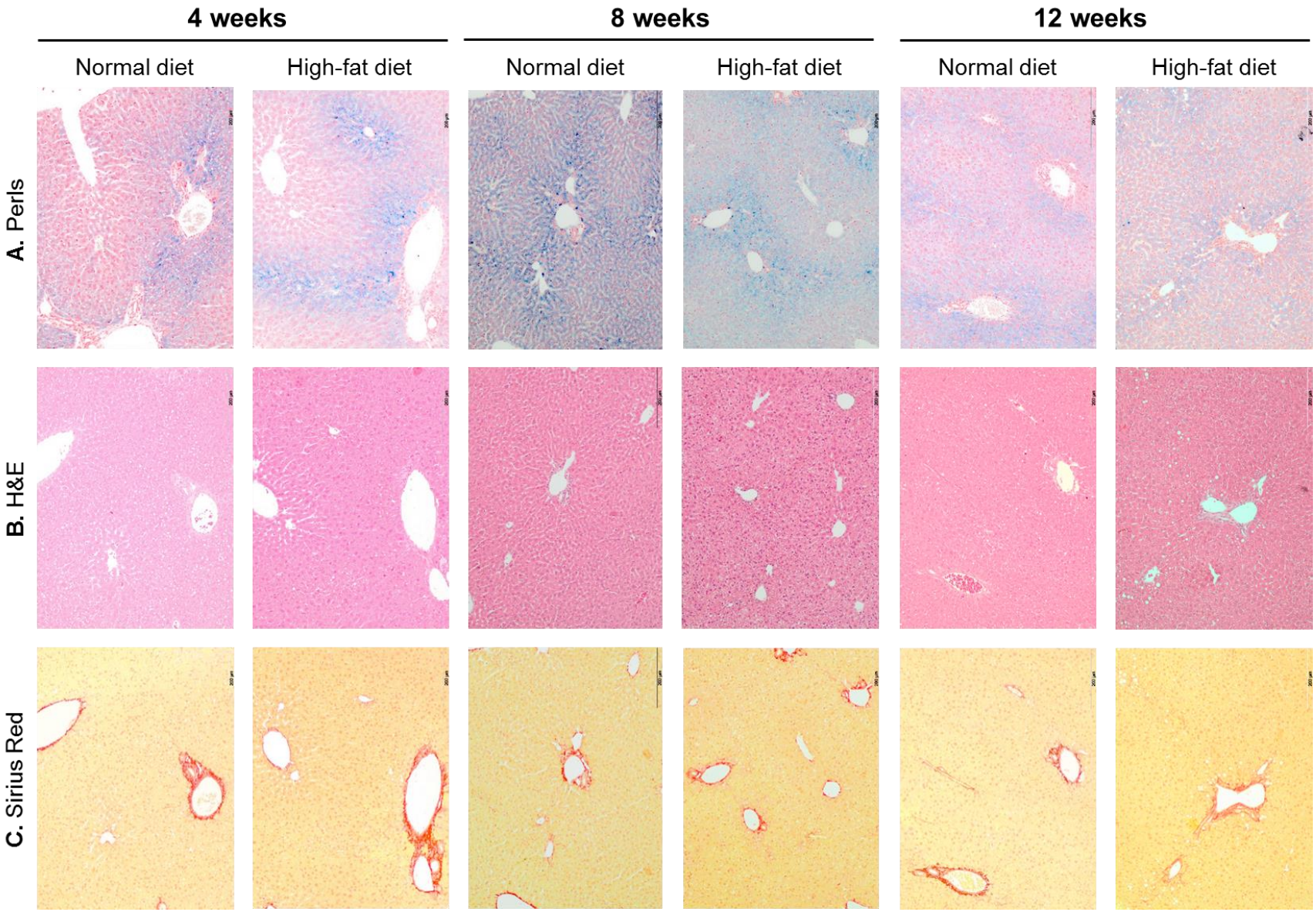

Figure 13. Representative liver sections from *Hfe*$^{-/-}$ mice fed ND or HFD for 4, 8 and 12 weeks. **(A)** Histological detection of iron deposits by Perls iron staining. **(B)** H&E staining for assessment of tissue architecture, steatosis and necroinflammation. **(C)** Sirius red staining for assessment of liver fibrosis. Original magnification: 100x.

3. Effect of diet on hepatic steatosis

Hepatic steatosis grading was performed on liver sections stained with H&E. The majority of mice on ND did not show any histological signs of steatosis. On the other hand, nearly all mice from the HFD-fed groups developed light steatosis and one individual developed moderate steatosis after 12 weeks of HFD feeding **(Figure 14)**. Steatosis was mostly microvesicular and predominantly located in zone 1 **(Figure 13B and 15)**.

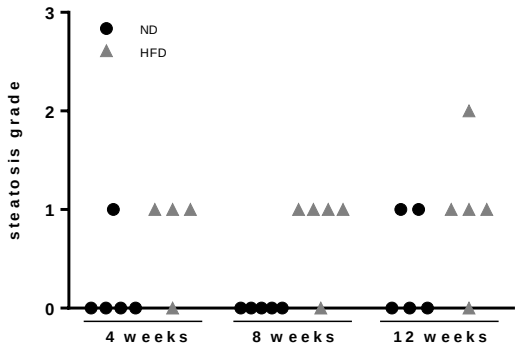

Figure 14. Grading of liver steatosis in *Hfe*$^{-/-}$ mice after 4, 8 and 12 weeks on ND or HFD. Steatosis was graded as 0. Absent (<5%), 1. Light (5%–33%), 2. Moderate (>33%–66%) or 3. Severe (>66%), according to the amount of surface area of parenchyma visually determined to be involved by steatosis.

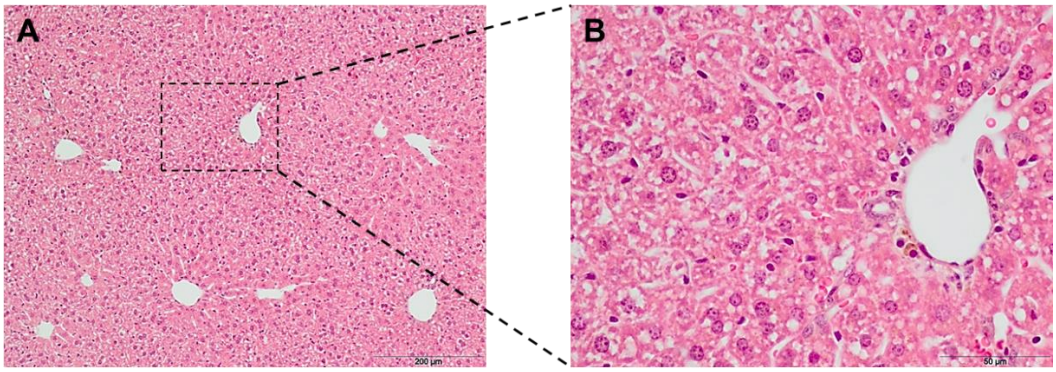

Figure 15. Representative liver sections of *Hfe*$^{-/-}$ mice fed HFD for 8 weeks **(A)**, and detailed magnified section showing mild microvesicular steatosis near periportal areas **(B)**. Original magnification: 100x and 400x.

4. Effect of diet on hepatic inflammation and fibrosis

Liver sections stained with H&E were also inspected for histological evidence of inflammation. Grading of hepatic inflammation revealed the existence of very mild infiltration of inflammatory cells in every experimental group, especially in mice fed ND **(Figure 16A)**. However, no statistical significance was reached. No hepatocyte ballooning was documented in any of the experimental groups.

Histological staging of liver fibrosis was performed on sections stained with Sirius red. None or mild fibrosis was observed in mice of all experimental groups. However, no statistically significant differences were observed between experimental groups **(Figures 13C and 16B)**.

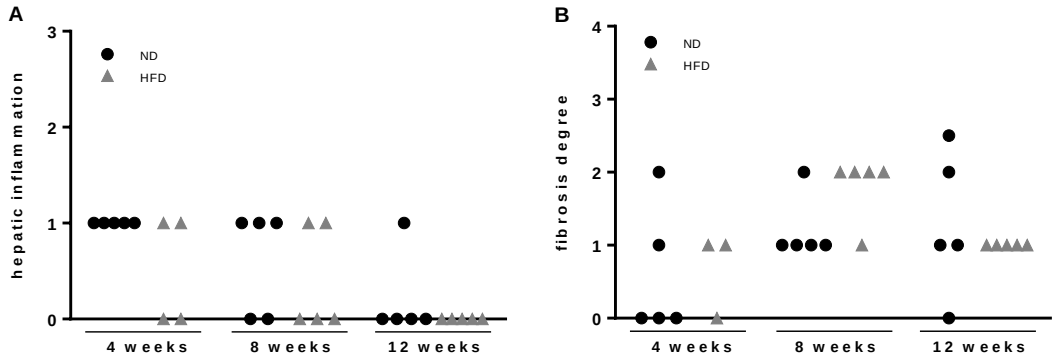

Figure 16. Histological grading and staging of liver sections by H&E and Sirius red staining of *Hfe*$^{-/-}$ fed ND or HFD for 4, 8 or 12 weeks. **(A)** Hepatic inflammation degree. Inflammation was graded according to the overall assessment of all inflammatory foci as 0. No foci, 1. <2 foci per 200X field, 2. 2-4 foci per 200X field and, 3. >4 foci per 200X field. **(B)** Hepatic fibrosis degree. Liver sections were graded according to the amount of parenchyma with visible fibrosis as 0. None, 1. Mild to moderate, zone 3, or portal/periportal only, 2. Portal/periportal and perisinusoidal, 3. Bridging fibrosis and 4. Cirrhosis.

The percentage of hepatic fibrotic area, representing the deposition of collagen fibers in the liver, was also assessed. No significant differences were observed throughout the 12 weeks period, regardless of the diet. If at all, the hepatic fibrotic area appeared to decrease with time in mice fed HFD **(Figure 17)**.

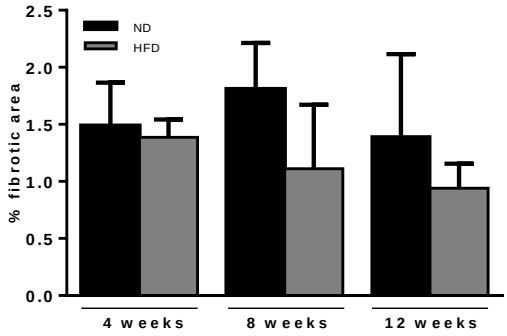

Figure 17. Percentage of hepatic fibrotic area of *Hfe*$^{-/-}$ mice on 4, 8 and 12 weeks of ND or HFD.

Gene expression analysis by qPCR was employed to measure the expression of the inflammatory tumor necrosis factor alpha (*Tnf-α*) gene. TNF-α is a cell signaling protein mainly produced by activated macrophages and involved in systemic inflammation. In mice fed HFD for 12 weeks there was a significant increase in *Tnf-α* expression ($p<0.01$), compared to mice on HFD for 4 weeks **(Figure 18A)**, but *Tnf-α* mRNA levels were not

significantly higher than in animals fed ND. The expression of *α-Sma*, a commonly used marker of hepatic stellate cell differentiation into myofibroblast was also measured by qPCR. *α-Sma* mRNA expression remained unchanged throughout the different experimental time points when mice were fed ND. On the other hand, in mice fed HFD there was a tendency for *α-Sma* expression to decrease with time, although no statistical significance was achieved **(Figure 18B)**.

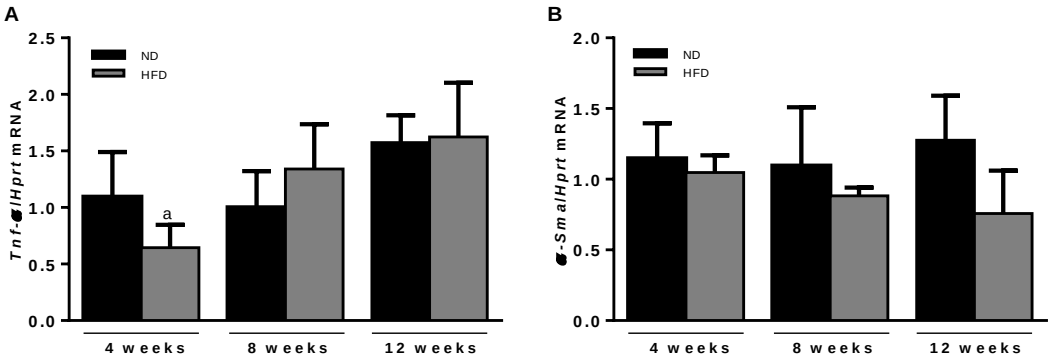

Figure 18. Hepatic pro-inflammatory and pro-fibrotic gene expression of *Hfe*$^{-/-}$ mice on 4, 8 and 12 weeks of ND or HFD. Expression of *Tnf-α* mRNA **(A)** and *α-Sma* mRNA **(B)** was determined by qRT-PCR. a. p<0.01 (one-way ANOVA vs. Hfe$^{-/-}$ mice on 12 weeks of HFD).

Part II

To evaluate the role of excessive parenchymal and mesenchymal hepatic iron deposition in the development of hepatic damage, 8 weeks old *Hfe*$^{-/-}$ and wt female mice, fed a high-fat, high-sucrose diet (HFD) or a normal diet (ND), were intraperitoneally injected with iron dextran every 2 weeks, for a total period of 8 weeks (ND+Fe and HFD+Fe), or left untreated.

1. Effects of diet, iron treatment and genotype on body weight

The food/energy intake and body weight were monitored once every week throughout the duration of the experiment. The percentage of body weight gain, liver weight and visceral fat weight were calculated at the end of the experiment. The daily food intake of HFD-fed wt mice was higher than in mice fed ND. In *Hfe*$^{-/-}$ mice, however, food consumption was independent of the diet **(Table 3)**. When iron was administered, we observed a drop in the consumption of both ND and HFD in mice of the two genotypes. The daily energy intake followed the same trend and is also depicted in **Table 3**.

Table 3. Daily food and energy intake.

Experimental group	Food intake (g/animal/day)		Energy intake (kcal/animal/day)	
	ND	HFD	ND	HFD
Wt mice	2.75	5.09	12.1	26.8
Wt mice+Fe	2.77	4.06	12.2	21.3
***Hfe*$^{-/-}$ mice**	2.98	3.13	13.1	16.5
***Hfe*$^{-/-}$ mice+Fe**	2.47	2.38	10.9	12.5

As expected, mice fed HFD exhibited increased body weight compared to mice on ND, independently of the genotype **(Figure 19A and 19B)**. However, when mice were treated with iron, this increase was less pronounced, especially on *Hfe*$^{-/-}$mice. *Hfe*$^{-/-}$ mice tended to gain more weight over time when fed either a HFD or a ND, compared to wt mice. Nevertheless, when iron was intraperitoneally administered to both genotypes, *Hfe*$^{-/-}$ mice tended to gain less weight than their counterparts. However, these results were only significant when comparing wt and *Hfe*$^{-/-}$ mice on a ND+Fe ($p<0.05$) **(Figure 19C)**.

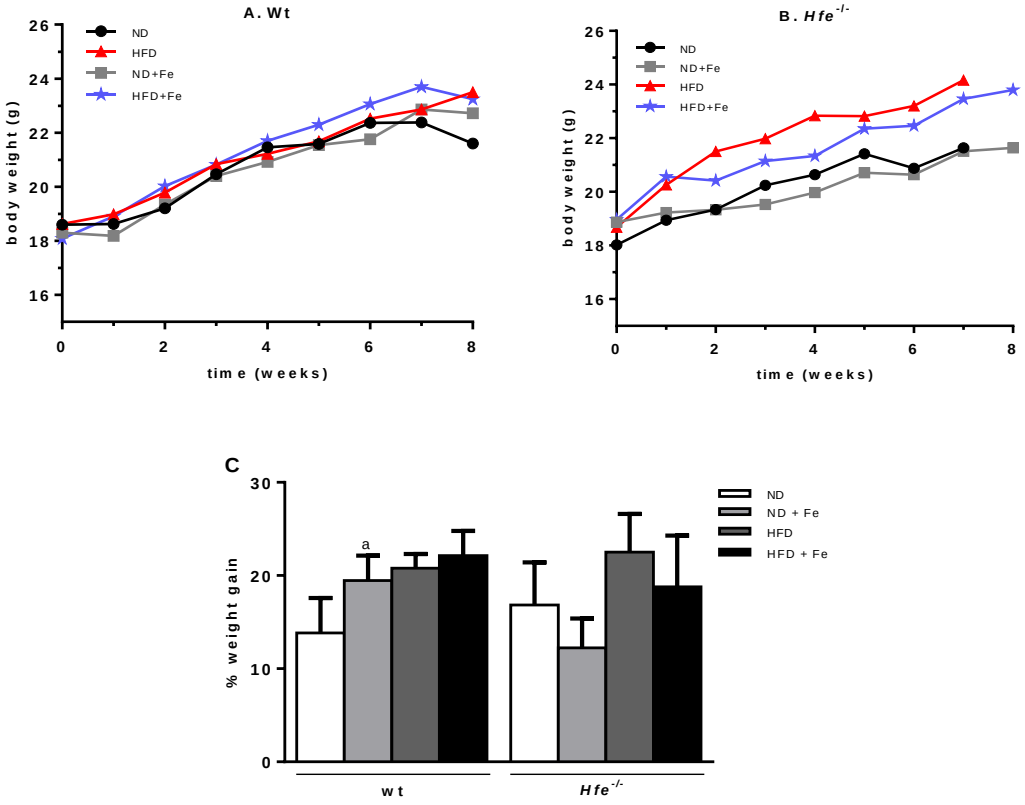

Figure 19. Eight-week old wild-type (wt) and *Hfe*$^{-/-}$ mice on a C57BL/6 background (n=5 females per group) were either placed on a normal diet (ND) or a high-fat diet (HFD). Additionally, wt and *Hfe*$^{-/-}$ mice (n=6 or 7 females per group) were given intraperitoneal injections of iron dextran complex every 2 weeks, for 8 weeks, while receiving ND (ND+Fe) or HFD (HFD+Fe). Body weight was monitored every week. **(A)** Body weight of wt mice. **(B)** Body weight of *Hfe*$^{-/-}$ mice. **(C)** Percentage of weight gain of wt and *Hfe*$^{-/-}$ mice. a. p<0.05 (one-way ANOVA vs. *Hfe*$^{-/-}$ mice on ND+Fe).

Even if not statistically significant, visceral fat weight increased when mice were fed a HFD and decreased when iron was administered, regardless of the genotype or diet **(Figure 20A)**. Liver weight was significantly lower in *Hfe*$^{-/-}$ mice, compared to wt mice, irrespective of the diet and iron treatment **(Figure 20B)**. There was also a trend for lower liver to body weight ratio in *Hfe*$^{-/-}$ mice regardless of diet and iron treatment **(Figure 20C)**. In *Hfe*$^{-/-}$ mice, both HFD and iron treatment increased liver weight. Iron treatment appeared to increase liver weight, although this effect only reached statistical significance in *Hfe*$^{-/-}$ on a ND+Fe, compared to *Hfe*$^{-/-}$ mice on a ND (p<0.001) **(Figure 20B)**. Iron dextran increased the liver/body weight ratio in wt mice fed ND or HFD (p<0.001) and in *Hfe*$^{-/-}$ mice fed ND (p<0.0001) **(Figure 20C)**.

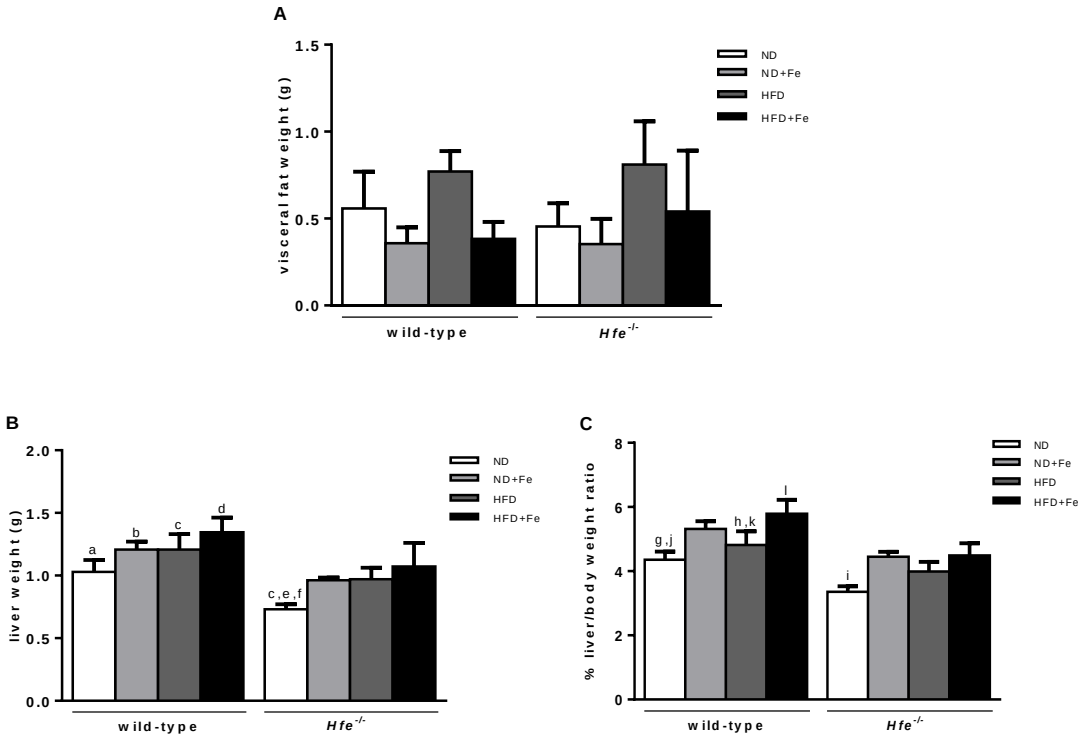

Figure 20. Eight-week old wild-type (wt) and *Hfe*$^{-/-}$ mice on a C57BL/6 background (n=5 females per group) were either placed on a normal diet (ND) or a high-fat diet (HFD). Additionally, wt and *Hfe*$^{-/-}$ mice (n=6 or 7 females per group) were given intraperitoneal injections of iron dextran complex every 2 weeks while receiving ND (ND+Fe) or HFD (HFD+Fe). Visceral fat weight **(A)**, liver weight **(B)** and liver/body weight ratio **(C)** in were determined at the end of 8 weeks. a. p<0.01 (one-way ANOVA vs. *Hfe*$^{-/-}$ mice on ND). b. p<0.01 (one-way ANOVA vs. *Hfe*$^{-/-}$ mice on ND+Fe). c. p<0.05 (one-way ANOVA vs. *Hfe*$^{-/-}$ mice on HFD). d. p<0.01 (one-way ANOVA vs. *Hfe*$^{-/-}$ mice on HFD+Fe). e. p<0.05 (one-way ANOVA vs. *Hfe*$^{-/-}$ mice on ND+Fe). f. p<0.001 (one-way ANOVA vs. Hfe$^{-/-}$ mice on HFD+Fe). g. p<0.001 (one-way ANOVA vs. wt mice on ND+Fe). h. p<0.001 (one-way ANOVA vs. wt mice on HFD+Fe). i. p<0.0001 (one-way ANOVA vs. *Hfe*$^{-/-}$ mice on ND+Fe). j. p<0.001 (one-way ANOVA vs. *Hfe*$^{-/-}$ mice on ND). k. p<0.01 (one-way ANOVA vs. *Hfe*$^{-/-}$ mice on HFD). l. p<0.0001 (one-way ANOVA vs. *Hfe*$^{-/-}$ mice on HFD+Fe).

2. Effects of diet, iron treatment and genotype on iron metabolism

Hfe$^{-/-}$ mice fed ND had higher hepatic iron content than wt mice **(Figure 21A)**. Serum iron (p<0.0001) **(Figure 21B)** and transferrin saturation (p<0.0001) **(Figure 21C)** were significantly elevated, and histologically detectable iron deposits in the liver parenchyma **(Figure 22A)** were also noticeable in *Hfe*$^{-/-}$ mice fed ND. Serum iron (p<0.0001) **(Figure 21B)** and transferrin saturation (p<0.0001) **(Figure 21C)** were also significantly higher in *Hfe*$^{-/-}$ mice fed HFD, compared to wt mice. The HFD *per se* had apparently no effect on the hepatic iron content **(Figure 21A)**. As expected, iron dextran administration increased the hepatic iron content significantly both in wt mice on ND (p<0.001) and on HFD (p<0.01). The same effect was observed in *Hfe*$^{-/-}$ mice on ND (p<0.0001) and *Hfe*$^{-/-}$ treated mice on HFD (p<0.0001). When comparing genotypes, the hepatic iron stores of

Hfe$^{-/-}$ mice were significantly higher than those of wt mice both on ND (p<0.0001) or HFD (p<0.0001) **(Figure 21A)**. Serum iron and transferrin saturation were also significantly increased in wt mice fed ND (p<0.0001 and p<0.001, respectively) or HFD (p<0.0001 and p<0.001, respectively) when iron was administered **(Figure 21B and 21C)**. On the other hand, the iron treatment caused no further increase in serum iron or transferrin saturation in *Hfe*$^{-/-}$ mice fed either ND or HFD.

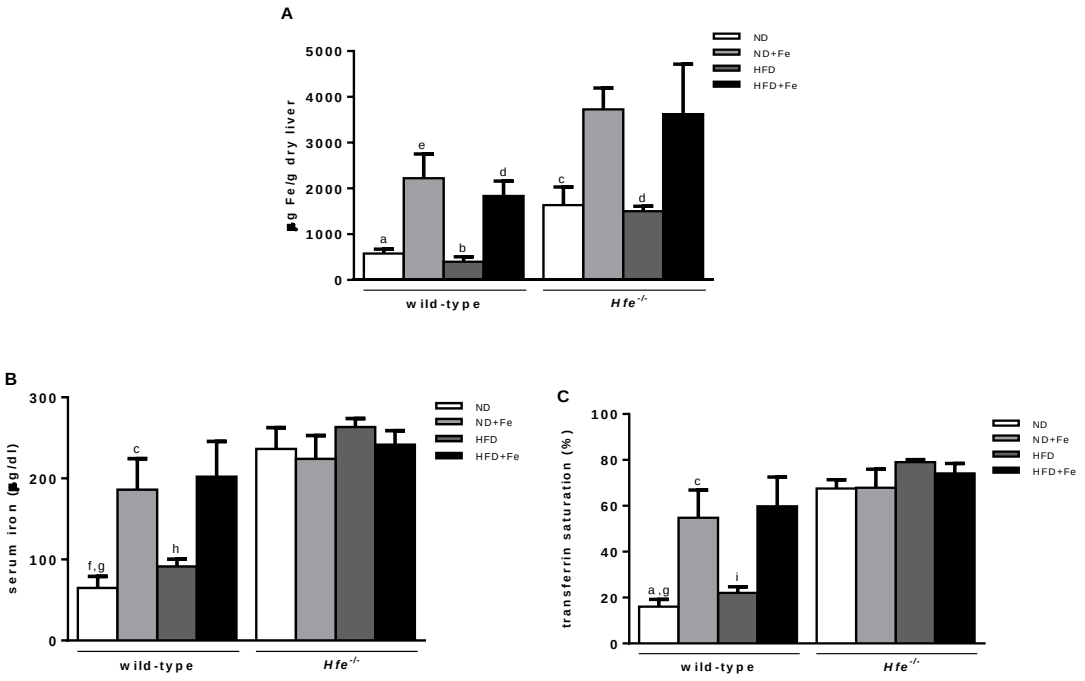

Figure 21. Eight-week old wild-type (wt) and *Hfe*$^{-/-}$ mice on a C57BL/6 background (n=5 females per group) were either placed on a normal diet (ND) or a high-fat diet (HFD). Additionally, wt and *Hfe*$^{-/-}$ mice (n=6 or 7 females per group) were given intraperitoneal injections of iron dextran complex every 2 weeks while receiving ND (ND+Fe) or HFD (HFD+Fe). Hepatic non-heme iron **(A)**, serum iron **(B)**, and transferrin saturation **(C)** determination on wt and *Hfe*$^{-/-}$ mice after 8 weeks of ND and HFD feeding and iron dextran administration. a. p<0.001 (one-way ANOVA vs. wt mice on ND+Fe). b. p<0.01 (one-way ANOVA vs. wt mice on HFD+Fe). c. p<0.0001 (one-way ANOVA vs. *Hfe*$^{-/-}$ mice on ND+Fe). d. p<0.0001 (one-way ANOVA vs. *Hfe*$^{-/-}$ mice on HFD+Fe). e. p<0.001 (one-way ANOVA vs. *Hfe*$^{-/-}$ mice on ND+Fe). f. p<0.0001 (one-way ANOVA vs. wt mice on ND+Fe). g. p<0.0001 (one-way ANOVA vs. *Hfe*$^{-/-}$ mice on ND). h. p<0.0001 (one-way ANOVA vs. wt mice on HFD+Fe). i. p<0.001 (one-way ANOVA vs. wt mice on HFD+Fe).

Parenchymal iron overload is related to increased intestinal iron absorption caused by deficient hepcidin expression. Iron enters the liver through the portal vein and deposits within hepatocytes according to a decreasing gradient from periportal to centrolobular areas (Deugnier and Turlin, 2007). Accordingly, liver histology showed that *Hfe*$^{-/-}$ mice accumulated iron in the parenchyma predominantly in periportal areas, irrespective of the diets **(Figure 22A)**. Hepatic parenchymal iron deposits were blindly graded and no

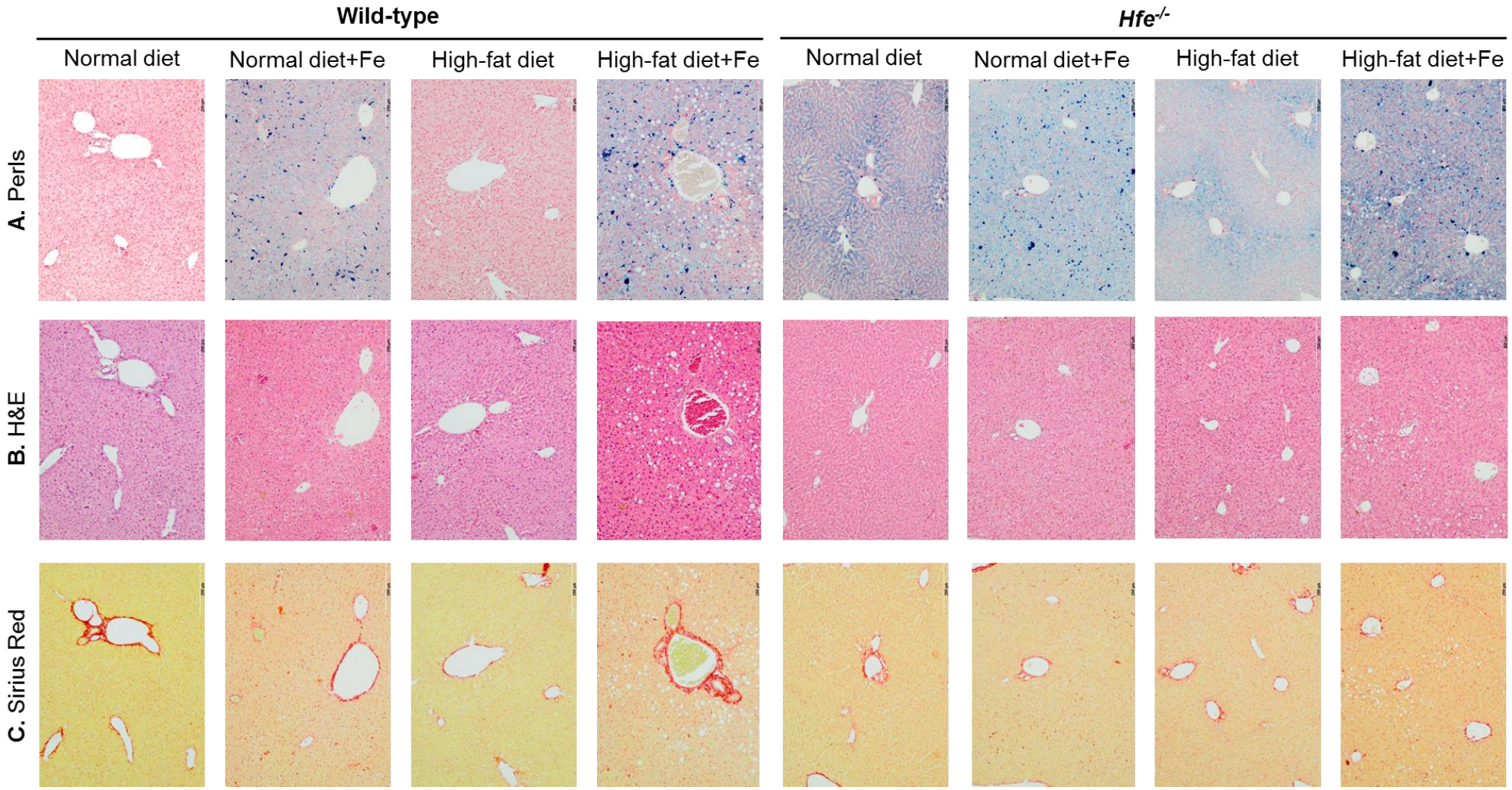

Figure 22. Representative liver sections from wt and *Hfe*$^{-/-}$ mice fed ND or HFD and treated with iron dextran complex. **(A)** Histological detection of iron deposits by Perls iron staining. **(B)** H&E staining for assessment of tissue architecture, steatosis and necroinflammation. **(C)** Sirius red staining for assessment of liver fibrosis. Original magnification: 100x.

histological differences were found between *Hfe*$^{-/-}$ mice fed ND or HFD, irrespective of the iron dextran treatment. On the other hand, wt mice did not accumulate iron within their hepatocytes unless iron was intraperitoneally administered **(Figures 22A and 23A)**.

Mesenchymal iron overload corresponds to iron deposition within Kupffer cells and/or portal macrophages (Deugnier and Turlin, 2007). These iron loaded cells, when present, were either isolated or grouped without any lobular systematization **(Figure 22A)**. Iron-rich macrophages were scarcely observed on periportal areas of *Hfe*$^{-/-}$ mice fed ND and HFD, and became abundant throughout the parenchyma of mice of both genotypes after iron dextran treatment. Interestingly, *Hfe*$^{-/-}$ mice fed a HFD+Fe exhibited significantly less iron-rich Kupffer cells than their counterparts on ND+Fe, which may indicate a modulation of iron metabolism caused by the high-fat diet **(Figure 23B)**.

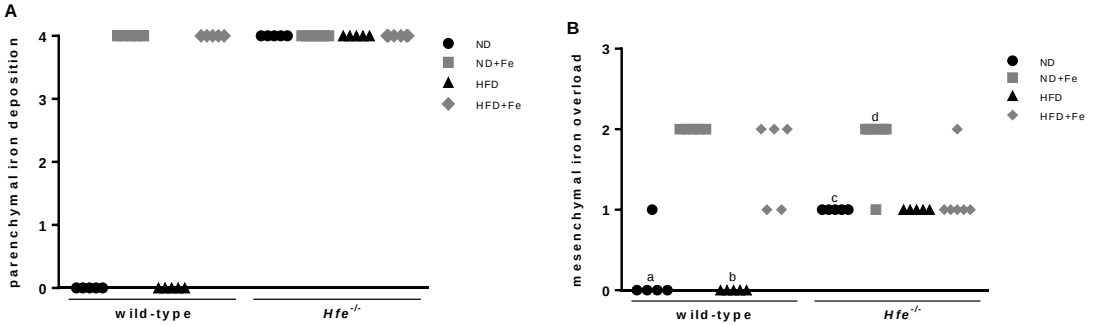

Figure 23. Iron deposits in liver parenchymal, mesenchymal and sinusoidal cells of wt and *Hfe*$^{-/-}$ mice fed ND or HFD, with or without iron dextran treatment. **(A)**. Parenchymal iron deposition. Iron in hepatocytes was graded as 0. No visible iron, 1. Iron in very few hepatocytes, 2. Iron in 5 – 10% of hepatocytes, 3. Iron in ≥ 40% of hepatocytes, and 4. Abundant iron in most hepatocytes (4). **(B)**. Mesenchymal iron deposition. Iron in Kupffer cells was classified as 0. No iron, 1. Iron in < one-third of cells, 2. Iron in one third to two thirds of cells and, 3.Abundant iron in more than two-thirds of cells. a. $p<0.0001$ (one-way ANOVA vs, wt mice on a ND+Fe). B. $p<0.0001$ (one-way ANOVA vs. wt mice on a HFD+Fe). c. $p<0.01$ (one-way ANOVA vs. *Hfe*$^{-/-}$ mice on a ND+Fe). d. $p<0.05$ (one-way ANOVA vs. *Hfe*$^{-/-}$ mice on a HFD+Fe).

The expression of the iron regulatory hormone hepcidin in the liver was analyzed by qPCR. As expected the iron treatment substantially increased *Hamp* mRNA expression in wt mice, independently of the diet ($p<0.0001$ vs. wt mice on ND and $p<0.0001$ vs. wt mice on HFD). In *Hfe*$^{-/-}$ mice, the expression of *Hamp* mRNA was lower and was not significantly altered by the iron treatment or diet **(Figure 24)**. Nevertheless, HFD feeding appeared to decrease *Hamp* levels both in wt and *Hfe*$^{-/-}$ mice.

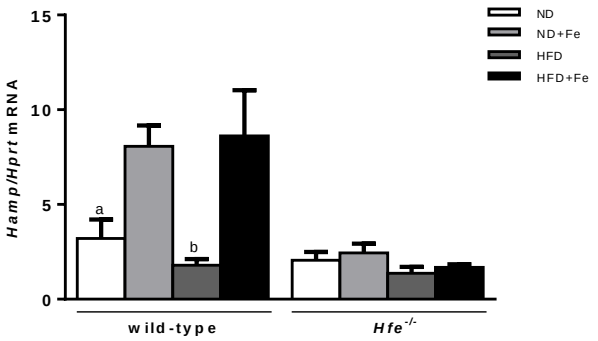

Figure 24. Eight-week old wild-type (wt) and *Hfe*$^{-/-}$ mice on a C57BL/6 background (n=5 females per group) were either placed on a normal diet (ND) or a high-fat diet (HFD). Additionally, wt and *Hfe*$^{-/-}$ mice (n=6 or 7 females per group) were given intraperitoneal injections of iron dextran complex every 2 weeks while receiving ND (ND+Fe) or HFD (HFD+Fe). Hepatic hepcidin (*Hamp*) mRNA expression was analyzed by qPCR at the end of 8 weeks. a. $p<0.0001$ (one-way ANOVA vs. wt mice on ND+Fe). b. $p<0.0001$ (one-way ANOVA vs. wt mice on HFD+Fe).

3. Effects of diet, iron treatment, and genotype on hepatic lipid metabolism

The main aim of these experiments was to examine the effects of iron treatment and dietary regimens on the development of NAFLD, the hepatic manifestation of the metabolic syndrome. Hyperglycemia is a condition in which blood glucose levels are elevated. The most common cause of hyperglycemia is diabetes, a condition in which the pancreas does not produce enough insulin or cells of the body become insulin resistant. Both conditions are associated with metabolic syndrome development. Under ND, *Hfe*$^{-/-}$ mice have lower serum glucose levels at starvation than wt animals **(Figure 25A)**. In wt mice, serum glucose levels were not affected by diet or iron treatment, although there was a trend for increased serum glucose in mice fed a HFD and treated with iron. On the other hand, in *Hfe*$^{-/-}$ mice, HFD intake seamed to increase serum glucose levels; however, no statistical significance was reached **(Figure 25A)**.

Animal fats are complex mixtures mostly comprised of triglycerides, with lower amounts of phospholipids and cholesterol. High blood cholesterol is one of the major risk factors for heart disease. As expected, the HFD promoted a significant increase in serum cholesterol levels, particularly in *Hfe*$^{-/-}$ mice **(Figure 25B)**. Triglycerides are the most common form of fat in the body and elevated levels may cause fatty liver disease. Serum triglyceride levels **(Figure 25C)** showed no significant differences between treatments within the same genotype. Nonetheless, serum triglyceride levels seemed to be higher in *Hfe*$^{-/-}$ mice fed HFD or HFD+Fe ($p<0.05$), compared to wt mice on a HFD. Concerning hepatic triglyceride content, no differences could be attributable to genotype or consumption of HFD. However, hepatic triglyceride levels were significantly lower in iron-

treated *Hfe*$^{-/-}$ mice fed ND and HFD (p<0.05), when compared to iron-treated wt animals **(Figure 25D)**.

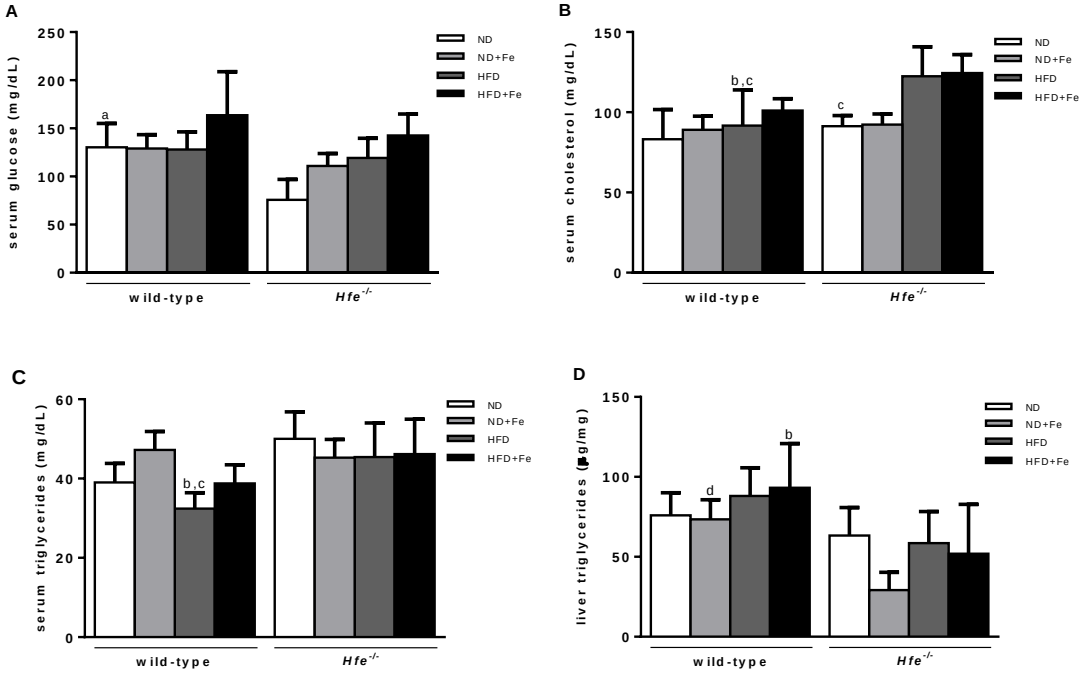

Figure 25. Eight-week old wild-type (wt) and *Hfe*$^{-/-}$ mice on a C57BL/6 background (n=5 females per group) were either placed on a normal diet (ND) or a high-fat diet (HFD). Additionally, wt and *Hfe*$^{-/-}$ mice (n=6 or 7 females per group) were given intraperitoneal injections of iron dextran complex every 2 weeks while receiving ND (ND+Fe) or HFD (HFD+Fe). Analysis of serum glucose at starvation **(A)**, serum cholesterol **(B)**, serum triglycerides **(C)**, and liver triglycerides were determined after 8 weeks on the diet. a. p<0.05 (one-way ANOVA vs *Hfe*$^{-/-}$ mice on ND). b. p<0.05 (one-way ANOVA vs *Hfe*$^{-/-}$ mice on HFD+Fe). c. p<0.05 (one-way ANOVA vs *Hfe*$^{-/-}$ mice on HFD). d. p<0.05 (one-way ANOVA vs *Hfe*$^{-/-}$ mice on ND+Fe).

The characterization of hepatic steatosis was performed by blinded grading of the histological degree of steatosis in each group. Under ND and ND+Fe, *Hfe*$^{-/-}$ mice did not develop any signs of steatosis and only one wt individual in the ND group and one individual in the ND+Fe group presented with light steatosis. On the other hand, practically all wt and *Hfe*$^{-/-}$ mice from the HFD groups developed light to moderate hepatic steatosis. Its degree was, however, higher in wt individuals fed a HFD (p<0.05) or a HFD+Fe (p<0.01), compared to *Hfe*$^{-/-}$ mice on the same set of experimental treatments. These results suggest a connection between elevated iron deposits as seen in *Hfe*$^{-/-}$ mice and fat deposition. Steatosis was either microvesicular, macrovesicular or mixed and it was predominantly located in zone 1. **(Figure 22B and 26)**.

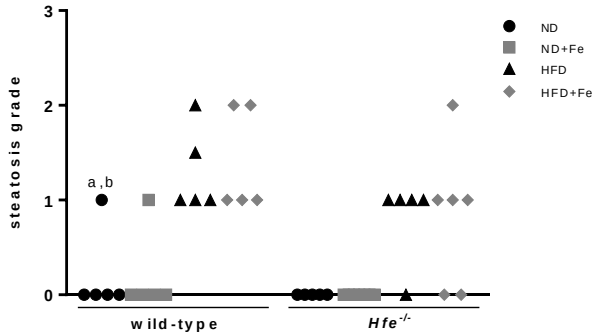

Figure 26. Grading of liver steatosis in wt and *Hfe*$^{-/-}$ mice on ND or HFD for 8 weeks and either treated or untreated with iron dextran complex. Steatosis was graded as 0. Absent (<5%), 1. Light (5%–33%), 2. Moderate (>33%–66%) or 3. Severe (>66%), according to the amount of surface area of parenchyma visually determined to be involved by steatosis a. p<0.05 (one-way ANOVA vs. wt mice on HFD). b. p<0.01 (one-way ANOVA vs. wt mice on HFD+Fe).

4. Effects of diet, iron treatment, and genotype on hepatic inflammation and fibrosis

The diagnosis of nonalcoholic steatohepatitis (NASH) is defined by the presence and pattern of specific histological abnormalities on liver biopsy such as steatosis, inflammation and hepatocyte ballooning in the absence of significant alcohol consumption. The presence of liver fibrosis is not necessary for a NASH diagnosis, but it is often a consequence of NASH development. Serum alanine transaminase (ALT) activity is commonly measured in the clinics as a part of a diagnostic evaluation of hepatocellular injury. Under ND or HFD, *Hfe*$^{-/-}$ mice did not exhibit elevated values of this liver-derived serum transaminase, compared to wt controls **(Figure 27)**. Iron treatment *per se* did not have an effect on serum ALT in *Hfe*$^{-/-}$ mice, but appeared to significantly decrease ALT activity in the livers of wt mice.

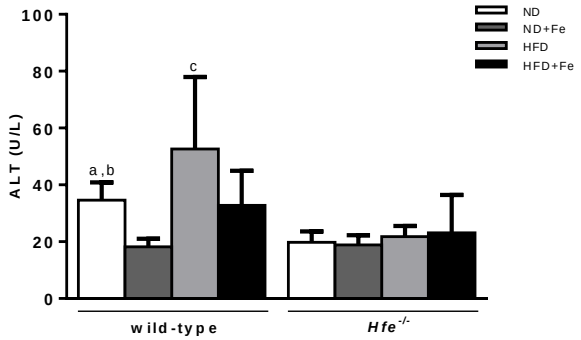

Figure 27. Analysis of serum transaminase ALT in wt and *Hfe*$^{-/-}$ mice on ND or HFD and either treated or untreated with iron for 8 weeks. a. p<0.0001 (one-way ANOVA vs. *wt* mice on ND+Fe). b. p<0.01 (one-way ANOVA vs. *Hfe*$^{-/-}$ mice on ND). c. p<0.001 (one-way ANOVA vs. *Hfe*$^{-/-}$ mice on HFD).

Liver sections stained with H&E were inspected for histological analysis and grading of inflammation. While areas with very mild infiltration of inflammatory cells were documented in every group **(Figure 28A)**, there was no evidence of iron-induced necroinflammation **(Figure 22B)**. Histological grading of liver sections stained with Sirius red showed none to mild or moderate zone 3 fibrosis, as well as portal/periportal and perisinusoidal fibrosis in every experimental group. However, the only significant increase was in *Hfe*$^{-/-}$ on HFD ($p<0.01$) which was normalized following HFD+Fe intake **(Figures 22C and 28B)**. No hepatocyte ballooning was documented in any of the experimental groups.

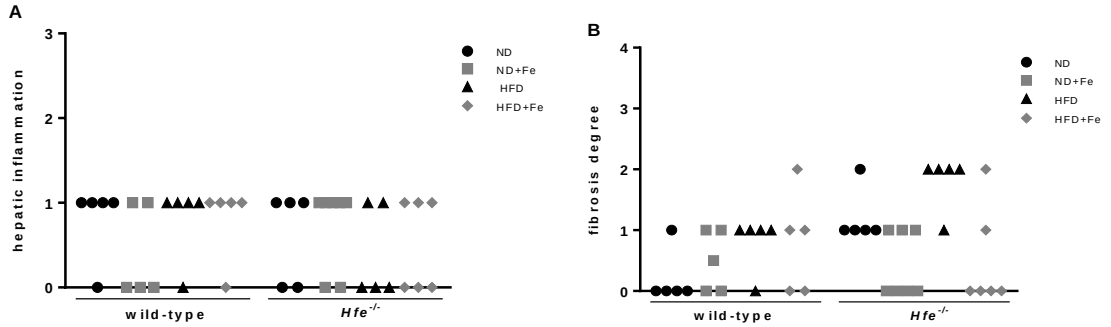

Figure 28. Histological grading of liver sections by H&E staining on wt and *Hfe*$^{-/-}$ fed ND or HFD for 8 weeks and either treated or untreated with iron dextran complex. **(A)** Hepatic inflammation degree. Inflammation was graded according to the overall assessment of all inflammatory foci as 0. No foci, 1. <2 foci per 200X field, 2. 2-4 foci per 200X field and, 3. >4 foci per 200X field. **(B)** Hepatic fibrosis degree. Liver sections were graded according to the amount of parenchyma with visible fibrosis as 0. None, 1. Mild to moderate, zone 3, or portal/periportal only, 2. Portal/periportal and perisinusoidal, 3. Bridging fibrosis and 4. Cirrhosis.

Gene expression analysis by qPCR was employed to measure the expression of *Tnf-α* and *α-Sma*. In wt mice, the expression of *Tnf-α* mRNA was significantly increased in response to iron, irrespective of the diet ($p<0.01$). In the *Hfe*$^{-/-}$ group, *Tnf-α* mRNA was also increased when both ND and HFD fed mice were given the iron treatment, but this increase was only significant for mice fed ND+Fe ($p<0.05$) **(Figure 29A)**. In wt mice, *α-Sma* expression also appeared to increase in response to iron, although the effect only reached statistical significance for wt mice fed ND+Fe **(Figure 29B)**.

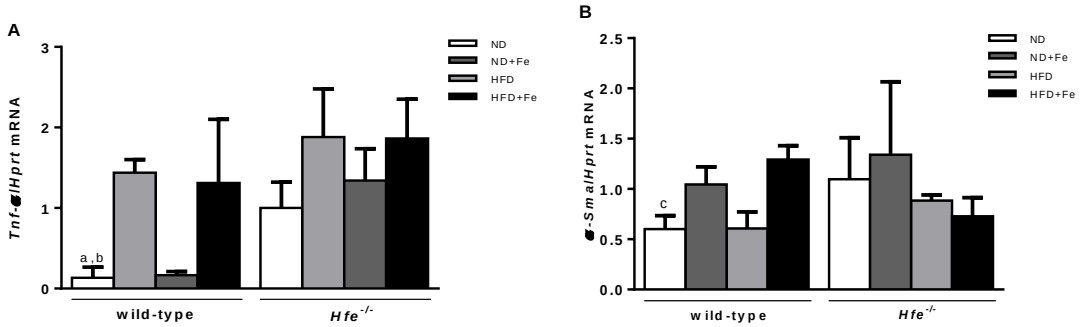

Figure 29. Hepatic pro-inflammatory and pro-fibrotic gene expression in wt and *Hfe*$^{-/-}$ mice fed ND or HFD and either treated or untreated with iron dextran complex. Expression of *Tnf-α* mRNA **(A)** and *α-Sma* mRNA **(B)** was determined by qRT-PCR at the end of 8 weeks. a. p<0.01 (one-way ANOVA vs. wt mice on a ND+Fe). b. p<0.01 (one-way ANOVA vs. wt mice on a HFD+Fe). c. p<0.05 (one-way ANOVA vs. *Hfe*$^{-/-}$ mice on a ND+Fe). d. p<0.05 (one-way ANOVA vs. wt mice on a ND+Fe).

Part III

To evaluate the effect of age on the development of hepatic steatosis and steatohepatitis, *Hfe*$^{-/-}$, *Nrf2*$^{-/-}$ and wt mice on C57BL/6 background received HFD for 12 weeks, starting at 8 or at approximately 52 weeks of age . These ages were selected to reflect the normal physiology of young and middle-aged mice, respectively. Control groups consisted of mice of the same genotype and age fed a standard rodent diet (SD). Since the samples from mice on SD had already been collected in the host laboratory, some data were only assessed for HFD-fed mice.

1. Effects of diet, age, and genotype on body weight

The food and energy intake, as well as the body weight of young and middle-aged wt, *Nrf2*$^{-/-}$ and *Hfe*$^{-/-}$ animals on HFD was monitored once every week. The percentage of body weight gain, liver weight and visceral fat weight were calculated at the end of the experiment. The daily food and energy intake of middle-aged wt and *Nrf2*$^{-/-}$ mice fed HFD was lower compared to younger counterparts, whereas in *Hfe*$^{-/-}$ mice food consumption was independent of age **(Table 4)**. Young *Hfe*$^{-/-}$ mice consumed less food/energy than their wt and *Nrf2*$^{-/-}$ counterparts.

Table 4. Daily food and energy intake.

Experimental group	Age	Food intake (g/animal/day)	Energy intake (kcal/animal/day)
		HFD	HFD
Wt	Young	4.94	25.99
	Middle-aged	3.44	18.09
Nrf2$^{-/-}$	Young	5.12	26.90
	Middle-aged	2.89	15.18
Hfe$^{-/-}$	Young	3.02	15.86
	Middle-aged	3.25	17.11

Feeding HFD for 12 weeks resulted in an increase in body weight in young mice of the 3 genotypes **(Figure 30A)**. Despite similar food/energy intake, *Nrf2*$^{-/-}$ mice displayed significantly higher body weight **(Figure 30A)** and weight gain **(Figure 30C)**, compared to their young wt counterparts ($p<0.0001$). The body weight and weight gain of young *Hfe*$^{-/-}$ mice, on the other hand, were not significantly different from those of wt mice. The HFD has also increased the body weight of middle-aged wt and *Nrf2*$^{-/-}$ mice **(Figure 30B)** but, contrary to young mice, the weight gain was similar in both groups **(Figure 30C)**. It is worth noting that middle-aged *Hfe*$^{-/-}$ mice did not appear to gain weight after 12 weeks of HFD feeding ($p<0.001$) **(Figure 30B and 30C)**. This may be explained by the

development of liver tumors in all mice of this experimental group, as depicted in **Figure 31**.

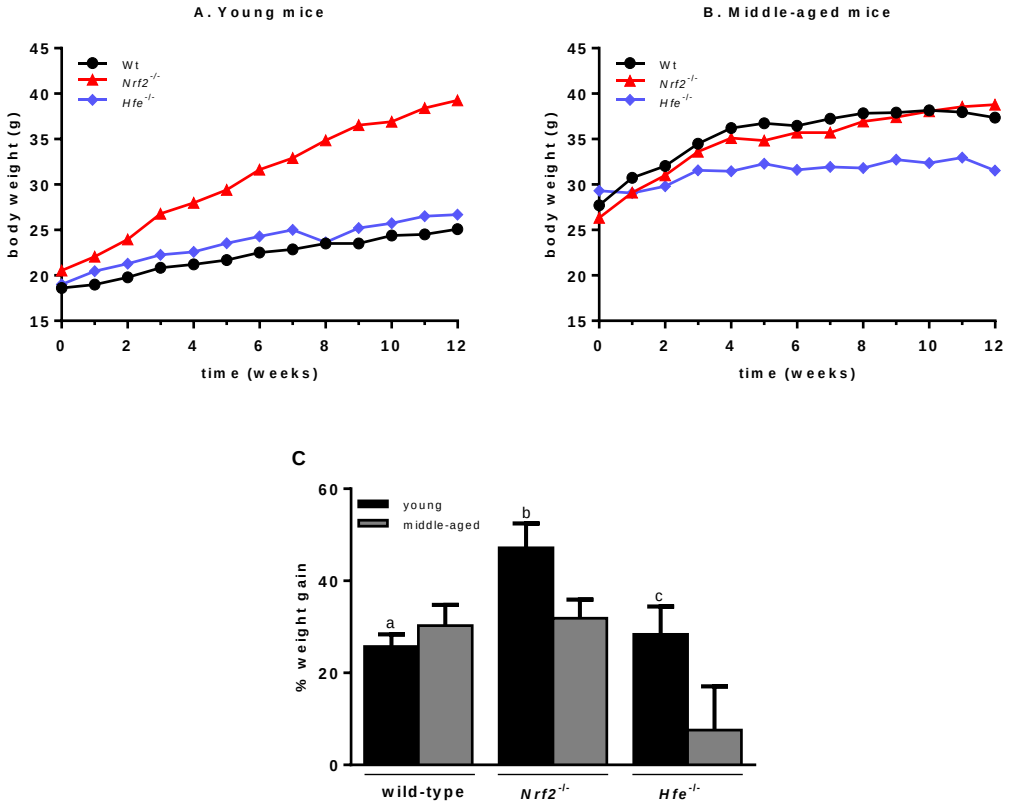

Figure 30. Body weight gain in young and middle-aged wt, *Nrf2*$^{-/-}$ and *Hfe*$^{-/-}$ mice after 12 weeks of HFD feeding. The body weight of **(A)** young and **(B)** middle-aged mice was determined weekly. **(C)** The percentage of weight gain was determined at the end of the experiment. a. p<0.0001 (one-way ANOVA vs. young *Nrf2*$^{-/-}$ mice on HFD). b. p<0.01 (one-way ANOVA vs. middle-aged *Nrf2*$^{-/-}$ mice on HFD). c. p<0.001 (one-way ANOVA vs. middle-aged *Hfe*$^{-/-}$ mice on HFD).

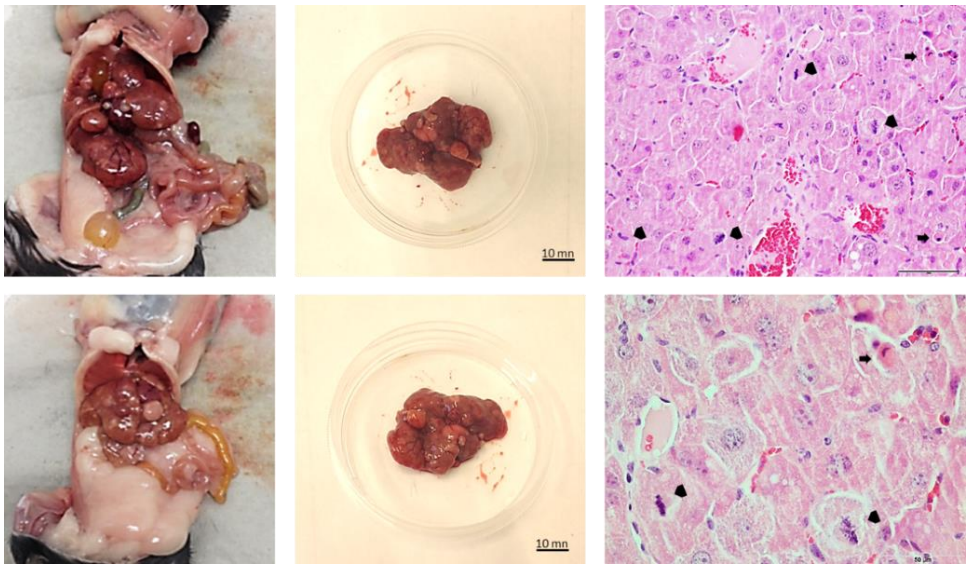

Figure 31. Hepatic tumors in middle-aged *Hfe*$^{-/-}$ mice fed HFD for 12 weeks. Two representative animals are shown. The right panels show H&E staining of a liver tumor section denoting abundant mitotic cells (arrowheads) and apoptotic bodies (arrows).

The visceral fat weight was also determined after the 12 weeks of HFD feeding. Young *Nrf2*$^{-/-}$ mice had considerably more visceral fat than wt and *Hfe*$^{-/-}$ animals of the same age. The visceral fat weight tended to increase in middle-aged wt and *Hfe*$^{-/-}$ mice, compared to younger counterparts, although statistical significance was not reached. The visceral fat weight of middle-aged *Nrf2*$^{-/-}$ mice was similar to what was observed in young mice of the same genotype and in middle-aged wt mice **(Figure 32A)**. Liver weight was determined for mice that received SD and HFD. As for the visceral fat, the HFD increased liver weight in middle-aged mice of all genotypes and in young *Nrf2*$^{-/-}$ mice **(Figure 32B)**. In middle-aged wt and *Hfe*$^{-/-}$ mice fed HFD, liver weight increased to a similar extent when comparing with both HFD-fed young mice ($p<0.0001$) and SD-fed middle-aged counterparts ($p<0.0001$). Young ($p<0.0001$) and middle-aged ($p<0.0001$) *Nrf2*$^{-/-}$ mice had significantly heavier livers when fed HFD, compared to SD-fed counterparts. The ratio was substantially higher in the *Hfe*$^{-/-}$ mice, likely reflecting the growth of liver tumors in these animals **(Figure 32C)**.

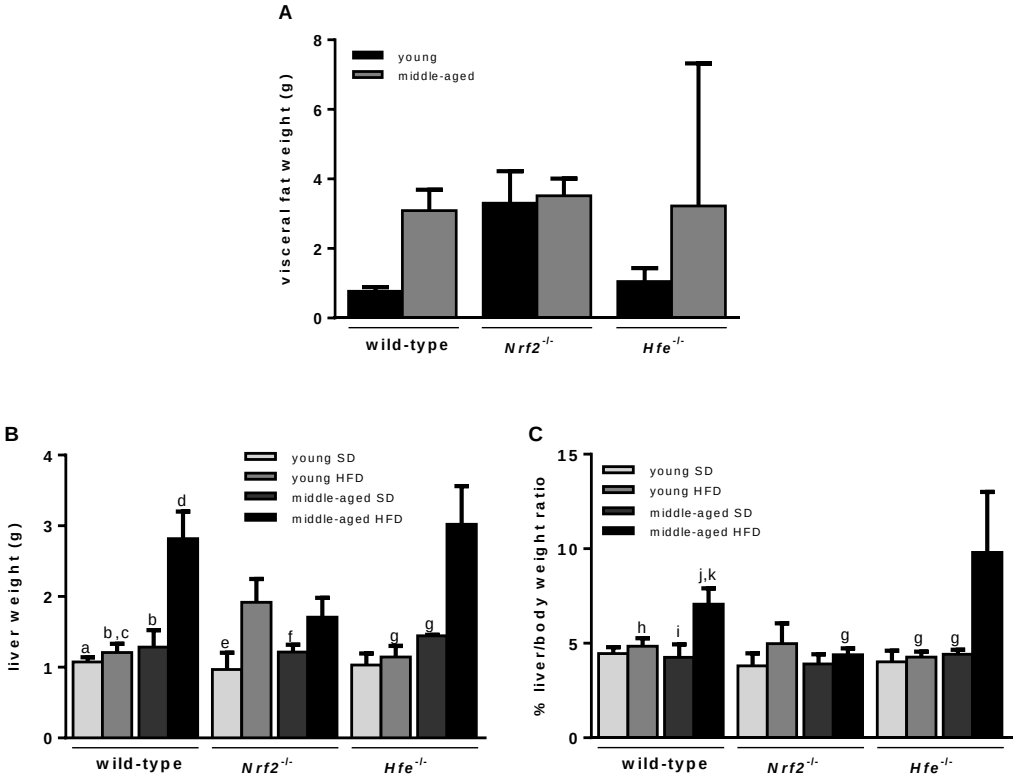

Figure 32. Visceral fat weight **(A)**, liver weight **(B)** and liver/body weight ratio **(C)** in young and middle-aged wt, *Nrf2*$^{-/-}$, and *Hfe*$^{-/-}$ mice after 12 weeks of SD or HFD feeding. a. $p<0.0001$ (one-way ANOVA vs. young Nrf2$^{-/-}$ mice on SD). b. $p<0.0001$ (one-way ANOVA vs. middle-aged wt mice on HFD). c. $p<0.001$ (one-way ANOVA vs. young *Nrf2*$^{-/-}$ mice on HFD). d. $p<0.0001$ (one-way ANOVA vs. middle-aged *Nrf2*$^{-/-}$ mice on HFD). e. $p<0.0001$ (one-way ANOVA vs. young *Nrf2*$^{-/-}$ mice on HFD). f. $p<0.05$ (one-way ANOVA vs. middle-aged *Nrf2*$^{-/-}$ mice on HFD). g. $p<0.0001$ (one-way ANOVA vs. middle-aged *Hfe*$^{-/-}$ mice on HFD). h. $p<0.05$ (one-way ANOVA vs. middle-aged wt mice on HFD). i. $p<0.001$ (one-way ANOVA vs. middle-aged wt mice on HFD). j. $p<0.01$ (one-way ANOVA vs. middle-aged *Nrf2*$^{-/-}$ mice on HFD). k. $p<0.01$ (one-way ANOVA vs. middle-aged *Hfe*$^{-/-}$ mice on HFD).

2. Effects of diet, age, and genotype on iron metabolism

As expected, young *Hfe*$^{-/-}$ mice fed SD or HFD showed significantly increased levels of hepatic iron concentration **(Figure 33A)**, serum iron **(Figure 33C)** and transferrin saturation **(Figure 33D)**, compared to young wt mice on the same diets. On the contrary, middle-aged *Hfe*$^{-/-}$ mice presented only a significant increase in serum iron, compared to wt counterparts. In agreement with the two previous experiments, both young ($p<0.0001$) and middle-aged ($p<0.05$) *Hfe*$^{-/-}$ mice on HFD showed significant lower non-heme iron concentrations, compared to mice fed SD. The same was, however, not evidenced for serum iron and transferrin saturation. Interestingly, middle-aged *Hfe*$^{-/-}$ mice on either SD ($p<0.0001$) or HFD ($p<0.0001$) presented a significant decrease in hepatic non-heme iron concentration compared to their younger counterparts. Wt and *Nrf2*$^{-/-}$ mice, on the other hand, did not present any significant variations in hepatic non-heme iron concentration, serum iron or transferrin saturation as a result of age or diet. The total amount of iron stored in the liver, however, increased significantly in HFD-fed middle-aged wt mice, compared to their young counterparts ($p<0.05$) **(Figure 33B)**, which is likely attributed to the increased liver weight of mice fed HFD **(Figure 32B)**. Iron stores were also significantly higher in HFD-fed middle-aged *Hfe*$^{-/-}$ mice ($p<0.001$), compared to their younger counterparts.

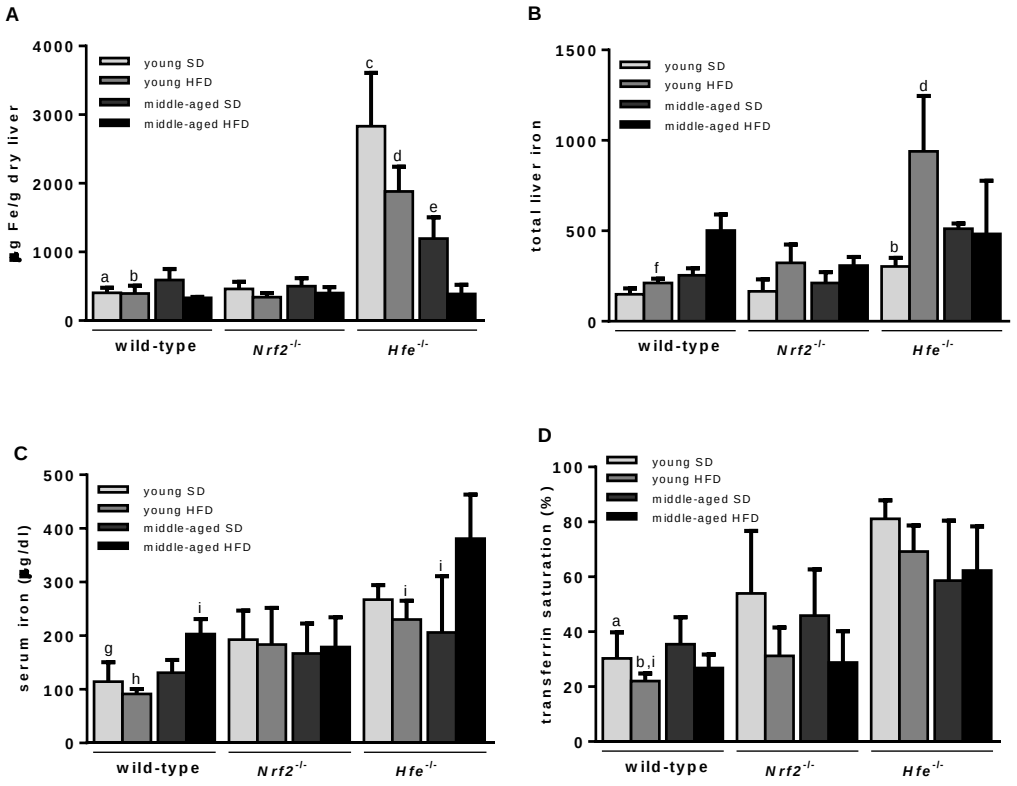

Figure 33. Hepatic non-heme iron, serum iron and transferrin saturation in young and middle-aged wt, *Nrf2*$^{-/-}$ and *Hfe*$^{-/-}$ mice after 12 weeks of SD or HFD feeding. Hepatic iron stores were expressed as **(A)** micrograms of iron per gram of dry

tissue weight or **(B)** total liver iron. **(C)** Serum iron. **(D)** Transferrin saturation. a. p<0.0001 (one-way ANOVA vs. young *Hfe*$^{-/-}$ mice on SD). b. p<0.0001 (one-way ANOVA vs. young *Hfe*$^{-/-}$ mice on HFD). c. p<0.0001 (one-way ANOVA vs. middle-aged *Hfe*$^{-/-}$ mice on SD). d. p<0.0001 (one-way ANOVA vs. middle-aged *Hfe*$^{-/-}$ mice on HFD). e. p<0.05 (one-way ANOVA vs. middle-aged *Hfe*$^{-/-}$ mice on HFD). f. p<0.05 (one-way ANOVA vs. middle-aged wt mice on HFD). g. p<0.001 (one-way ANOVA vs. young *Hfe*$^{-/-}$ mice on SD). h. p<0.01 (one-way ANOVA vs. young *Hfe*$^{-/-}$ mice on HFD). i. p<0.01 (one-way ANOVA vs. middle-aged *Hfe*$^{-/-}$ mice on HFD).

Parenchymal and mesenchymal iron load were blindly graded in histological liver sections stained with Perls Prussian blue. Young and middle-aged *Hfe*$^{-/-}$ mice on SD displayed a significantly greater parenchymal iron deposition, compared to wt mice of the same age and diet and to their HFD-fed counterparts **(Figure 34A)**. Analysis of liver sections stained with Perls Prussian blue revealed that iron accumulated predominantly periportal areas **(Figures 35A and 36A)**. On the other hand, parenchymal iron deposition was nearly undetected in middle-aged *Hfe*$^{-/-}$ mice fed HFD. Young **(Figure 35A)** and middle-aged **(Figure 36A)** wt and *Nrf2*$^{-/-}$ mice also did not exhibit significant iron deposits in liver parenchyma. Mesenchymal iron deposition, in turn, was rarely observed in *Hfe*$^{-/-}$ mice and was practically absent in wt and *Nrf2*$^{-/-}$ mice **(Figure 34B)**.

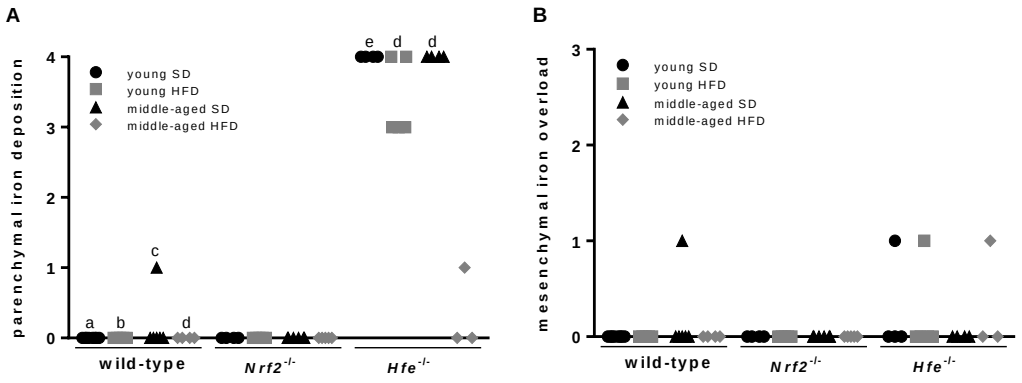

Figure 34. Histological grading of hepatic iron load in young and middle-aged wt, *Nrf2*$^{-/-}$, and *Hfe*$^{-/-}$ mice after 12 weeks of SD or HFD feeding. **(A)** Parenchymal iron deposition. Iron in hepatocytes was graded as 0. No visible iron, 1. Iron in very few hepatocytes, 2. Iron in 5 – 10% of hepatocytes, 3. Iron in ≥ 40% of hepatocytes, and 4. Abundant iron in most hepatocytes (4). **(B)** Mesenchymal iron deposition. Iron in Kupffer cells was classified as 0. No iron, 1. Iron in < one-third of cells, 2. Iron in one third to two thirds of cells and, 3.Abundant iron in more than two-thirds of cells. a. p<0.0001 (one-way ANOVA vs. young *Hfe*$^{-/-}$ mice on SD). b. p<0.0001 (one-way ANOVA vs. young *Hfe*$^{-/-}$ mice on HFD). c. p<0.0001 (one-way ANOVA vs. middle-aged *Hfe*$^{-/-}$ mice on SD). d. p<0.0001 (one-way ANOVA vs. middle-aged *Hfe*$^{-/-}$ mice on HFD). e. p<0.05 (one-way ANOVA vs. young *Hfe*$^{-/-}$ mice on HFD).

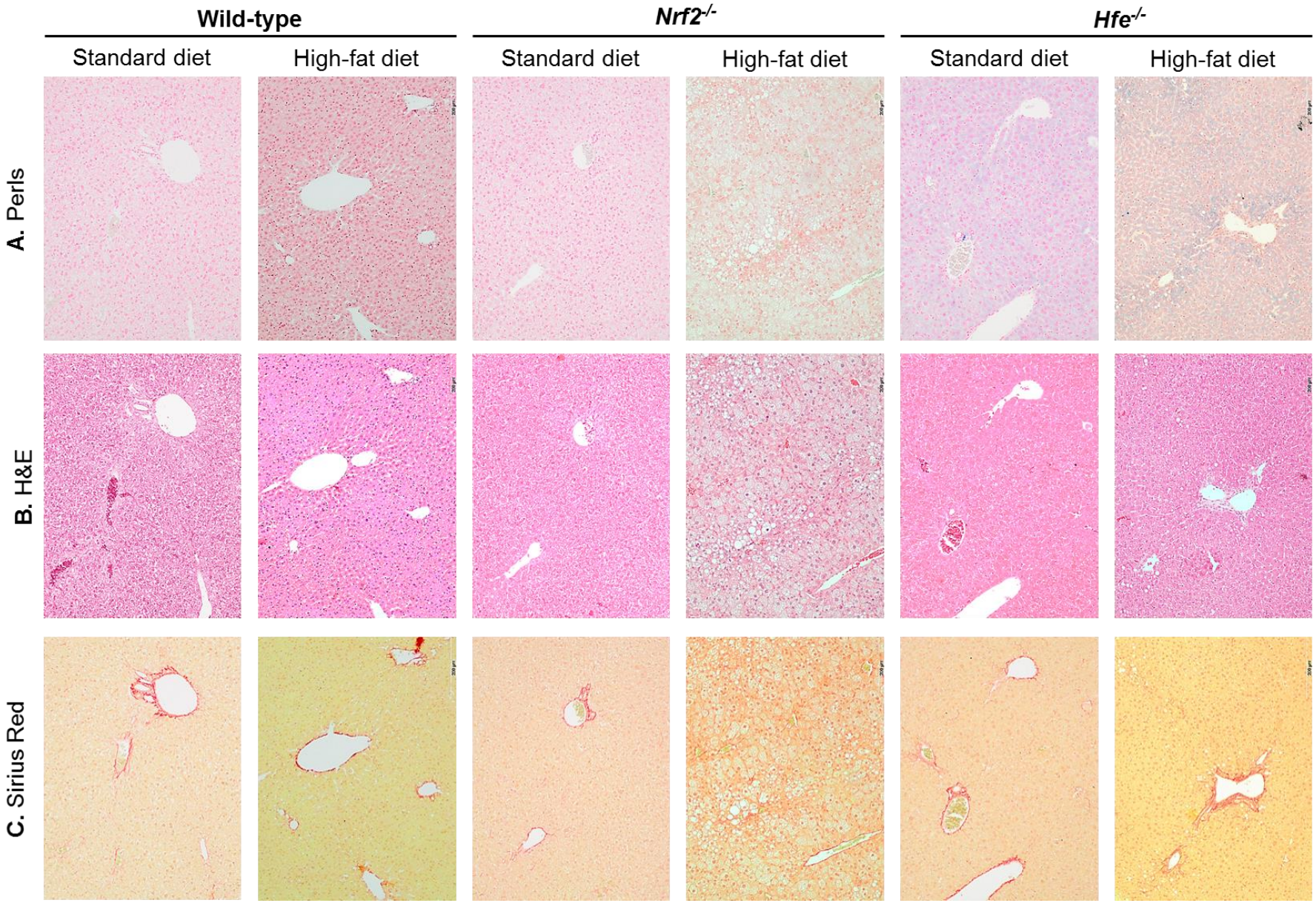

Figure 35. Representative liver sections from young wt, *Hfe*$^{-/-}$, and *Nrf2*$^{-/-}$ mice fed SD or HFD for 12 weeks. **(A)** Histological detection of iron deposits by Perls iron staining. **(B)** H&E staining for assessment of tissue architecture, steatosis and inflammation. **(C)** Sirius red staining for assessment of liver fibrosis. Original magnification: 100x.

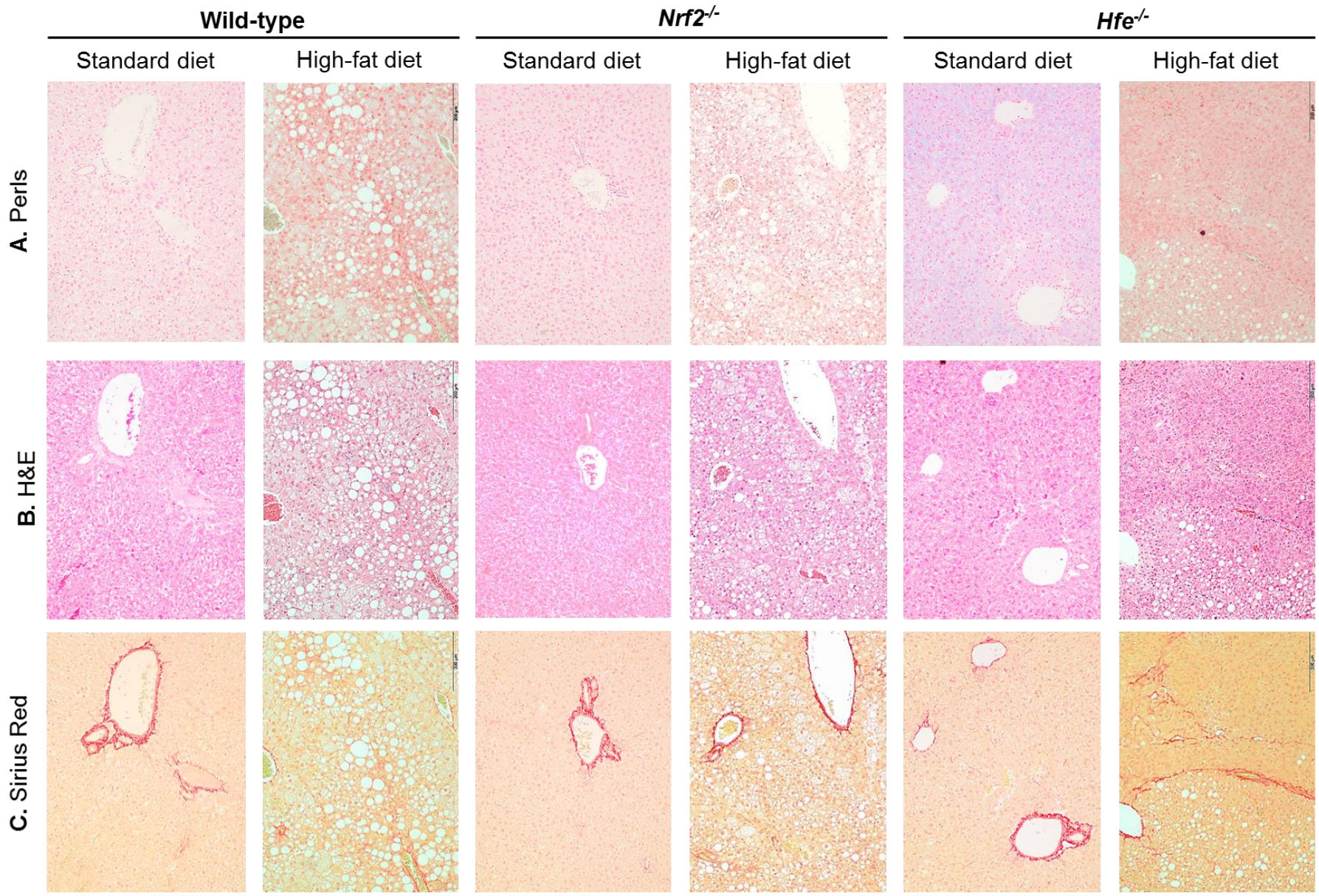

Figure 36. Representative liver sections from middle-aged wt, *Nrf2*$^{-/-}$ and *Hfe*$^{-/-}$ mice fed SD or HFD for 12 weeks. **(A)** Histological detection of iron deposits by Perls iron staining. **(B)** H&E staining for assessment of tissue architecture, steatosis and inflammation. **(C)** Sirius red staining for assessment of liver fibrosis. Original magnification: 100x.

3. Effects of diet, age, and genotype on glucose tolerance and hepatic lipid metabolism

To establish whether mice of different age and genotype acquire insulin resistance after administration of HFD, an intraperitoneal glucose tolerance test (IGTT) was performed. After fasting for 6 h, baseline blood glucose levels were determined and mice were administered glucose intraperitoneally. Blood glucose measurements were repeated at 30, 60, 90 and 120 min after the glucose bolus. IGTT showed that, unlike their young counterparts, middle-aged wt mice fed HFD for 12 weeks were not able to clear glucose from the peripheral circulation within 120 minutes post glucose administration **(Figure 37A)**. On the other hand, the rate of glucose clearance in young and middle-aged *Nrf2*$^{-/-}$ mice was similar **(Figure 37B)**. Notably, young *Nrf2*$^{-/-}$ mice displayed a lower glucose disposal rate, as illustrated by significantly higher estimates of the area under the curve (AUC), similar to the AUCs observed for older mice of both genotypes **(Figure 37D)**. Whilst the test was not performed on young *Hfe*$^{-/-}$ mice, middle-aged *Hfe*$^{-/-}$ animals fed HFD showed a normal IGTT, compared to wt counterparts **(Figure 37C)**.

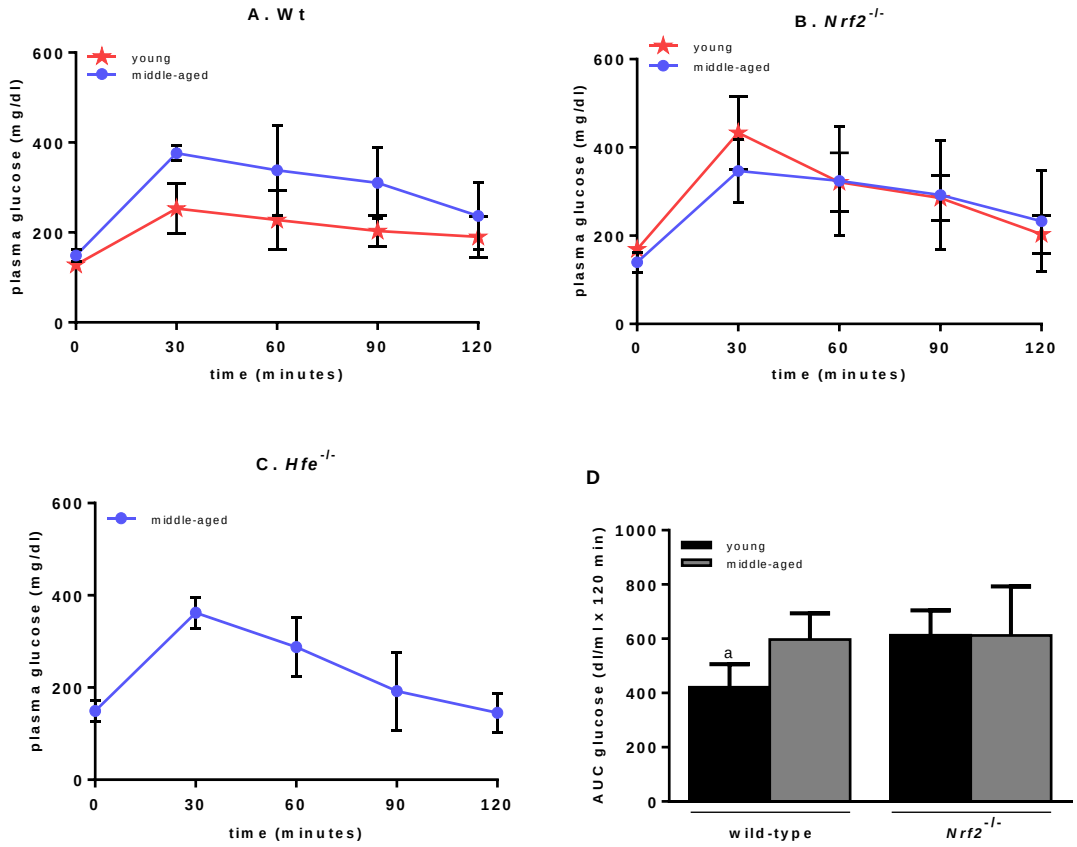

Figure 37. Intraperitoneal glucose tolerance test (IGTT) on young and middle-aged wt, *Nrf2*$^{-/-}$, and *Hfe*$^{-/-}$ mice after 12 weeks of HFD feeding. **(A, B and C)** Blood glucose levels in wt, *Nrf2*$^{-/-}$, and *Hfe*$^{-/-}$, respectively, over a 2 h interval. **(D)** The amount of glucose cleared from the circulation as calculated from the area under the curve (AUC) from (A), (B) and (C). a. $p<0.05$ (one-way ANOVA vs. young *Nrf2*$^{-/-}$ mice on HFD).

Regarding serum cholesterol levels **(Figure 38A)**, no significant differences could be attributed to age in the wt and *Nrf2*$^{-/-}$ groups fed HFD. However, middle-aged *Hfe*$^{-/-}$ mice on HFD showed significantly higher levels of serum cholesterol, compared to wt and *Nrf2*$^{-/-}$ counterparts and to young *Hfe*$^{-/-}$ mice. Serum triglyceride levels **(Figure 38B)** showed no significant differences between treatments within the same genotype, except for *Hfe*$^{-/-}$ mice, which exhibited significantly higher serum triglyceride levels in middle-aged mice fed HFD ($p<0.01$), compared to younger counterparts. Nonetheless, serum triglyceride levels were significantly higher in young *Nrf2*$^{-/-}$ mice, compared to wt counterparts, and in middle-aged *Hfe*$^{-/-}$ mice, compared to wt counterparts. Concerning the hepatic triglyceride content **(Figure 38C)**, *Nrf2*$^{-/-}$ mice fed HFD presented with significantly higher hepatic triglyceride levels, compared to younger wt and *Hfe*$^{-/-}$ counterparts and middle-aged *Nrf2*$^{-/-}$ animals. Under HFD, both young and middle-aged *Hfe*$^{-/-}$ mice had significantly lower levels of hepatic triglycerides than wt counterparts.

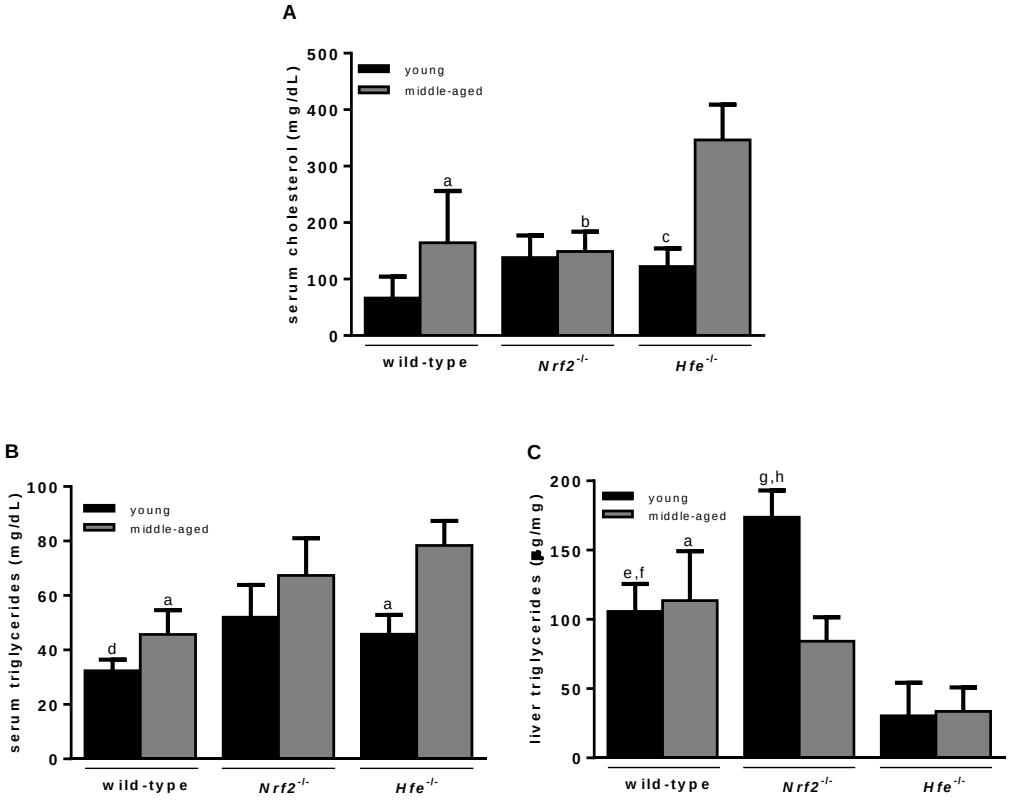

Figure 38. Analysis of serum cholesterol **(A)**, serum triglycerides **(B)**, and liver triglycerides **(C)** of young and middle-aged wt, *Nrf2*$^{-/-}$, and *Hfe*$^{-/-}$ mice after 12 weeks of HFD feeding. a. $p<0.01$ (one-way ANOVA vs. middle-aged *Hfe*$^{-/-}$ mice on HFD). b. $p<0.001$ (one-way ANOVA vs. middle-aged *Hfe*$^{-/-}$ mice on HFD). c. $p<0.0001$ (one-way ANOVA vs. middle-aged *Hfe*$^{-/-}$ mice on HFD). d. $p<0.05$ (one-way ANOVA vs. young *Nrf2*$^{-/-}$ mice on HFD). e. $p<0.01$ (one-way ANOVA vs. young *Nrf2*$^{-/-}$ mice on HFD). f. $p<0.001$ (one-way ANOVA vs. young *Hfe*$^{-/-}$ mice on HFD). g. $p<0.0001$ (one-way ANOVA vs. middle-aged *Nrf2*$^{-/-}$ mice on HFD). h. $p<0.0001$ (one-way ANOVA vs. young *Hfe*$^{-/-}$ mice on HFD).

4. Effects of diet, age, and genotype on steatohepatitis and fibrosis

Under SD, young and middle-aged mice did not exhibit elevated serum ALT activity, regardless of genotype **(Figure 39)**. The HFD caused significantly higher levels of this liver-derived serum transaminase in middle-aged wt, *Hfe*$^{-/-}$ and Nrf2$^{-/-}$ mice and also in young *Nrf2*$^{-/-}$ mice. Middle-aged *Hfe*$^{-/-}$ mice had the most elevated levels of serum ALT activity, likely due to the presence of hepatic tumors in mice from this experimental group.

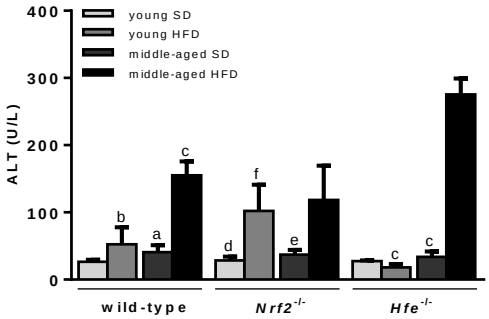

Figure 39. Analysis of serum ALT activity in young and middle-aged wt, *Nrf2*$^{-/-}$, and *Hfe*$^{-/-}$ mice after 12 weeks of SD or HFD feeding. a. p<0.0001 (one-way ANOVA vs. middle-aged wt mice on HFD). b. p<0.05 (one-way ANOVA vs. young *Nrf2*$^{-/-}$ mice on HFD). c. p<0.0001 (one-way ANOVA vs. middle-aged *Hfe*$^{-/-}$ mice on HFD). d. p<0.001 (one-way ANOVA vs. young *Nrf2*$^{-/-}$ mice on HFD). e. p<0.0001 (one-way ANOVA vs. middle-aged *Nrf2*$^{-/-}$ mice on HFD). f. p<0.0001 (one-way ANOVA vs. young *Hfe*$^{-/-}$ mice on HFD).

The characterization of hepatic steatosis was performed by blind grading of the histological degree of steatosis in liver sections stained with H&E. Mixed sized vesicles (microvesicles and macrovesicles) were only visible in the HFD-fed groups, independently of the genotype. Young and middle-aged wt, *Nrf2*$^{-/-}$ and *Hfe*$^{-/-}$ mice exhibited signs of zone 1 macrovesicular steatosis and zone 3 microvesicular steatosis **(Figures 35B and 36B)**. Upon HFD feeding, all young *Nrf2*$^{-/-}$ mice and middle-aged wt and *Nrf2*$^{-/-}$ mice developed severe steatosis. *Hfe*$^{-/-}$ mice and young wt mice exhibited light to moderate steatosis **(Figure 40)**. Young and middle-aged individuals fed SD did not develop any signs of hepatic steatosis.

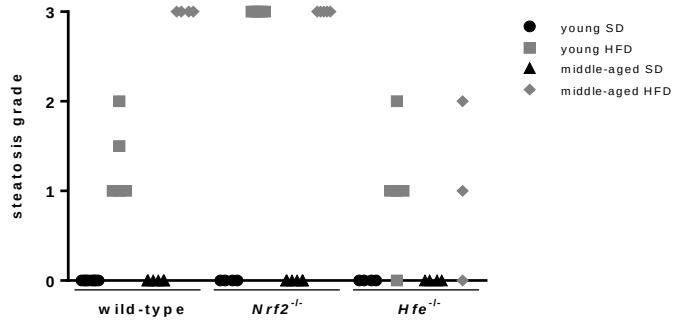

Figure 40. Grading of liver steatosis in young and middle-aged wt, *Nrf2*$^{-/-}$, and *Hfe*$^{-/-}$ mice after 12 weeks of SD or HFD feeding. Steatosis was graded as 0. Absent (<5%), 1. Light (5%–33%), 2. Moderate (>33%–66%) or 3. Severe (>66%), according to the amount of surface area of parenchyma visually determined to be involved by steatosis.

Liver sections stained with H&E were also inspected for histological analysis and grading of inflammation. Areas with mild infiltration of inflammatory cells were documented in nearly every experimental group, especially in mice fed HFD **(Figure 41A)**. Inflammation was significantly higher in middle-aged *Nrf2*$^{-/-}$ and *Hfe*$^{-/-}$ mice fed HFD, compared to younger HFD-fed and middle-aged ND-fed counterparts. Hepatocyte ballooning is a form of liver parenchymal cell death that is usually associated with fatty degeneration. Ballooned cells are typically two to three times the size of adjacent hepatocytes and are characterized by a clear or vacuolated cytoplasm and pyknotic nuclei on H&E stained sections (Yip and Burt, 2006). Significant hepatocyte ballooning was observed in middle-aged wt mice fed HFD and, to a greater extent, in young and middle-aged *Nrf2*$^{-/-}$ mice fed the same diet **(Figure 41B)**. For illustration purposes, **Figures 42A and 42B** depict a contiguous patch of hepatocytes with prominent ballooning injury in a middle-aged *Nrf2*$^{-/-}$ mouse after 12 weeks of HFD feeding.

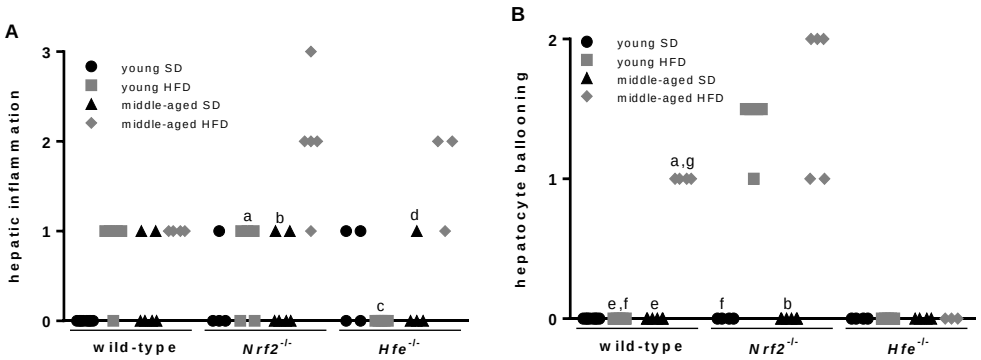

Figure 41. Histological grading of hepatic inflammation and hepatocyte ballooning in young and middle-aged wt, *Nrf2*$^{-/-}$, and *Hfe*$^{-/-}$ mice after 12 weeks of SD or HFD feeding. **(A)** Hepatic inflammation degree. Inflammation was graded according to the overall assessment of all inflammatory foci as 0. No foci, 1. <2 foci per 200X field, 2. 2-4 foci per 200X field and, 3. >4 foci per 200X field. **(B)** Hepatocyte ballooning degree. Hepatocyte ballooning was classified as 0. None, 1. Few ballooned cells, and 2. Many ballooned cells. a. $p<0.001$ (one-way ANOVA vs. middle-aged *Nrf2*$^{-/-}$ mice on HFD). b. $p<0.0001$ (one-way ANOVA vs. middle-aged *Nrf2*$^{-/-}$ mice on HFD). c. $p<0.001$ (one-way ANOVA vs. middle-aged *Hfe*$^{-/-}$

mice on HFD). d. p<0.01 (one-way ANOVA vs. middle-aged *Hfe*$^{-/-}$ mice on HFD). e. p<0.0001 (one-way ANOVA vs. middle-aged wt mice on HFD). f. p<0.0001 (one-way ANOVA vs. young *Nrf2*$^{-/-}$ mice on HFD). g. p<0.0001 (one-way ANOVA vs. middle-aged *Hfe*$^{-/-}$ mice on HFD).

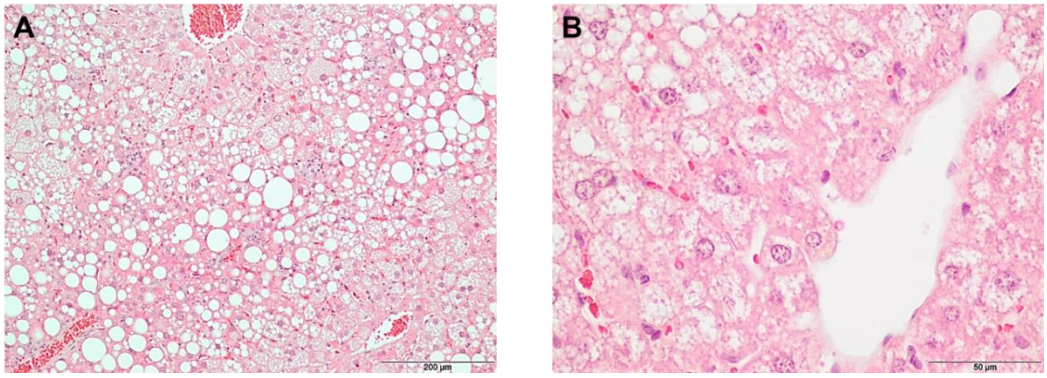

Figure 42. Representative liver sections from middle-aged *Nrf2*$^{-/-}$ mice on HFD for 12 weeks. **(A)** Periportal (zone 1) macrovesicular steatosis and perivenular (zone 3) microsteatosis and ballooning degeneration of hepatocytes. **(B)** Ballooned hepatocytes with enlarged, rarefied cytoplasm. Original magnification: 100x and 400x.

The staging of hepatic fibrosis was performed on liver sections stained with Sirius red. Within each genotype, the highest stages of fibrosis were seen in middle-aged mice fed HFD. Middle-aged wt and *Nrf2*$^{-/-}$ mice showed mild to moderate zone 3 fibrosis, as well as portal/periportal and perisinusoidal fibrosis **(Figure 43A)**. More advanced stages of liver fibrosis, such as bridging fibrosis and cirrhosis were only detected in middle-aged *Hfe*$^{-/-}$ mice fed HFD. The percentage of hepatic fibrotic area was also determined and corroborated the staging **(Figure 43B)**. It is worth noting that young *Nrf2*$^{-/-}$ mice fed HFD presented a significant increase in the percentage of fibrotic area, compared to wt and *Hfe*$^{-/-}$ counterparts and to SD-fed young *Nrf2*$^{-/-}$ mice.

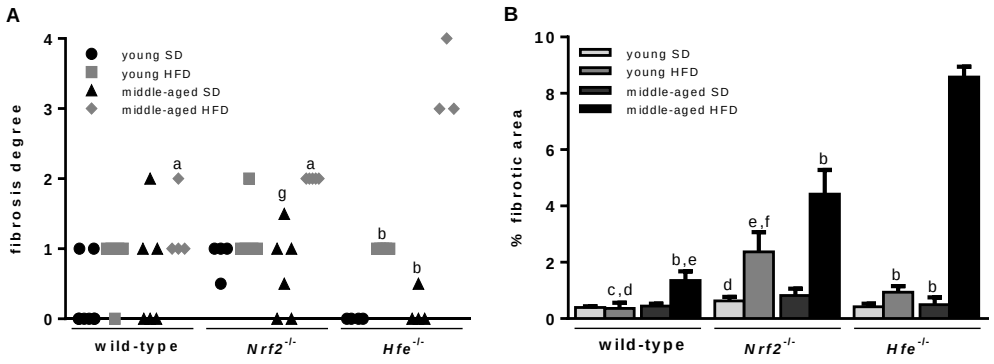

Figure 43. Histological evaluation of liver fibrosis by Sirius red staining of young and middle-aged wt, *Nrf2*$^{-/-}$, and *Hfe*$^{-/-}$ mice after 12 weeks of SD or HFD feeding. **(A)** Hepatic fibrosis degree. Liver sections were graded according to the amount of parenchyma with visible fibrosis as 0. None, 1. Mild to moderate, zone 3, or portal/periportal only, 2. Portal/periportal and perisinusoidal, 3. Bridging fibrosis and 4. Cirrhosis. **(B)** Percentage of hepatic fibrotic area. a. p<0.05 (one-way ANOVA vs. middle-aged *Hfe*$^{-/-}$ mice on HFD). b. p<0.0001 (one-way ANOVA vs. middle-aged *Hfe*$^{-/-}$ mice on HFD). c. p<0.05 (one-way ANOVA vs. middle-aged wt mice on HFD). d. p<0.0001 (one-way ANOVA vs. young *Nrf2*$^{-/-}$

mice on HFD). e. p<0.0001 (one-way ANOVA vs. middle-aged *Nrf2*$^{-/-}$ mice on HFD). f. p<0.0001 (one-way ANOVA vs. young *Hfe*$^{-/-}$ mice on HFD). g. p<0.01 (one-way ANOVA vs. middle-aged *Nrf2*$^{-/-}$ mice on HFD).

The NAFLD activity score (NAS) is the sum of the separate scores for steatosis (0–3), hepatocellular ballooning (0–2) and lobular inflammation (0–3) and is represented in **Figure 44**. The HFD elevated the NAS score in wt mice, but the effect appeared to be age-dependent. In *Nrf2*$^{-/-}$ mice, however, the NAS score was greatly elevated by the HFD in both young and middle-aged animals.

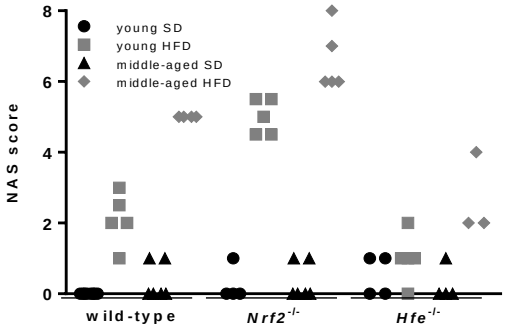

Figure 44. NAFLD activity score (NAS) in young and middle-aged wt, *Nrf2*$^{-/-}$, and *Hfe*$^{-/-}$ mice after 12 weeks of SD or HFD feeding.

Gene expression analysis by qPCR was employed to measure the hepatic expression of NAD(P)H dehydrogenase [quinone] 1 (*Nqo1*), *Tnf-α*, *α-Sma* and *Hamp*. *Nqo1* encodes a 2-electron reductase and its enzymatic activity includes the detoxification of reactive oxygen species. *Nqo1* induction is regulated through the Keap1/NRF2/ARE pathway (Dinkova-Kostova et al., 2002). As expected, hepatic *Nqo1* mRNA expression was lower in *Nrf2*$^{-/-}$ mice, compared to wt and *Hfe*$^{-/-}$ mice **(Figure 45A)**. Middle-aged *Hfe*$^{-/-}$ fed HFD mice displayed significantly increased levels of *Nqo1* mRNA, compared to wt and *Nrf2*$^{-/-}$ counterparts and to young *Hfe*$^{-/-}$ mice fed HFD and middle-aged *Hfe*$^{-/-}$ mice fed SD. *Tnf-α* mRNA expression increased in middle-aged wt, *Nrf2*$^{-/-}$ and *Hfe*$^{-/-}$ mice and also in young *Nrf2*$^{-/-}$ and *Hfe*$^{-/-}$ mice **(Figure 45B)**. However, this increase was only statistically significant in young *Hfe*$^{-/-}$ mice fed HFD and middle-aged wt mice. The expression of *α-Sma* was also measured by qPCR **(Figure 45C)**. A trend for increased *α-Sma* expression was observed in young and middle-aged *Nrf2*$^{-/-}$ mice and in middle-aged *Hfe*$^{-/-}$ mice, although no statistical significance was achieved. Interestingly, the consumption of HFD appeared to reduce the *Hamp* transcript levels in mice of all genotypes and age groups **(Figure 45D)**.

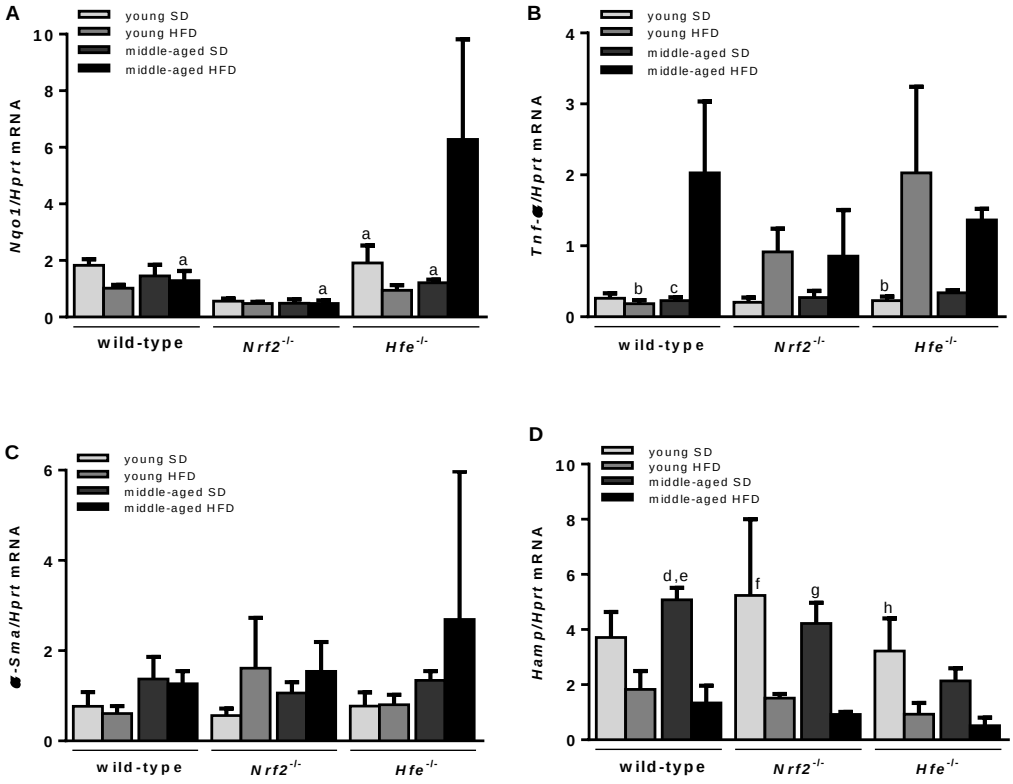

Figure 45. Hepatic gene expression in young and middle-aged wt, *Nrf2*$^{-/-}$, and *Hfe*$^{-/-}$ mice after 12 weeks of SD or HFD feeding. Expression of *Nqo1* mRNA **(A)**, *Tnf-α* mRNA **(B)** and *α-Sma* mRNA **(C)** was determined by qRT-PCR. a. p<0.0001 (one-way ANOVA vs. middle-aged *Hfe*$^{-/-}$ mice on HFD). b. p<0.001 (one-way ANOVA vs. young *Hfe*$^{-/-}$ mice on HFD). c. p<0.01 (one-way ANOVA vs. middle-aged wt mice on HFD). d. p<0.001 (one-way ANOVA vs. middle-aged wt mice on HFD). e. p<0.01 (one-way ANOVA vs. middle-aged *Hfe*$^{-/-}$ mice on ND). f. p<0.0001 (one-way ANOVA vs. young *Nrf2*$^{-/-}$ mice on HFD). g. p<0.001 (one-way ANOVA vs. middle-aged *Nrf2*$^{-/-}$ mice on HFD). h. p<0.05 (one-way ANOVA vs. young *Hfe*$^{-/-}$ mice on HFD).

5. Effects of diet, age, and genotype on lipid peroxidation

To evaluate the degree of lipid peroxidation, hepatic TBARS (thiobarbituric acid reactive substances) were quantified and reported as MDA equivalents. TBARS are formed as a byproduct of lipid peroxidation and thus represent markers of oxidative stress. Levels of MDA equivalents were unchanged in *Hfe*$^{-/-}$ mice but were significantly increased in middle-aged wt and *Nrf2*$^{-/-}$ mice fed HFD, compared to young counterparts fed HFD and middle-aged mice fed SD **(Figure 46)**.

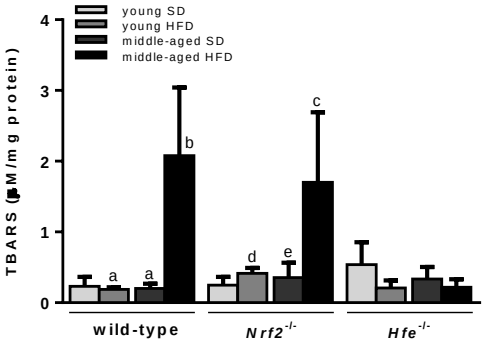

Figure 46. Hepatic MDA equivalents in young and middle-aged wt, *Nrf2*$^{-/-}$, and *Hfe*$^{-/-}$ mice after 12 weeks of SD or HFD feeding. a. p<0.0001 (one-way ANOVA vs. middle-aged wt mice on HFD). b. p<0.0001 (one-way ANOVA vs. middle-aged *Hfe*$^{-/-}$ mice on HFD). c. p<0.01 0001 (one-way ANOVA vs. middle-aged *Hfe*$^{-/-}$ mice on HFD). d. p<0.01 (one-way ANOVA vs. middle-aged *Nrf2*$^{-/-}$ mice on HFD). e. p<0.001 (one-way ANOVA vs. middle-aged *Nrf2*$^{-/-}$ mice on HFD).

Discussion

NASH is characterized by the presence of hepatocellular steatosis, fatty degeneration of hepatocytes and lobular inflammation. The deposition of collagen fibers, although not obligatory, is often observed. NASH may arise from a “two-step” process in which fat accumulation derived from insulin resistance first leads to hepatic steatosis. The liver is the prime target for fat deposition and the mechanism whereby TG accumulate within hepatocytes is attributed to both an increase uptake of FFA and a reduced TG secretion via VLDL (Rinella et al., 2008). Subsequently, oxidative stress derived from increased lipid *β*-oxidation and a number of other intracellular and extracellular triggers may drive inflammation and hepatocyte ballooning (Day and James, 1998; Tanaka et al., 2008; Tariq et al., 2014). The triad of steatosis, inflammation and hepatocyte ballooning is considered essential for a NASH diagnosis, while the presence of fibrosis is not required for diagnostic purposes.

In this study a high-fat, high-sucrose diet model was used to assess the development of NASH in mice. Several studies have focused on the effects of other steatosis-inducing diets such as the methionine- and choline-deficient diet (MCD), which promotes intrahepatic lipid accumulation in rodents (Chowdhry et al., 2010; Sugimoto et al., 2010; Zhang et al., 2010). However, the MCD diet is of limited value as a human disease model, as mice fed this diet only develop hepatic symptomatology and do not exhibit any signs of insulin resistance. The high-fat, high-sucrose diet (or ‘western-type’ diet), on the other hand, is the most reliable representation of the clinical situation whereby patients develop NASH in the settings of obesity, insulin resistance, dyslipidemia and metabolic syndrome. Several authors have demonstrated that the over-nutrition provided by a modern Western-type diet, not only from vegetable or animal fat sources (fatty acids and cholesterol), but also from the inclusion of carbohydrates in the diet (fructose and sucrose) is of utmost importance for steatohepatitis development (Fakhoury-Sayegh et al., 2015; Meli et al., 2013; Moriya et al., 2012; Ragab et al., 2015; Takai et al., 2015; Tan et al., 2011).

1. Parenchymal and mesenchymal iron overload did not promote hepatic injury in wild-type and *Hfe knock-out* mice fed a high-fat diet

The liver is one of the main sites for iron storage in the organism. Hepatocytes have at least two distinct mechanisms for iron uptake: a transferrin/TfR1 cycle and another important iron uptake pathway that takes up NTBI when serum iron levels exceed Tf biding capacity. Recycling macrophages are also major players in iron flux into extracellular fluid, exceeding the contribution of dietary iron absorption and the release

of stored iron from hepatocytes (Ganz, 2012). The HFE protein is a regulator of circulating iron uptake and systemic iron balance. HFE mutations may cause iron overload disorders such as Hereditary Hemochromatosis. In humans, the contribution of HFE mutations to NAFLD is controversial, but increased hepatic stores are often encountered in NAFLD patients (O'Brien and Powell, 2012). Excessive iron deposition is thought to aggravate the disease and favor the progression to NASH (Maliken et al., 2013; Nelson et al., 2011; Valenti et al., 2010). Conversely, HH patients often present with hepatic steatosis (Bonkovsky et al., 1999; Powell et al., 2005). As steatosis, together with cellular iron loading, produces a combination of factors that may result in the production of ROS, we aimed to determine experimentally whether excessive parenchymal hepatic iron deposition, as seen in HFE-related HH, is an aggravating factor in the progression from hepatic steatosis to steatohepatitis and to NASH-related fibrosis.

In the first set of experiments, we studied the development of hepatic steatosis, inflammation and fibrosis in an animal model of parenchymal iron overload. *Hfe*$^{-/-}$ mice at 8 weeks of age were fed high-fat, high-sucrose diet (HFD) or normal diet (ND) for experimental periods of 4, 8 or 12 weeks. Parenchymal iron load was visible in most hepatocytes, especially in periportal areas, independently of the diet. Nevertheless, non-heme iron concentration decreased when mice were fed HFD. This decrease in iron concentration can perhaps be explained through the fat source in the high-fat diet. It has been documented by several authors that a diet rich in animal fats tends to decrease hepatic iron concentration (Chung et al., 2011; Sonnweber et al., 2012; Takai et al., 2015), while diets rich in vegetable fats increase iron deposition (Ahmed and Oates, 2013; Johnson et al., 1987; Meli et al., 2013; Otogawa et al., 2007). Iron deposits within macrophages were also mildly present after 8 weeks of ND and HFD feeding. However, hepatic macrophages became iron-depleted after 12 weeks on the diets, a characteristic of mouse models of HH (Fleming et al., 2011). This depletion may have been caused by decreasing levels of hepatic hepcidin expression after 12 weeks of ND and HFD feeding, causing overexpression of ferroportin in macrophages and recapitulating the late onset of the human disease.

After 12 weeks of HFD feeding, *Hfe*$^{-/-}$ mice exhibited higher body, visceral fat and liver weight than their ND-fed counterparts. These mice also developed light to moderate microvesicular steatosis and signs of hepatic inflammation denoted by the elevated levels of *Tnf-α* transcript, but no other evidence of liver injury. In particular, we have not observed other signs of severe fatty liver disease phenotype akin to human NASH, including hepatocyte ballooning and early fibrogenesis. These results suggest that longer periods of high-fat diet feeding may represent a risk factor for developing NAFLD

and possibly NASH. But, under our experimental conditions, parenchymal iron overload coupled with high-fat diet feeding for up to 12 weeks failed to trigger the progression from steatosis to advanced liver disease.

Whilst the *Hfe*$^{-/-}$ mouse is a model of parenchymal iron deposition, mixed hepatocellular and mesenchymal iron deposition has been reported in NAFLD and NASH (Corradini and Pietrangelo, 2012; Nelson et al., 2011; Otogawa et al., 2007; Sorrentino et al., 2009). It can be hypothesized that the iron-loaded hepatic macrophages would become activated and promote steatohepatitis and fibrosis, while iron loading of hepatocytes would not contribute significantly to disease progression. To replicate the mixed (parenchymal and mesenchymal) iron deposition characteristic of some NAFLD patients, wt and *Hfe*$^{-/-}$ mice were given intraperitoneal injections of iron dextran. Intraperitoneal administration of iron dextran complex increased hepatic iron concentration, transferrin saturation and serum iron significantly in wt mice. In *Hfe*$^{-/-}$ mice, iron dextran increased the hepatic iron content even further without increasing serum iron concentration or transferrin saturation, independently of the diet. In iron overload disorders, serum iron concentration may exceed the transferrin binding capacity, generating NTBI. We speculate that, in *Hfe*$^{-/-}$ mice, iron administration may have increased serum NTBI and its uptake by the liver. In what concerns hepatic iron distribution, a mixed (parenchymal and mesenchymal) iron deposition was achieved with the iron treatment in both wt and *Hfe*$^{-/-}$ mice **(Figure 22)**. In theory, basal hepcidin expression is low in genetic mouse models of HH, hence ferroportin is overexpressed in reticuloendothelial cells, rendering them iron-depleted. It has been shown, however, that parenteral iron treatment or high-iron diets induce residual hepcidin expression, which leads to iron retention within macrophages (Daba et al., 2013; Gkouvatsos et al., 2014; Padda et al., 2015). In wt mice, it is plausible to assume that ND+Fe and HFD+Fe treatments promoted iron loading in Kupffer cells due to increased hepcidin expression. However, iron injections did not increase hepcidin expression significantly in *Hfe*$^{-/-}$ mice **(Figure 24)**. We speculate that the low basal hepcidin levels of *Hfe*$^{-/-}$ mice may enable some iron-retention within hepatic reticuloendothelial cells.

The iron treatment per se did not cause liver injury in animals of either genotype. After 8 weeks on HFD, both wt and *Hfe*$^{-/-}$ mice developed hepatic steatosis. It is interesting to note that while 8 weeks of HFD feeding increased body and visceral fat weight in wt and *Hfe*$^{-/-}$ mice compared to their normal diet-fed counterparts, mice that received iron intraperitoneally failed to gain as much weight and visceral fat as non-iron-treated mice. On the other hand, iron treatment did not alter the hepatic steatosis degree, as all wt and *Hfe*$^{-/-}$ mice fed HFD developed light to moderate microvesicular steatosis. Evidence of mild hepatic inflammation was also present in mice given iron dextran injections. No

hepatocyte ballooning or fibrosis were observed. We conclude that, despite substantial parenchymal and mesenchymal iron overload, the steatosis did not evolve to steatohepatitis in the iron-treated groups. One possible explanation is that neither the strictly parenchymal iron overload nor the mixed iron overload in our experiments were sufficient to increase oxidative stress and trigger the progression from simple steatosis to steatohepatitis. Similar results were obtained by (Padda et al., 2015) using the *Hjv*$^{-/-}$ mice model coupled with a high-fat and iron-rich diet. On the other hand, another study showed that *Hfe*$^{-/-}$ mice develop a NASH-like phenotype and early fibrosis in response to HFD-feeding for 8 weeks (Tan et al., 2011). We speculate that the striking differences may be attributable to the higher cholesterol and carbohydrate composition of the diets employed by (Tan et al., 2011).

2. Aging and *Nrf2* deletion promote steatosis and steatohepatitis in mice fed high-fat diet

Nrf2$^{-/-}$ mice are an established model of compromised antioxidant response and deleting *Nrf2* from mice results in rapid onset and progression of methionine- and choline-deficient diet-induced NASH (Chowdhry et al., 2010; Sugimoto et al., 2010). To examine the potential effects of aging on NAFLD development, we challenged wt and *Nrf2*$^{-/-}$ female mice of different ages with high-fat, high-sucrose diet for a period of 12 weeks to induce metabolic syndrome and NASH. This experimental design was intended to question whether the age altered the development of steatosis and steatohepatitis in response to a defined period of diet, as the prevalence of the metabolic syndrome increases significantly with age (Ford et al., 2002). NAFLD, the hepatic manifestation of the metabolic syndrome, has also been associated with aging. In particular, several population based studies have reported increased incidence of steatohepatitis and mortality in older individuals (Daryani et al., 2010; Gan et al., 2011; Williams et al., 2011). The link between aging and the development of the metabolic syndrome may result from age-related increases in obesity and diabetes, mainly derived from lifestyle factors such as diet and the lack of physical activity.

The transcription factor NRF2, besides playing a pivotal role in the activation of antioxidant and detoxification genes in response to electrophilic or oxidative stress, has an important role in hepatic fatty acid metabolism. NRF2 has been reported as a repressor of genes involved in FA synthesis (Kitteringham et al., 2010; Yates et al., 2009) and inflammation (Kohler et al., 2015; Reddy et al., 2011). NRF2 has also been shown to play a crucial role in the regulation of hepatic lipid metabolism not only in mice fed MCD, but also in mice fed HFD (Huang et al., 2010; Tanaka et al., 2008; Tanaka et al.,

2012). Furthermore, pharmacological activation of *Nrf2* down-regulates lipogenesis genes (Shin et al., 2009). As loss of *Nrf2* seems to increase both the expression of lipogenesis genes and sensitivity to oxidative stress, it may also contribute to the etiology of NASH.

Middle-aged wt mice exhibited higher levels of body, visceral fat and liver weight than their younger counterparts. On the other hand, features of the metabolic syndrome, such as increased body mass and visceral fat weight that developed as a consequence of the HFD-feeding, were similarly elevated in young and middle-aged *Nrf2*$^{-/-}$ mice. Moreover, middle-aged wt and *Nrf2*$^{-/-}$ mice and young *Nrf2*$^{-/-}$ mice developed signs of insulin resistance, as they were not able to clear glucose from their peripheral circulation 2 hours after glucose administration. We conclude that the age-associated metabolic changes observed in HFD-fed wt mice, such as obesity and insulin resistance, occur prematurely in *Nrf2*$^{-/-}$ animals.

We have also observed that young *Nrf2*$^{-/-}$ mice developed zone 1 macrovesicular steatosis and zone 3 microvesicular steatosis more rapidly and with greater severity than young wt and *Hfe*$^{-/-}$ mice when fed HFD. Notably, the severe steatotic phenotype displayed by young *Nrf2*$^{-/-}$ mice was similar to that observed in middle-aged wt and *Nrf2*$^{-/-}$ mice. This finding is not surprising in light of the similar extent of weight gain and insulin resistance in *Nrf2*$^{-/-}$ mice and middle-aged wt mice. This indicates that *Nrf2 knock-out* predisposes mice to hepatic lipid accumulation and that the phenotype is unaffected by age. Correlating with the severe steatosis, TG concentration of liver tissues was significantly increased in young *Nrf2*$^{-/-}$ mice fed HFD. On the other hand, liver TG were not as elevated in middle-aged *Nrf2*$^{-/-}$ mice, which might be explained by the lower liver weight observed in these animals. Serum TG and cholesterol levels were also increased in *Nrf2*$^{-/-}$ mice and middle-aged wt mice. We can thus speculate that the differences may result from changes in the expression of genes involved in lipid metabolism, namely in synthesis, catabolism, uptake and secretion of lipids. It would be useful to investigate the expression of genes involved in FA synthesis and uptake. Nevertheless, these results are in agreement with the previously reported *Nrf2*-mediated inhibition of fat accumulation in the liver of mice fed HFD (Tanaka et al., 2008) or MCD diet (Sugimoto et al., 2010).

Correlating with liver histology grading of inflammation and staging of fibrosis, the expression of the inflammatory cytokine *Tnf-α* and of the pro-fibrogenic gene *α-Sma* were significantly increased in middle-aged wt mice and *Nrf2*$^{-/-}$ mice fed HFD. Considering the well-established immune response depression with aging (Weiskopf et al., 2009), we believe that the increase in liver inflammation in older mice is related with a secondary response to liver injury in response to the HFD. Accordingly, middle-aged

wt mice and *Nrf2*$^{-/-}$ mice fed HFD had significantly increased hepatocyte ballooning and serum ALT activity, confirming that the lack of *Nrf2* and aging promoted liver injury in our experimental settings.

The levels of hepcidin mRNA were also measured in the livers of wt and *Nrf2*$^{-/-}$ mice. It has been shown that mice fed a high-fat diet undergo sustained hepatic inflammation. Inflammation increases hepatic hepcidin expression, which results in a reduction of the hepatic iron level (Chung et al., 2011). Our data are not in agreement with the literature, as *Nrf2*$^{-/-}$ mice on HFD and middle-aged wt mice on HFD, the experimental groups exhibiting the lowest hepcidin mRNA levels, were precisely the ones exhibiting more hepatic inflammation. Furthermore, we would expect the decreased hepcidin expression of mice fed HFD to result in increased intestinal iron absorption, elevated levels of serum iron and transferrin saturation, and higher hepatic iron accumulation. This was, however, not the case, which points to alternative pathways of hepcidin regulation. CREB-H (cyclic AMP response element–binding protein H) is an ER stress-activated liver-specific transcription factor originally recognized for its involvement in the induction of acute-phase response genes (Omori et al., 2001). Recent studies indicate that CREB-H is activated by fasting, obesity and diabetes, disorders associated with active gluconeogenesis and insulin resistance, and that its expression up-regulates lipid metabolism genes. CREB-H has also been reported to activate the transcription of hepcidin, linking glucose and iron homeostasis (Vecchi et al., 2014). This mechanism is, however, not a likely explanation for our results, as the expression of CREB-H would have been higher in middle-aged wt mice and *Nrf2*$^{-/-}$ mice in response to the HFD feeding. The increase in CREB-H expression would have up-regulated the expression of hepcidin, which is the opposite effect to what we observed in the current study. Further investigation about the interaction between the iron and lipid metabolism is required.

Our data are suggestive of oxidative stress in middle-aged wt and *Nrf2*$^{-/-}$ mice on HFD, as evidenced by increased hepatic malondialdehyde. Furthermore, mRNA levels of the detoxifying enzyme *Nqo1* was significantly decreased in the livers of *Nrf2*$^{-/-}$ mice. It seems plausible that the inability of *Nrf2*$^{-/-}$ mice to up-regulate their antioxidant defenses results in lipid peroxidation, facilitating the development of NASH, as reported by (Ikura et al., 2006). Moreover, these results also suggest that aging plays a prominent role in decreasing NRF2-dependent oxidative stress defenses, contributing to the rapid onset of NASH in *Nrf2*$^{-/-}$ animals, comparable to the phenotype of older wt mice.

The nonoccurrence of steatohepatitis within 12 weeks of HFD feeding in young wt mice clearly shows that a HFD per se does not trigger the development of NASH in the young. The aging process coupled with HFD, however, was sufficient to promote the

development of liver injury and inflammation in wt animals. Importantly, what our results also disclose is that the lack of *Nrf2* is as efficient as the age-related factors to prompt the metabolic events leading to NASH.

3. High-fat diet feeding promoted the development of liver tumors in middle-aged *Hfe*$^{-/-}$ mice

Herein, we have also studied of effects of age and dietary treatment in the development of steatosis and steatohepatitis in *Hfe*$^{-/-}$ mice, as altered lipid metabolism in *Hfe*$^{-/-}$ mice reportedly promotes severe NAFLD and early fibrosis in response to HFD (Tan et al., 2011). *Hfe*$^{-/-}$ mice of different ages were also challenged with high-fat, high-sucrose diet feeding for a period of 12 weeks to induce the metabolic syndrome and NAFLD. Young *Hfe*$^{-/-}$ mice exhibited similar body, visceral and liver weight compared to wt counterparts, but middle-aged *Hfe*$^{-/-}$ mice fed HFD tended to gain less weight. The most significant finding of this experiment was that every single middle-aged *Hfe*$^{-/-}$ mouse fed HFD developed liver tumors, evidenced by the macroscopic appearance of the livers and abnormal histology **(Figures 31 and 36)**. Another two individuals from this experimental group died before the end of the 12 weeks of high-fat diet feeding and at least one of these mice also exhibited a liver tumor. We found no evidence of hepatocyte ballooning (a NASH signature) in these mice. Moreover, young mice of the same genotype did not develop inflammation, hepatocyte ballooning or fibrosis in response to the HFD, so we cannot confidently attribute the development of liver tumors in middle-aged mice to HFD-induced steatohepatitis. Nevertheless, we consider it unlikely that the development of hepatic tumors derived just from old age, since no tumors were observed in middle-aged *Hfe*$^{-/-}$ fed SD or in considerably older *Hfe*$^{-/-}$ mice (up to 24 months old) (Tiago Duarte, personal communication). The identification of the tumor type will be performed soon in collaboration with an experienced pathologist, which is expected to help understand its etiology. But we can speculate that the apparently rather advanced stage of the tumors is responsible for the discrepancies in several biological parameters, compared to their younger counterparts. For example, the rapid glucose clearance from their bloodstream might have been caused by the high metabolic activity of the hepatic tumor, as rapidly dividing cells need great amounts of energy to proliferate. Despite being a model of iron overload and having significantly lower hepatic hepcidin mRNA levels than their younger HFD-fed counterparts, these mice exhibited decreased hepatic iron deposits. We can also speculate that the hepatic tumors may have consumed the hepatic iron deposits. Serum iron and transferrin saturation, on the other hand, had normal values in this experimental group, compared to *Hfe*$^{-/-}$ counterparts. This might indicate that the tumor was only using local hepatic iron, instead of having a systemic effect in circulating iron.

Serum cholesterol and triglyceride levels were also significantly higher in middle-aged *Hfe*$^{-/-}$ mice fed HFD than in younger counterparts, despite a lower degree of steatosis and lower hepatic triglyceride content.

Another consequence of the tumors was a dramatic elevation of serum ALT activity, which is indicative of hepatocellular injury. The grading of inflammation and staging of fibrosis in liver sections, as well as the levels of *Tnf-α* and *α-Sma* transcripts, showed that middle-aged *Hfe*$^{-/-}$ mice fed HFD exhibited significant liver inflammation, which was accompanied by bridging fibrosis and cirrhosis. Substantial amounts of collagen deposition were seen surrounding the hepatic tumors **(Figure 36C)**.

In many cancers, uncontrolled NRF2 activity increases the expression of cytoprotective genes and, consequently, provides growth advantage to cancerous cells (Kanninen et al., 2015). The mRNA levels of *Nqo1,* a prototypical target of NRF2, were significantly elevated in middle-aged *Hfe*$^{-/-}$ mice fed HFD, which suggests that NRF2 may have a protective role in the proliferation of this type of tumor.

Conclusions

Our results show that, in young animals, the mild parenchymal iron overload associated with the loss of *Hfe*$^{-/-}$ was not sufficient to prompt the development of NASH upon feeding a 'Western-type diet'. Moreover, wt and *Hfe*$^{-/-}$ mice intraperitoneally injected with iron to increase both the parenchymal and mesenchymal hepatic iron overload also failed to develop features of NASH, such as obesity, hepatocyte ballooning or fibrosis.

The nonoccurrence of steatohepatitis in young wt mice fed HFD clearly shows that this diet *per se* does not trigger the development of NASH in the young. The aging process coupled with HFD, however, was sufficient to promote the development of liver injury and inflammation in wt animals. We demonstrated that aging promotes obesity, steatosis and steatohepatitis in wt mice fed high-fat diet. Importantly, we also demonstrated that *Nrf2* deletion leads to rapid progression of nutritional steatohepatitis in young as well as middle-aged mice fed a Western-type diet. We thus conclude that the lack of *Nrf2* is as efficient as the age-related factors to prompt the metabolic events leading to NASH, as age-associated metabolic changes observed in HFD-fed wt mice occurred prematurely in *Nrf2*$^{-/-}$ animals. Moreover, our data suggest that the decrease in NRF2-dependent oxidative stress defenses that occurs as part of the aging process may contributing significantly to the onset of NASH in the elder.

Finally, we showed that feeding a high-fat, high-sucrose diet promotes the development of liver tumors in middle-aged *Hfe*$^{-/-}$ mice. These animals exhibited extensive hepatocellular injury, as evidenced by the dramatic elevation of serum ALT activity, and significant liver inflammation, which was accompanied by bridging fibrosis and cirrhosis. However, young mice of the same genotype did not develop features of NASH such as obesity, insulin resistance, hepatic steatosis, inflammation, hepatocyte ballooning or fibrosis in response to the HFD. Hence, we cannot confidently attribute the development of liver tumors in middle-aged mice to HFD-induced steatohepatitis.

Future perspectives

The results of the current work suggest that *Nrf2* is an interesting therapeutic target for the prevention and treatment of NAFLD and NASH. It would be interesting to investigate whether *Nrf2* target therapy with thiol-reactive, electrophilic compounds, such as sulphoraphane, would be capable of activating NRF2/ARE-dependent gene expression in old wt and *Hfe*$^{-/-}$ mice, and prevent the progression of nonalcoholic steatohepatitis and hepatic tumors, respectively.

Future work could also focus on the study of the *Hamp knock-out* mouse, a more severe model of iron overload. This model would enable the deposition of massive amounts of hepatic iron that, when coupled with the high-fat, high-sucrose diet feeding, may be sufficient to trigger the development of NASH in young mice. Additionally, it would be interesting to determine whether iron overload in *Hamp*$^{-/-}$ individuals fed a Western-type diet would also favor the development of hepatic tumors in middle-aged mice.

Publications

Chambel, S.S., Santos-Goncalves, A., and Duarte, T.L. (2015). The Dual Role of *Nrf2* in Nonalcoholic Fatty Liver Disease: Regulation of Antioxidant Defenses and Hepatic Lipid Metabolism. BioMed Research International *2015*, 597134.

Appendixes

Appendix I

Table 1. Dietary composition of experimental diets.

	Standard rodent diet (Mucedola)	Control diet (ssniff)	Western-type diet (ssniff)
Energy [kJ %]			
From protein	27	18	15
From carbohydrate	60	70	43
From fat	6.5	12	42
Metabolizable energy (kcal/g)	2.675	3.726	4.562
Total calories (kcal/g)	3.952	4.398	5.258
Crude nutrients [%]			
Dry matter	-	95.9	94.6
Crude Protein	19.4	17.1	17.5
Crude Fat	2.6	5.1	21.2
Crude fiber	5.5	5.0	5.0
Crude ash	6.8	4.2	4.5
N free extracts	54.6	64.5	48.8
Starch	-	39.0	14.6
Sugar	4	23.3	33.2
Minerals [%]			
Calcium	0.91	0.77	0.76
Phosphorus	0.76	0.46	0.46
Sodium	0.36	0.22	0.37
Magnesium	0.20	0.08	0.10
Potassium	0.84	0.55	0.54
Fatty acids [%]			
Butyric acid 4:0	-	-	0.80
Caproic acid 6:0	-	-	0.53
Caprylic acid 8:0	-	-	0.29
Capric acid 10:0	-	-	0.63
Lauric acid 12:0	-	-	0.72
Myristic acid 14:0	-	0.02	2.21
Palmitic acid 16:0	4.39	0.55	5.74
Palmitoleic acid 16:1	0.20	0.03	0.38
Margaric acid 17:0	-	-	0.13
Stearic acid 18:0	0.68	0.23	2.04
Oleic acid 18:1	5.05	1.32	4.63
Linoleic acid 18:2	12.3	2.65	0.38
Linolenic acid 18:3	1.20	0.33	0.11

Arachidic acid 20:0	-	0.03	0.04
Paullinic acid 20:1	-	-	0.02
Cholesterol [mg/kg]	-	-	500-600
Amino acids [%]			
Lysine	9.72	1.39	1.42
Methionine	4.45	0.91	0.63
Met+Cys	-	0.99	1.00
Threonine	-	0.75	0.76
Tryptophan	2.83	0.22	0.23
Arginine	10.94	0.62	0.67
Histidine	-	0.53	0.52
Valine	-	1.15	1.19
Isoleucine	-	0.88	0.93
Leucine	-	1.66	1.70
Phenylalanine	-	0.91	0.90
Phe+Tyr	-	1.81	1.80
Glycine	8.75	0.35	0.36
Glutamic acid	-	3.81	3.84
Aspartic acid	-	1.26	1.27
Proline	-	1.95	1.97
Alanine	-	0.55	0.57
Serine	-	1.01	1.02
Cystine	3.86	-	-
Vitamins [IU]			
Vitamin A	14400	15000	15000
Vitamin D3	1260	1500	1500
Vitamins [mg]			
Vitamin E	64.3	150	150
Vitamin K	3.2	20	20
Vitamin C	-	1030	1030
Thiamin (B1)	17.2	16	16
Riboflavin (B2)	15.2	16	16
Pyridoxine (B6)	10.7	18	18
Cobalamin (B12)	0.027	30	30
Nicotinic acid	-	45	45
Panthothenic acid	24.8	55	55
Folic acid	2.3	19	19
Biotin	0.40	305	305
Choline-Chloride	2256	2040	2040
Inositol	-	80	80
Niacin	95.8	-	-
Trace elements [mg]			
Iron	480	200	200

Manganese	86	23	23
Zinc	103	39	39
Copper	25.7	11	11
Iodine	1	0.28	0.28
Selenium	-	0.14	0.14
Cobalt	0.85	0.02	0.02

References

Abboud, S., and Haile, D.J. (2000). A novel mammalian iron-regulated protein involved in intracellular iron metabolism. J Biol Chem *275*, 19906-19912.

Ahmed, U., and Oates, P.S. (2013). Dietary fat level affects tissue iron levels but not the iron regulatory gene HAMP in rats. Nutrition research (New York, NY) *33*, 126-135.

Alberti, K.G., Zimmet, P., and Shaw, J. (2006). Metabolic syndrome--a new world-wide definition. A Consensus Statement from the International Diabetes Federation. Diabet Med *23*, 469-480.

Andrews, N.C. (2000). Iron homeostasis: insights from genetics and animal models. Nat Rev Genet *1*, 208-217.

Andrews, N.C., and Schmidt, P.J. (2007). Iron homeostasis. Annu Rev Physiol *69*, 69-85.

Andriopoulos, B., Jr., Corradini, E., Xia, Y., Faasse, S.A., Chen, S., Grgurevic, L., Knutson, M.D., Pietrangelo, A., Vukicevic, S., Lin, H.Y.*, et al.* (2009). BMP6 is a key endogenous regulator of hepcidin expression and iron metabolism. Nat Genet *41*, 482-487.

Angulo, P. (2002). Nonalcoholic fatty liver disease. The New England journal of medicine *346*, 1221-1231.

Arezes, J., and Nemeth, E. (2015). Hepcidin and iron disorders: new biology and clinical approaches. Int J Lab Hematol *37 Suppl 1*, 92-98.

Arezzini, B., Lunghi, B., Lungarella, G., and Gardi, C. (2003). Iron overload enhances the development of experimental liver cirrhosis in mice. The international journal of biochemistry & cell biology *35*, 486-495.

Batts, K.P. (2007). Iron overload syndromes and the liver. Mod Pathol *20 Suppl 1*, S31-39.

Beutler, E., Felitti, V.J., Koziol, J.A., Ho, N.J., and Gelbart, T. (2002). Penetrance of 845G--> A (C282Y) HFE hereditary haemochromatosis mutation in the USA. Lancet *359*, 211-218.

Bonkovsky, H.L., Jawaid, Q., Tortorelli, K., LeClair, P., Cobb, J., Lambrecht, R.W., and Banner, B.F. (1999). Non-alcoholic steatohepatitis and iron: increased prevalence of mutations of the HFE gene in non-alcoholic steatohepatitis. Journal of hepatology *31*, 421-429.

Boudreau, D.M., Malone, D.C., Raebel, M.A., Fishman, P.A., Nichols, G.A., Feldstein, A.C., Boscoe, A.N., Ben-Joseph, R.H., Magid, D.J., and Okamoto, L.J. (2009). Health care utilization and costs by metabolic syndrome risk factors. Metab Syndr Relat Disord *7*, 305-314.

Bridle, K.R., Frazer, D.M., Wilkins, S.J., Dixon, J.L., Purdie, D.M., Crawford, D.H., Subramaniam, V.N., Powell, L.W., Anderson, G.J., and Ramm, G.A. (2003). Disrupted hepcidin regulation in HFE-associated haemochromatosis and the liver as a regulator of body iron homoeostasis. Lancet *361*, 669-673.

Brunt, E.M., Kleiner, D.E., Wilson, L.A., Belt, P., and Neuschwander-Tetri, B.A. (2011). The NAS and The Histopathologic Diagnosis in NAFLD: Distinct Clinicopathologic Meanings. Hepatology (Baltimore, Md) *53*, 810-820.

Byrne, C.D., and Targher, G. (2015). NAFLD: a multisystem disease. Journal of hepatology *62*, S47-64.

Cheng, Y., Zak, O., Aisen, P., Harrison, S.C., and Walz, T. (2004). Structure of the human transferrin receptor-transferrin complex. Cell *116*, 565-576.

Chowdhry, S., Nazmy, M.H., Meakin, P.J., Dinkova-Kostova, A.T., Walsh, S.V., Tsujita, T., Dillon, J.F., Ashford, M.L., and Hayes, J.D. (2010). Loss of *Nrf2* markedly exacerbates nonalcoholic steatohepatitis. Free radical biology & medicine *48*, 357-371.

Chung, J., Kim, M.S., and Han, S.N. (2011). Diet-induced obesity leads to decreased hepatic iron storage in mice. Nutrition research (New York, NY) *31*, 915-921.

Collins, A.R., Lyon, C.J., Xia, X., Liu, J.Z., Tangirala, R.K., Yin, F., Boyadjian, R., Bikineyeva, A., Pratico, D., Harrison, D.G.*, et al.* (2009). Age-accelerated atherosclerosis correlates with failure to upregulate antioxidant genes. Circ Res *104*, e42-54.

Corradini, E., and Pietrangelo, A. (2012). Iron and steatohepatitis. Journal of gastroenterology and hepatology *27 Suppl 2*, 42-46.

D'Alessio, F., Hentze, M.W., and Muckenthaler, M.U. (2012). The hemochromatosis proteins HFE, TfR2, and HJV form a membrane-associated protein complex for hepcidin regulation. Journal of hepatology *57*, 1052-1060.

Daba, A., Gkouvatsos, K., Sebastiani, G., and Pantopoulos, K. (2013). Differences in activation of mouse hepcidin by dietary iron and parenterally administered iron dextran: compartmentalization is critical for iron sensing. Journal of molecular medicine (Berlin, Germany) *91*, 95-102.

Daniels, T.R., Delgado, T., Rodriguez, J.A., Helguera, G., and Penichet, M.L. (2006). The transferrin receptor part I: Biology and targeting with cytotoxic antibodies for the treatment of cancer. Clin Immunol *121*, 144-158.

Daryani, N.E., Daryani, N.E., Alavian, S.M., Zare, A., Fereshtehnejad, S.M., Keramati, M.R., Pashaei, M.R., and Habibollahi, P. (2010). Non-alcoholic steatohepatitis and influence of age and gender on histopathologic findings. World journal of gastroenterology : WJG *16*, 4169-4175.

Day, C.P., and James, O.F. (1998). Hepatic steatosis: innocent bystander or guilty party? Hepatology (Baltimore, Md) *27*, 1463-1466.

Deugnier, Y., and Turlin, B. (2007). Pathology of hepatic iron overload. World journal of gastroenterology : WJG *13*, 4755-4760.

Dietrich, P., and Hellerbrand, C. (2014). Non-alcoholic fatty liver disease, obesity and the metabolic syndrome. Best Pract Res Clin Gastroenterol *28*, 637-653.

Dinkova-Kostova, A.T., Holtzclaw, W.D., Cole, R.N., Itoh, K., Wakabayashi, N., Katoh, Y., Yamamoto, M., and Talalay, P. (2002). Direct evidence that sulfhydryl groups of Keap1 are the sensors regulating induction of phase 2 enzymes that protect against carcinogens and oxidants. Proceedings of the National Academy of Sciences of the United States of America *99*, 11908-11913.

Dinkova-Kostova, A.T., Holtzclaw, W.D., and Kensler, T.W. (2005). The role of Keap1 in cellular protective responses. Chem Res Toxicol *18*, 1779-1791.

Donovan, A., Brownlie, A., Zhou, Y., Shepard, J., Pratt, S.J., Moynihan, J., Paw, B.H., Drejer, A., Barut, B., Zapata, A*., et al.* (2000). Positional cloning of zebrafish ferroportin1 identifies a conserved vertebrate iron exporter. Nature *403*, 776-781.

Ekstedt, M., Franzen, L.E., Mathiesen, U.L., Thorelius, L., Holmqvist, M., Bodemar, G., and Kechagias, S. (2006). Long-term follow-up of patients with NAFLD and elevated liver enzymes. Hepatology (Baltimore, Md) *44*, 865-873.

Elpek, G.O. (2014). Cellular and molecular mechanisms in the pathogenesis of liver fibrosis: An update. World journal of gastroenterology : WJG *20*, 7260-7276.

Enomoto, H., Bando, Y., Nakamura, H., Nishiguchi, S., and Koga, M. (2015). Liver fibrosis markers of nonalcoholic steatohepatitis. World journal of gastroenterology : WJG *21*, 7427-7435.

Evstatiev, R., and Gasche, C. (2012). Iron sensing and signalling. Gut *61*, 933-952.

Fabbrini, E., and Magkos, F. (2015). Hepatic Steatosis as a Marker of Metabolic Dysfunction. Nutrients *7*, 4995-5019.

Fakhoury-Sayegh, N., Trak-Smayra, V., Khazzaka, A., Esseily, F., Obeid, O., Lahoud-Zouein, M., and Younes, H. (2015). Characteristics of nonalcoholic fatty liver disease induced in wistar rats following four different diets. Nutrition research and practice *9*, 350-357.

Feder, J.N., Gnirke, A., Thomas, W., Tsuchihashi, Z., Ruddy, D.A., Basava, A., Dormishian, F., Domingo, R., Jr., Ellis, M.C., Fullan, A.*, et al.* (1996). A novel MHC class I-like gene is mutated in patients with hereditary haemochromatosis. Nat Genet *13*, 399-408.

Fleming, R.E., Feng, Q., and Britton, R.S. (2011). Knockout mouse models of iron homeostasis. Annual review of nutrition *31*, 117-137.

Ford, E.S., Giles, W.H., and Dietz, W.H. (2002). Prevalence of the metabolic syndrome among US adults: findings from the third National Health and Nutrition Examination Survey. Jama *287*, 356-359.

Gan, L., Chitturi, S., and Farrell, G.C. (2011). Mechanisms and implications of age-related changes in the liver: nonalcoholic Fatty liver disease in the elderly. Current gerontology and geriatrics research *2011*, 831536.

Ganz, T. (2012). Macrophages and systemic iron homeostasis. J Innate Immun *4*, 446-453.

Ganz, T. (2013). Systemic iron homeostasis. Physiol Rev *93*, 1721-1741.

Ganz, T., and Nemeth, E. (2012). Hepcidin and iron homeostasis. Biochim Biophys Acta *1823*, 1434-1443.

Gkouvatsos, K., Fillebeen, C., Daba, A., Wagner, J., Sebastiani, G., and Pantopoulos, K. (2014). Iron-dependent regulation of hepcidin in *Hjv*$^{-/-}$ mice: evidence that hemojuvelin is dispensable for sensing body iron levels. PloS one *9*, e85530.

Gkouvatsos, K., Papanikolaou, G., and Pantopoulos, K. (2012). Regulation of iron transport and the role of transferrin. Biochim Biophys Acta *1820*, 188-202.

Goswami, T., and Andrews, N.C. (2006). Hereditary hemochromatosis protein, HFE, interaction with transferrin receptor 2 suggests a molecular mechanism for mammalian iron sensing. J Biol Chem *281*, 28494-28498.

Gulec, S., Anderson, G.J., and Collins, J.F. (2014). Mechanistic and regulatory aspects of intestinal iron absorption. American journal of physiology Gastrointestinal and liver physiology *307*, G397-409.

Gupte, A.A., Lyon, C.J., and Hsueh, W.A. (2013). Nuclear factor (erythroid-derived 2)-like-2 factor (Nrf2), a key regulator of the antioxidant response to protect against atherosclerosis and nonalcoholic steatohepatitis. Curr Diab Rep *13*, 362-371.

Harrison, P.M., and Arosio, P. (1996). The ferritins: molecular properties, iron storage function and cellular regulation. Biochim Biophys Acta *1275*, 161-203.

Hayes, J.D., and Dinkova-Kostova, A.T. (2014). The *Nrf2* regulatory network provides an interface between redox and intermediary metabolism. Trends in biochemical sciences *39*, 199-218.

Hentze, M.W., Muckenthaler, M.U., and Andrews, N.C. (2004). Balancing acts: molecular control of mammalian iron metabolism. Cell *117*, 285-297.

Hentze, M.W., Muckenthaler, M.U., Galy, B., and Camaschella, C. (2010). Two to tango: regulation of Mammalian iron metabolism. Cell *142*, 24-38.

Hernaez, R., Yeung, E., Clark, J.M., Kowdley, K.V., Brancati, F.L., and Kao, W.H. (2011). Hemochromatosis gene and nonalcoholic fatty liver disease: a systematic review and meta-analysis. Journal of hepatology *55*, 1079-1085.

Hirayama, A., Yoh, K., Nagase, S., Ueda, A., Itoh, K., Morito, N., Hirayama, K., Takahashi, S., Yamamoto, M., and Koyama, A. (2003). EPR imaging of reducing activity in Nrf2 transcriptional factor-deficient mice. Free radical biology & medicine *34*, 1236-1242.

Holmstrom, K.M., Baird, L., Zhang, Y., Hargreaves, I., Chalasani, A., Land, J.M., Stanyer, L., Yamamoto, M., Dinkova-Kostova, A.T., and Abramov, A.Y. (2013). *Nrf2* impacts cellular bioenergetics by controlling substrate availability for mitochondrial respiration. Biol Open *2*, 761-770.

Huang J, B.K., Reddy JK (2011). Hepatic Lipid Metabolism Chapter 10. In Molecular Pathology of Liver Diseases

Huang, J., Tabbi-Anneni, I., Gunda, V., and Wang, L. (2010). Transcription factor *Nrf2* regulates SHP and lipogenic gene expression in hepatic lipid metabolism. American journal of physiology Gastrointestinal and liver physiology *299*, G1211-1221.

Ikura, Y., Ohsawa, M., Suekane, T., Fukushima, H., Itabe, H., Jomura, H., Nishiguchi, S., Inoue, T., Naruko, T., Ehara, S.*, et al.* (2006). Localization of oxidized

phosphatidylcholine in nonalcoholic fatty liver disease: impact on disease progression. Hepatology (Baltimore, Md) *43*, 506-514.

Ilyin, G., Courselaud, B., Troadec, M.B., Pigeon, C., Alizadeh, M., Leroyer, P., Brissot, P., and Loreal, O. (2003). Comparative analysis of mouse hepcidin 1 and 2 genes: evidence for different patterns of expression and co-inducibility during iron overload. FEBS letters *542*, 22-26.

Itoh, K., Chiba, T., Takahashi, S., Ishii, T., Igarashi, K., Katoh, Y., Oyake, T., Hayashi, N., Satoh, K., Hatayama, I.*, et al.* (1997). An *Nrf2*/small Maf heterodimer mediates the induction of phase II detoxifying enzyme genes through antioxidant response elements. Biochem Biophys Res Commun *236*, 313-322.

Jenkitkasemwong, S., Wang, C.Y., Mackenzie, B., and Knutson, M.D. (2012). Physiologic implications of metal-ion transport by ZIP14 and ZIP8. Biometals *25*, 643-655.

Johnson, P.E., Lukaski, H.C., and Bowman, T.D. (1987). Effects of level and saturation of fat and iron level and type in the diet on iron absorption and utilization by the rat. The Journal of nutrition *117*, 501-507.

Jungermann, K., and Kietzmann, T. (1996). Zonation of parenchymal and nonparenchymal metabolism in liver. Annual review of nutrition *16*, 179-203.

Kaji, K., Yoshiji, H., Kitade, M., Ikenaka, Y., Noguchi, R., Shirai, Y., Aihara, Y., Namisaki, T., Yoshii, J., Yanase, K.*, et al.* (2011). Combination treatment of angiotensin II type I receptor blocker and new oral iron chelator attenuates progression of nonalcoholic steatohepatitis in rats. American journal of physiology Gastrointestinal and liver physiology *300*, G1094-1104.

Kanninen, K.M., Pomeshchik, Y., Leinonen, H., Malm, T., Koistinaho, J., and Levonen, A.L. (2015). Applications of the Keap1-Nrf2 system for gene and cell therapy. Free radical biology & medicine.

Kansanen, E., Jyrkkanen, H.K., and Levonen, A.L. (2012). Activation of stress signaling pathways by electrophilic oxidized and nitrated lipids. Free radical biology & medicine *52*, 973-982.

Katz, N., Teutsch, H.F., Jungermann, K., and Sasse, D. (1977). Heterogeneous reciprocal localization of fructose-1,6-bisphosphatase and of glucokinase in microdissected periportal and perivenous rat liver tissue. FEBS letters *83*, 272-276.

Kawabata, H., Germain, R.S., Vuong, P.T., Nakamaki, T., Said, J.W., and Koeffler, H.P. (2000). Transferrin receptor 2-alpha supports cell growth both in iron-chelated cultured cells and *in vivo*. J Biol Chem *275*, 16618-16625.

Kawabata, H., Yang, R., Hirama, T., Vuong, P.T., Kawano, S., Gombart, A.F., and Koeffler, H.P. (1999). Molecular cloning of transferrin receptor 2. A new member of the transferrin receptor-like family. The Journal of biological chemistry *274*, 20826-20832.

Kehrer, J.P. (2000). The Haber-Weiss reaction and mechanisms of toxicity. Toxicology *149*, 43-50.

Kell, D.B. (2009). Iron behaving badly: inappropriate iron chelation as a major contributor to the aetiology of vascular and other progressive inflammatory and degenerative diseases. BMC Med Genomics *2*, 2.

Kensler, T.W., Wakabayashi, N., and Biswal, S. (2007). Cell survival responses to environmental stresses via the Keap1-*Nrf2*-ARE pathway. Annu Rev Pharmacol Toxicol *47*, 89-116.

Kitteringham, N.R., Abdullah, A., Walsh, J., Randle, L., Jenkins, R.E., Sison, R., Goldring, C.E., Powell, H., Sanderson, C., Williams, S.*, et al.* (2010). Proteomic analysis of *Nrf2* deficient transgenic mice reveals cellular defence and lipid metabolism as primary *Nrf2*-dependent pathways in the liver. J Proteomics *73*, 1612-1631.

Kohler, U.A., Bohm, F., Rolfs, F., Egger, M., Hornemann, T., Pasparakis, M., Weber, A., and Werner, S. (2015). NF-kappaB/RelA and Nrf2 cooperate to maintain hepatocyte integrity and to prevent development of hepatocellular adenoma. Journal of hepatology.

Koyama, Y., and Brenner, D.A. (2015). New therapies for hepatic fibrosis. Clinics and research in hepatology and gastroenterology.

Kristiansen, M., Graversen, J.H., Jacobsen, C., Sonne, O., Hoffman, H.J., Law, S.K., and Moestrup, S.K. (2001). Identification of the haemoglobin scavenger receptor. Nature *409*, 198-201.

Lane, D.J., Bae, D.H., Merlot, A.M., Sahni, S., and Richardson, D.R. (2015a). Duodenal cytochrome b (DCYTB) in iron metabolism: an update on function and regulation. Nutrients *7*, 2274-2296.

Lane, D.J., Merlot, A.M., Huang, M.L., Bae, D.H., Jansson, P.J., Sahni, S., Kalinowski, D.S., and Richardson, D.R. (2015b). Cellular iron uptake, trafficking and metabolism: Key molecules and mechanisms and their roles in disease. Biochim Biophys Acta *1853*, 1130-1144.

LeCluyse, E.L., Witek, R.P., Andersen, M.E., and Powers, M.J. (2012). Organotypic liver culture models: meeting current challenges in toxicity testing. Critical reviews in toxicology *42*, 501-548.

Lee, J.M., Calkins, M.J., Chan, K., Kan, Y.W., and Johnson, J.A. (2003). Identification of the NF-E2-related factor-2-dependent genes conferring protection against oxidative stress in primary cortical astrocytes using oligonucleotide microarray analysis. J Biol Chem *278*, 12029-12038.

Levonen, A.L., Hill, B.G., Kansanen, E., Zhang, J., and Darley-Usmar, V.M. (2014). Redox regulation of antioxidants, autophagy, and the response to stress: implications for electrophile therapeutics. Free radical biology & medicine *71*, 196-207.

Liu, K., and Czaja, M.J. (2013). Regulation of lipid stores and metabolism by lipophagy. Cell Death Differ *20*, 3-11.

Mackenzie, B., and Garrick, M.D. (2005). Iron Imports. II. Iron uptake at the apical membrane in the intestine. American journal of physiology Gastrointestinal and liver physiology *289*, G981-986.

Maliken, B.D., Nelson, J.E., Klintworth, H.M., Beauchamp, M., Yeh, M.M., and Kowdley, K.V. (2013). Hepatic reticuloendothelial system cell iron deposition is associated with increased apoptosis in nonalcoholic fatty liver disease. Hepatology (Baltimore, Md) *57*, 1806-1813.

McKie, A.T., Barrow, D., Latunde-Dada, G.O., Rolfs, A., Sager, G., Mudaly, E., Mudaly, M., Richardson, C., Barlow, D., Bomford, A*., et al.* (2001). An iron-regulated ferric reductase associated with the absorption of dietary iron. Science *291*, 1755-1759.

McKie, A.T., Marciani, P., Rolfs, A., Brennan, K., Wehr, K., Barrow, D., Miret, S., Bomford, A., Peters, T.J., Farzaneh, F*., et al.* (2000). A novel duodenal iron-regulated transporter, IREG1, implicated in the basolateral transfer of iron to the circulation. Mol Cell *5*, 299-309.

Meli, R., Mattace Raso, G., Irace, C., Simeoli, R., Di Pascale, A., Paciello, O., Pagano, T.B., Calignano, A., Colonna, A., and Santamaria, R. (2013). High Fat Diet Induces Liver Steatosis and Early Dysregulation of Iron Metabolism in Rats. PloS one *8*, e66570.

Meynard, D., Kautz, L., Darnaud, V., Canonne-Hergaux, F., Coppin, H., and Roth, M.P. (2009). Lack of the bone morphogenetic protein BMP6 induces massive iron overload. Nat Genet *41*, 478-481.

Moriya, T., Kitamori, K., Naito, H., Yanagiba, Y., Ito, Y., Yamagishi, N., Tamada, H., Jia, X., Tsuchikura, S., Ikeda, K.*, et al.* (2012). Simultaneous changes in high-fat and high-cholesterol diet-induced steatohepatitis and severe fibrosis and those underlying molecular mechanisms in novel SHRSP5/Dmcr rat. Environmental health and preventive medicine *17*, 444-456.

Muckenthaler, M.U. (2014). How mutant HFE causes hereditary hemochromatosis. Blood *124*, 1212-1213.

Nagamoto, T., Eguchi, G., and Beebe, D.C. (2000). Alpha-smooth muscle actin expression in cultured lens epithelial cells. Investigative ophthalmology & visual science *41*, 1122-1129.

Nelson, J.E., Wilson, L., Brunt, E.M., Yeh, M.M., Kleiner, D.E., Unalp-Arida, A., and Kowdley, K.V. (2011). Relationship between the pattern of hepatic iron deposition and histological severity in nonalcoholic fatty liver disease. Hepatology (Baltimore, Md) *53*, 448-457.

Nemeth, E., Tuttle, M.S., Powelson, J., Vaughn, M.B., Donovan, A., Ward, D.M., Ganz, T., and Kaplan, J. (2004). Hepcidin regulates cellular iron efflux by binding to ferroportin and inducing its internalization. Science *306*, 2090-2093.

Nicolas, G., Bennoun, M., Devaux, I., Beaumont, C., Grandchamp, B., Kahn, A., and Vaulont, S. (2001). Lack of hepcidin gene expression and severe tissue iron overload in upstream stimulatory factor 2 (USF2) knockout mice. Proceedings of the National Academy of Sciences of the United States of America *98*, 8780-8785.

Nicolas, G., Chauvet, C., Viatte, L., Danan, J.L., Bigard, X., Devaux, I., Beaumont, C., Kahn, A., and Vaulont, S. (2002). The gene encoding the iron regulatory peptide hepcidin is regulated by anemia, hypoxia, and inflammation. J Clin Invest *110*, 1037-1044.

O'Brien, J., and Powell, L.W. (2012). Non-alcoholic fatty liver disease: is iron relevant? Hepatology international *6*, 332-341.

Ohgami, R.S., Campagna, D.R., Greer, E.L., Antiochos, B., McDonald, A., Chen, J., Sharp, J.J., Fujiwara, Y., Barker, J.E., and Fleming, M.D. (2005). Identification of a ferrireductase required for efficient transferrin-dependent iron uptake in erythroid cells. Nat Genet *37*, 1264-1269.

Omori, Y., Imai, J., Watanabe, M., Komatsu, T., Suzuki, Y., Kataoka, K., Watanabe, S., Tanigami, A., and Sugano, S. (2001). CREB-H: a novel mammalian transcription factor belonging to the CREB/ATF family and functioning via the box-B element with a liver-specific expression. Nucleic acids research *29*, 2154-2162.

Otogawa, K., Kinoshita, K., Fujii, H., Sakabe, M., Shiga, R., Nakatani, K., Ikeda, K., Nakajima, Y., Ikura, Y., Ueda, M.*, et al.* (2007). Erythrophagocytosis by liver macrophages (Kupffer cells) promotes oxidative stress, inflammation, and fibrosis in a rabbit model of steatohepatitis: implications for the pathogenesis of human nonalcoholic steatohepatitis. The American journal of pathology *170*, 967-980.

Padda, R.S., Gkouvatsos, K., Guido, M., Mui, J., Vali, H., and Pantopoulos, K. (2015). A high-fat diet modulates iron metabolism but does not promote liver fibrosis in hemochromatotic *Hjv*$^{(-)/(-)}$ mice. American journal of physiology Gastrointestinal and liver physiology *308*, G251-261.

Papanikolaou, G., and Pantopoulos, K. (2005). Iron metabolism and toxicity. Toxicol Appl Pharmacol *202*, 199-211.

Park, C.H., Valore, E.V., Waring, A.J., and Ganz, T. (2001). Hepcidin, a urinary antimicrobial peptide synthesized in the liver. J Biol Chem *276*, 7806-7810.

Pietrangelo, A. (2006). Hereditary hemochromatosis. Biochim Biophys Acta *1763*, 700-710.

Pietrangelo, A. (2010). Hereditary hemochromatosis: pathogenesis, diagnosis, and treatment. Gastroenterology *139*, 393-408, 408.e391-392.

Powell, E.E., Ali, A., Clouston, A.D., Dixon, J.L., Lincoln, D.J., Purdie, D.M., Fletcher, L.M., Powell, L.W., and Jonsson, J.R. (2005). Steatosis is a cofactor in liver injury in hemochromatosis. Gastroenterology *129*, 1937-1943.

Ragab, S.M., Abd Elghaffar, S., El-Metwally, T.H., Badr, G., Mahmoud, M.H., and Omar, H.M. (2015). Effect of a high fat, high sucrose diet on the promotion of non-alcoholic fatty liver disease in male rats: the ameliorative role of three natural compounds. Lipids in health and disease *14*, 83.

Rappaport, A.M. (1977). Microcirculatory units in the mammalian liver. Their arterial and portal components. Bibliotheca anatomica, 116-120.

Reddy, N.M., Potteti, H.R., Mariani, T.J., Biswal, S., and Reddy, S.P. (2011). Conditional deletion of *Nrf2* in airway epithelium exacerbates acute lung injury and impairs the resolution of inflammation. American journal of respiratory cell and molecular biology *45*, 1161-1168.

Rinella, M.E., Elias, M.S., Smolak, R.R., Fu, T., Borensztajn, J., and Green, R.M. (2008). Mechanisms of hepatic steatosis in mice fed a lipogenic methionine choline-deficient diet. Journal of lipid research *49*, 1068-1076.

Rochette, L., Gudjoncik, A., Guenancia, C., Zeller, M., Cottin, Y., and Vergely, C. (2015). The iron-regulatory hormone hepcidin: a possible therapeutic target? Pharmacol Ther *146*, 35-52.

Rozen, S., and Skaletsky, H. (2000). Primer3 on the WWW for general users and for biologist programmers. Methods Mol Biol *132*, 365-386.

Ryter, S.W., Alam, J., and Choi, A.M. (2006). Heme oxygenase-1/carbon monoxide: from basic science to therapeutic applications. Physiol Rev *86*, 583-650.

Ryter, S.W., and Tyrrell, R.M. (2000). The heme synthesis and degradation pathways: role in oxidant sensitivity. Heme oxygenase has both pro- and antioxidant properties. Free radical biology & medicine *28*, 289-309.

Sebastiani, G., Gkouvatsos, K., Maffettone, C., Busatto, G., Guido, M., and Pantopoulos, K. (2011). Accelerated CCl4-induced liver fibrosis in *Hjv*$^{-/-}$ mice, associated with an oxidative burst and precocious profibrogenic gene expression. PloS one *6*, e25138.

Seifert, E.L., Estey, C., Xuan, J.Y., and Harper, M.E. (2010). Electron transport chain-dependent and -independent mechanisms of mitochondrial H2O2 emission during long-chain fatty acid oxidation. J Biol Chem *285*, 5748-5758.

Serviddio, G., Bellanti, F., and Vendemiale, G. (2013). Free radical biology for medicine: learning from nonalcoholic fatty liver disease. Free radical biology & medicine *65*, 952-968.

Sharp, P.A. (2010). Intestinal iron absorption: regulation by dietary & systemic factors. Int J Vitam Nutr Res *80*, 231-242.

Sheedfar, F., Di Biase, S., Koonen, D., and Vinciguerra, M. (2013). Liver diseases and aging: friends or foes? Aging cell *12*, 950-954.

Shih, P.H., and Yen, G.C. (2007). Differential expressions of antioxidant status in aging rats: the role of transcriptional factor *Nrf2* and MAPK signaling pathway. Biogerontology *8*, 71-80.

Shin, S., Wakabayashi, J., Yates, M.S., Wakabayashi, N., Dolan, P.M., Aja, S., Liby, K.T., Sporn, M.B., Yamamoto, M., and Kensler, T.W. (2009). Role of *Nrf2* in prevention of high-fat diet-induced obesity by synthetic triterpenoid CDDO-imidazolide. Eur J Pharmacol *620*, 138-144.

Silva, B., and Faustino, P. (2015). An overview of molecular basis of iron metabolism regulation and the associated pathologies. Biochim Biophys Acta *1852*, 1347-1359.

Sonnweber, T., Ress, C., Nairz, M., Theurl, I., Schroll, A., Murphy, A.T., Wroblewski, V., Witcher, D.R., Moser, P., Ebenbichler, C.F.*, et al.* (2012). High-fat diet causes iron deficiency via hepcidin-independent reduction of duodenal iron absorption. The Journal of nutritional biochemistry *23*, 1600-1608.

Sorrentino, P., D'Angelo, S., Ferbo, U., Micheli, P., Bracigliano, A., and Vecchione, R. (2009). Liver iron excess in patients with hepatocellular carcinoma developed on non-alcoholic steato-hepatitis. Journal of hepatology *50*, 351-357.

Stein, Y., and Shapiro, B. (1960). Uptake and metabolism of triglycerides by the rat liver. Journal of lipid research *1*, 326-331.

Steinbicker, A.U., Bartnikas, T.B., Lohmeyer, L.K., Leyton, P., Mayeur, C., Kao, S.M., Pappas, A.E., Peterson, R.T., Bloch, D.B., Yu, P.B.*, et al.* (2011). Perturbation of hepcidin expression by BMP type I receptor deletion induces iron overload in mice. Blood *118*, 4224-4230.

Sugimoto, H., Okada, K., Shoda, J., Warabi, E., Ishige, K., Ueda, T., Taguchi, K., Yanagawa, T., Nakahara, A., Hyodo, I.*, et al.* (2010). Deletion of nuclear factor-E2-related factor-2 leads to rapid onset and progression of nutritional steatohepatitis in mice. American journal of physiology Gastrointestinal and liver physiology *298*, G283-294.

Suh, J.H., Shenvi, S.V., Dixon, B.M., Liu, H., Jaiswal, A.K., Liu, R.M., and Hagen, T.M. (2004). Decline in transcriptional activity of Nrf2 causes age-related loss of glutathione synthesis, which is reversible with lipoic acid. Proceedings of the National Academy of Sciences of the United States of America *101*, 3381-3386.

Suzuki, T., Motohashi, H., and Yamamoto, M. (2013). Toward clinical application of the Keap1-Nrf2 pathway. Trends Pharmacol Sci *34*, 340-346.

Takai, K., Funaba, M., and Matsui, T. (2015). Steatohepatitis is developed by a diet high in fat, sucrose, and cholesterol without increasing iron concentration in rat liver. Biological trace element research.

Tan, T.C., Crawford, D.H., Jaskowski, L.A., Murphy, T.M., Heritage, M.L., Subramaniam, V.N., Clouston, A.D., Anderson, G.J., and Fletcher, L.M. (2011). Altered lipid metabolism in Hfe-knockout mice promotes severe NAFLD and early fibrosis. American journal of physiology Gastrointestinal and liver physiology *301*, G865-876.

Tanaka, Y., Aleksunes, L.M., Yeager, R.L., Gyamfi, M.A., Esterly, N., Guo, G.L., and Klaassen, C.D. (2008). NF-E2-related factor 2 inhibits lipid accumulation and oxidative stress in mice fed a high-fat diet. J Pharmacol Exp Ther *325*, 655-664.

Tanaka, Y., Ikeda, T., Yamamoto, K., Ogawa, H., and Kamisako, T. (2012). Dysregulated expression of fatty acid oxidation enzymes and iron-regulatory genes in livers of *Nrf2*-null mice. Journal of gastroenterology and hepatology *27*, 1711-1717.

Tariq, Z., Green, C.J., and Hodson, L. (2014). Are oxidative stress mechanisms the common denominator in the progression from hepatic steatosis towards non-alcoholic steatohepatitis (NASH)? Liver international : official journal of the International Association for the Study of the Liver *34*, e180-190.

Theil, E.C. (2003). Ferritin: at the crossroads of iron and oxygen metabolism. The Journal of nutrition *133*, 1549S-1553S.

Tilg, H., and Moschen, A.R. (2010). Evolution of inflammation in nonalcoholic fatty liver disease: the multiple parallel hits hypothesis. Hepatology (Baltimore, Md) *52*, 1836-1846.

Tong, K.I., Kobayashi, A., Katsuoka, F., and Yamamoto, M. (2006). Two-site substrate recognition model for the Keap1-*Nrf2* system: a hinge and latch mechanism. Biological chemistry *387*, 1311-1320.

Torrance, J.D., and Bothwell, T.H. (1980). Methods in Hematology *1*, 90-115.

Umbreit, J. (2008). Intestinal absorption of iron (I): Fe(III). In Iron metabolism and disease, H. Fuchs, ed. (Germany: Research Signpost), pp. 1-30.

Valenti, L., Fracanzani, A.L., Bugianesi, E., Dongiovanni, P., Galmozzi, E., Vanni, E., Canavesi, E., Lattuada, E., Roviaro, G., Marchesini, G.*, et al.* (2010). HFE genotype, parenchymal iron accumulation, and liver fibrosis in patients with nonalcoholic fatty liver disease. Gastroenterology *138*, 905-912.

Vecchi, C., Montosi, G., Garuti, C., Corradini, E., Sabelli, M., Canali, S., and Pietrangelo, A. (2014). Gluconeogenic signals regulate iron homeostasis via hepcidin in mice. Gastroenterology *146*, 1060-1069.

Weiskopf, D., Weinberger, B., and Grubeck-Loebenstein, B. (2009). The aging of the immune system. Transplant international : official journal of the European Society for Organ Transplantation *22*, 1041-1050.

Williams, C.D., Stengel, J., Asike, M.I., Torres, D.M., Shaw, J., Contreras, M., Landt, C.L., and Harrison, S.A. (2011). Prevalence of nonalcoholic fatty liver disease and nonalcoholic steatohepatitis among a largely middle-aged population utilizing ultrasound and liver biopsy: a prospective study. Gastroenterology *140*, 124-131.

Wu, X.G., Wang, Y., Wu, Q., Cheng, W.H., Liu, W., Zhao, Y., Mayeur, C., Schmidt, P.J., Yu, P.B., Wang, F.*, et al.* (2014). HFE interacts with the BMP type I receptor ALK3 to regulate hepcidin expression. Blood *124*, 1335-1343.

Yates, M.S., Tran, Q.T., Dolan, P.M., Osburn, W.O., Shin, S., McCulloch, C.C., Silkworth, J.B., Taguchi, K., Yamamoto, M., Williams, C.R.*, et al.* (2009). Genetic versus chemoprotective activation of Nrf2 signaling: overlapping yet distinct gene expression profiles between Keap1 knockout and triterpenoid-treated mice. Carcinogenesis *30*, 1024-1031.

Yip, W.W., and Burt, A.D. (2006). Alcoholic liver disease. Seminars in diagnostic pathology *23*, 149-160.

Yun, S., and Vincelette, N.D. (2015). Update on iron metabolism and molecular perspective of common genetic and acquired disorder, hemochromatosis. Crit Rev Oncol Hematol *95*, 12-25.

Zambo, V., Simon-Szabo, L., Szelenyi, P., Kereszturi, E., Banhegyi, G., and Csala, M. (2013). Lipotoxicity in the liver. World J Hepatol *5*, 550-557.

Zhang, Y.K., Wu, K.C., Liu, J., and Klaassen, C.D. (2012). Nrf2 deficiency improves glucose tolerance in mice fed a high-fat diet. Toxicol Appl Pharmacol *264*, 305-314.

Zhang, Y.K., Yeager, R.L., Tanaka, Y., and Klaassen, C.D. (2010). Enhanced expression of Nrf2 in mice attenuates the fatty liver produced by a methionine- and choline-deficient diet. Toxicol Appl Pharmacol *245*, 326-334.

Zhou, X.Y., Tomatsu, S., Fleming, R.E., Parkkila, S., Waheed, A., Jiang, J., Fei, Y., Brunt, E.M., Ruddy, D.A., Prass, C.E.*, et al.* (1998). HFE gene knockout produces mouse model of hereditary hemochromatosis. Proceedings of the National Academy of Sciences of the United States of America *95*, 2492-2497.